A STUDY ON THE DEVELOPMENT ON TUNABLE OPTO-FLUIDIC DEVICES BY DIAMOND TURNING AND SOFT LITHOGRAPHY

LEUNG HUI MIN

NATIONAL UNIVERSITY OF SINGAPORE

2009

A STUDY ON THE DEVELOPMENT ON TUNABLE OPTO-FLUIDIC DEVICES BY DIAMOND TURNING AND SOFT LITHOGRAPHY

LEUNG HUI MIN
(B. Eng(Hons.), NUS)

A THESIS SUBMITTED FOR THE DEGREE OF MASTER OF ENGINEERING

DEPARTMENT OF MECHANICAL ENGINEERING
NATIONAL UNIVERSITY OF SINGAPORE

2009

Acknowledgement

I would like to express heartfelt gratitude towards my project supervisors Assoc. Prof A. Senthil Kumar and Asst. Prof Zhou Guangya. They have been most helpful and supportive throughout the course of project. Their continuous guidance and insights are utmost important in enabling the smooth progress of the project.

I would also like to thank the staff at Advance Manufacturing Laboratory (AML) especially Mr Tan Choon Huat and Mr Nelson Yeo Eng Huat. Mr Tan often kindly offered technical advice regarding the usage of various machineries, which is very helpful in facilitating the fabrication processes. It is also much appreciated that Mr Nelson has always been very dependable in operating the diamond turning machine and in explaining the technicalities required for the programming of the machine.

Not forgetting the staff and colleagues in Microsystem Technology Initiative (MSTI) laboratory, which include laboratory technologist Mr Suhaimi Bin Daud, postdoctoral fellow Mr Yu Hongbin, research scholars Mr Cheo Koon Lin, Mr Wang Shouhua, Mr Du Yu, Mr Jason Chew Xiong Yew and Mr Mu Xiaojing, I would like to thank their continuous encouragement and advice. The learning process will surely not be as fruitful and enjoyable without them.

Last but not least, I appreciate the enduring patience and generous help from Mr Ooi Boon Hooi, a fellow science enthusiast acquainted since undergraduate days. His expertise in computing has often helped relieve me from frustrations I had with many programmes such as MatLab.

Table of Contents

Summary

Single-point diamond machining methods, namely diamond turning and shaping, are combined with a rapid replication technique known as soft lithography to develop an efficient and affordable fabrication process flow to obtain various types of liquid tunable lenses. The tunability of all of the liquid tunable microlenses developed in this project works on the same principle. Through the pumping of distilled water via micro liquid channels, the radius of curvature of a deformable membrane above a carefully designed optical surface can be adjusted, thereby acting as a tunable refractive lens.

First, the diamond machining processes are explored on various types of substrate materials. Based on a few important considerations such as post-machining surface quality, hardness, material compatibility with the diamond cutter, cost and availability, Polymethylmethacrylate (PMMA) is found to be the most suitable substrate material for diamond machining. Next, the main parameters of diamond turning, which include rotational speed of spindle, feedrate and depth of cut are chosen to be 1000 rpm, 0.1 mm/min and 5 μm respectively to obtain a suitably smooth optical surface without premature damage to the cutting tool.

Next, the fabrication processes involving soft lithography with PDMS are developed and refined to ensure good surface quality and mold replica integrity. As determined by atomic force microscope (AFM) test results, the mean surface roughness of the diamond cut PMMA mold and the final PDMS replica are 36.5 nm and 13.1 nm respectively. Surface profiles of the replica and the mold are also compared to verify the reliability of the replication processes.

Meanwhile, the optical surfaces of four different types of microlenses are designed in this work. Firstly, a diffractive/refractive hybrid lens is designed to reduce chromatic aberration in the visible range with an optimum focal length of 15 mm. Secondly, a double focusing lens that consists of a central and peripheral spherical surface with different radii of curvatures is designed to simultaneously give two lateral focal points. This type of lens could be used to process data from two positions at the same time to increase efficiency. The central spherical surface has a diameter of 2 mm and radius of curvature of 3 mm while those of the peripheral spherical surface are 12 mm and 100 mm respectively. Thirdly, an aspherical lens is designed to reduce third order aspherical aberration at an optimum focal length of 20 mm. ZEMAX, an optical ray tracing software is used to simulate the required aspherical surface based on the optical properties of the lens materials and the surrounding medium. Lastly, by displacing the optical center of the diffractive Fresnel lens by a small distance, a toroidal lens is obtained. This toroidal lens can produce two traverse focal points that are close together. If those two focal points are close enough to be non-distinguishable, the toroidal lens can increase the depth of focus.

The surface quality, integrity of the replicated molds and the optical performances of the four types of lenses are experimentally tested and verified. In addition, analysis and discussion of the results of each lens will also be given.

List of Tables

List of Figures

List of Symbols

f	Focal length
V	Abbe number
ϕ	Optical power
n	Refractive index
λ	wavelength
h	Height
m	Fresnel zone number
r	Distance from a point of the surface relief of the diffractive lens to the focal point
R_m	Radius of the zone ring of a certain zone number
W(x,y)	Wavefront error as a function of x and y coordinates
S	Shear
R	Radius of curvature of lens
t	thickness of lens
S_o	object distance
S_i	image distance
D	Diameter of lens aperture

Chapter 1. Introduction

1.1 Aim and Objectives

The main objective of this project work is to develop a fabrication flow process that combines diamond machining techniques and soft lithographic replication processes to efficiently produce high quality liquid tunable microlenses. This would serve as an alternative to building optical systems that are more cost effective, compact and have expanded functionalities as compared to conventional systems that use multiple fixed focal length lenses. At the same time, it would also provide a convenient and reliable way for engineers to design and produce free-form optical surface reliefs that can have specific imaging properties.

The fabrication process developed here should be able to fully utilize the versatile capabilities of ultrahigh precision diamond machining to fabricate 3-D rotationally symmetrical optical surfaces and accompanying necessary structural architecture to make a complete liquid tunable lens device. To demonstrate the feasibility of the fabrication flow process and the usefulness in applying the developed methods to improve numerous aspects of the imaging qualities of microlenses, this work also aim to include the fabrication and testing of the functionalities of a few different types of microlenses.

The contents of this thesis are arranged as follow. First, a literature study on various types of microlenses, different diamond machining techniques and soft lithography are given. Next, the motivation in combining diamond machining and soft lithographic methods to fabricate liquid tunable microlenses is elaborated. This is followed by giving the general fabrication flow process that is applicable to all the different types of microlenses developed in this work. After which, the discussion on working material suitability and the fabrication parameters used during machining, soft

lithography are presented in detail. Based on the established fabrication method, the design of four different types of liquid tunable microlenses, each of them with specific imaging improvements from conventional tunable lenses, are discussed and analysed. Together, the results of their optical performances and surface characterization are presented. Finally, a few directions which related future work could be carried out are given in the concluding chapter.

1.2 Microlenses

In early designs of optical systems, it is common to use multiple bulky solid lenses which require mounting and painstaking optical alignment between each of them. And if the configuration within the optical systems needs to be modified, for zooming purposes for instance, one or more lenses to have to be shifted to change the relative distance between the optical components within the system. If a lens is bulky, especially if compound lenses are required for considerations like aberrations, moving them will need a large amount of power input and their response might be slow. As technologies advance, there seems to be a ceaseless drive to develop increasingly miniaturized devices. Since optical systems are omnipresent in a wide range of applications, which include fiber-optic communication networks, handheld medical devices, bio-imaging systems and consumer products like pocket cameras, there is a need to develop optical systems which have reduced complexities, higher performance, enhanced compactness and affordability. Thus, it is natural that bulky lenses are often replaced by microlenses.

Owing to their sizes, microlenses can often be easily integrated in many important applications, which include wavefront sensing, laser shaping, confocal microscopes, endoscopes and miniaturised cameras in mobile phones, to achieve enhanced performance and miniaturization. There are a myriad of fabrication methods to realise microlenses.

1.2.1 Liquid Tunable Lenses

Despite the increasing sophistication in fabrication methods, fixed focal length microlenses is becoming insufficient to meet the demands of real-time acquisition of information, whereby the focal lengths of the lenses often need to vary dynamically. To address this concern, there are research groups that successfully used the property of variation of crystal orientation of liquid crystals in the presence of an electrical field to fabricate variable focusing microlenses [1]. The refractive index of liquid crystal is dependent on the crystal orientation which can be tuned by applying a potential applied across it. Liquid crystal cells are usually thin and lightweight, making them useful for fabricating compact optical devices. However, the low optical transmittance of thick liquid crystals and the polarisers that are necessary to ensure the incident light is parallel to the crystal orientation of the lenses result in low light efficiency. In addition, the response time of liquid crystal lenses, which is dependent on the thickness of the lens, tend to be long and could vary across the lens profile, such as in the case of convex or concave lenses. In addition to the fact that focal length tuning of the liquid crystal lenses is voltage frequency dependent, there could be potential problems implementing liquid crystal lenses in optical systems that demand high frequency response.

Another actuation method of variable focusing microlens that requires an external voltage source is known as electrowetting on dielectrics (EWOD) [2, 3]. The surface tension and hence, the curvature of the liquid lens, is controlled electrostatically, giving rise to smaller response times. This type of liquid lens needs to be encapsulated in a liquid chamber, mainly to prevent liquid loss through evaporation and to ensure the lens remains optically aligned in the presence of external disturbances. The liquid for the lens and the liquid encapsulating it need to be well

matched in density in a certain range of working temperature. In addition, the former needs to be electrically conductive, while the latter insulating. The dispersion characteristics of each liquid needs to be considered, too, if the lens is an achromat. The proper design and control of two suitable liquids can be a time consuming process.

To avoid the use of multiple liquids to achieve variable focusing microlenses, soft lithography could be utilised. Commonly, a suitable substrate, such as SU8, is first lithographically patterned before subsequently used as a master mold for replication processes. Since PDMS, an elastomer, has excellent optical transmittance over a wide spectral range, it is often used as the material for replicas. Bio-optical sensing systems [4] and Shack-Hartmann wavefront sensors [5], among others, have been shown to benefit from microlenses fabricated using soft lithography.

In 2003, Zhang et. al. published a work on a liquid tunable lens that consist of a PSMD liquid chamber sealed with a thin layer of PDMS [6] with accessible liquid channels. By tuning the hydraulic pressure applied through the pumping of liquid via the channels, the PDMS film bulges out in varying radius of curvatures, forming liquid lenses with varying focal lengths. Due to the high elasticity of the film, this liquid lens is able to achieve a high tunability of 131 mm. Both the design and actuation method of the lens design is simple and straightforward. There is a similar design published by Chen et. al. which consists of a similar liquid chamber. But instead of using a uniform thin film to seal it, the deformable seal has a profile of a convex lens [7]. The focal length of such a lens ranges between approximately 4 and 11 mm.

Other than liquid tunable lenses that require the pumping in and out of liquid from an external reservoir, there are designs that work with a fixed volume of water in a completely sealed cavity. For example, the liquid tunable lens published in [8] makes

use of a fixed volume cavity with two non-overlapping deformable elastic membrane. One of it is an actuator, which can be deformed with a ball indenter, while the other is the tunable liquid lens. When the ball indenter compresses one of the elastic membrane, the liquid pressure is transferred to deforming the other liquid membrane, forming a variable focus convex lens. Another example of a fixed volume liquid tunable lens is published in [8]. The radius of curvature of the lens is tuned by varying the diameter of the annular sealing ring. Experimental results show that that lens has a focal length tunability of over 120 mm.

1.2.2 Fixed Focus Microlenses

Despite the increasing importance in dynamically tunable lenses, the development of fixed focus microlenses is also instrumental in the development of micro optical systems. One method of fabricating fixed focus lenses uses bulk machining techniques to selectively etch a boron doped silicon wafer to obtain microlenses [9]. The diffusion time and drive-in time during boron doping of the silicon wafer define the dimensions and, hence, the focal length of the microlenses. The process requires a temperature of above 1000^0C for approximately 20 hours. Thus it can be seen that this process is power intensive and specialized equipment is required. Furthermore, this method is not suitable for the fabrication of microlenses that have diameters greater than 50 um as their profiles tend to deviate from spherical shapes.

In another published work, e-beam lithography was used to fabricate micro-sized Fresnel zone plate lenses [10]. Despite the fact that e-beam is a highly precise fabrication method, it limits the size of the lenses which can be fabricated mainly because it is not an efficient etching process. The lens which was fabricated has a diameter of 80 µm and the depth of the zone rings are only 110 nm tall. Because the height of the annular zone rings is too small, the focusing efficiency is too low to be tested in that work. Moreover, the efficiency of e-beam etching limits the diameter of

lens and it in turn limits the number of annular rings that can be accommodated within that diameter. The low number of annular rings in a zone plate lens results in low spatial resolution [11].

Another way to fabricate microlenses is known as the photoresist thermal reflow method whereby micro-sized columns of photoresist is first lithographically defined before being heated to temperatures above their glass temperature to form dome shaped lenses under the influence of interfacial tension. The profile has to be transferred to the silicon substrate through another step of etching process. The characteristics of such microlenses have non-linear dependency on a number of fabrication parameters, such as thermal reflow temperature and time. Therefore it can be a tedious task to optimise all the fabrication parameters [12]. It is possible to eliminate the final step of transferring the pattern from the photoresist to the substrate by using photo-curable optical polymer instead of conventional photoresist in the thermal reflow method. With the use of micro-contact printing to form wettability patterns on substrate, the positions of individual microlenses can be defined [13]. One problem of this fabrication process is the difficulty to avoid contamination of water droplets on the microlenses, which can lead to unpredictable degradation of performance.

In conclusion, it is apparent from the vast amount of work reviewed in this chapter that the development of novel fabrication methods to enhance the functionality and performance of microlenses are currently being actively pursued by research teams throughout the academia.

1.3 Machining Using Diamond Inserts

1.3.1 Turning Using Diamond Tool

Single-point diamond turning is a high precision cutting process that uses a diamond tool tip controlled by an actuator to cut a free form surface on a rotating substrate. A schematic of diamond turning is shown in Figure 1.1. A free form surface could be broadly understood as any continuous surface profile. The high precision of diamond turning is usually achieved by the use of piezoelectric actuators with various types of feedback control systems to minimize the error arising from both the slides and spindle systems in the machine [14-16].

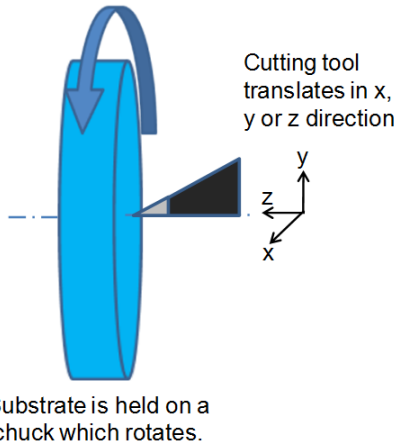

Figure 1.1: A schematic on how diamond turning is carried out.

Most commonly, diamond turning produces rotationally symmetrical profiles which the z-position of the spindle during machining is constant at a particular radius from the centre of rotation. In this case, translation of the cutting tool in the z-direction is just a function of x or y coordinates. The simplest example will be a spherical reflective lens that can be diamond turned on metallic substrates.

In cases when non-rotationally symmetrical profiles are required, such as a lens array or rectangular features, an additional parameter of time is required to define the z-coordinate of the cutting tool. This is because for a constant rotational speed, the rotational orientation will be known for any point of time. Since the angular position is controlled by high frequency response piezoelectric actuators, the system is also known as fast tool servo [17]. An alternative method to control the z position at a certain radius of cut is through the use of feedback response of mechanical slides, and this method is referred to as slow tool servo [18]. It should be noted that lens arrays composed of rotationally symmetrical elements are often encountered in many optical systems and they could theoretically be easily fabricated without the need to correlate time with the position of z but by varying the centers of rotation on the lathe. However, this functionality is often not incorporated in most diamond machining lathes. Hence, they are often considered to be non-rotationally symmetrical profiles as a whole.

The main difference between diamond turning of miniaturized components and conventional turning of bulky components is that the small variations in surface profile needs to be suppressed as they might over-shadow the micrometer features important to the design. Because of this, a dual servo system, one which is used for coarse rectification over a long distance and one for high frequency error correction within a short distance, might be necessary [15]. With the advance of technologies, commercial diamond turning lathes can now have a precision of 1 nm, although it is common to have a lower precision of a few microns.

However, those values could probably only be used as a coarse gauge as they are derived solely based on the control of the tool's positioning. Situations in which precision is of utmost importance, the actual cutting precision ought to take into account of the material's characteristics, such as the material's viscoelasticity,

ductility range, crystallographic orientation, thermal response and chemical stability at elevated temperature. For example, when high feed rate and rotational speed are used during cutting, the point of contact is usually heated to temperatures high enough to cause significant local thermal expansion. More severe damage could result when the elevated temperature changes a ductile material into a brittle one, resulting in pits and cracks on the surface of the work piece. Sometimes the damaging effects do not just pertain to the substrate. High temperatures can encourage the substrate material to react with the diamond tool tip, damaging the two [19]. Therefore, it can be seen that the effectiveness of the control system of the machine, the chemical stability of the substrate material and working parameters, such as feed rate, rotational speed, depth of cut and dwell time need to be optimized if a high quality product is desired [20].

The capability of diamond machining to produce smooth optical surfaces is not the only reason why it has been attracting global interest among researchers.

- Firstly, its precise actuators make diamond turning a viable technique to fabricate miniaturized 3-dimensional (3-D) components with extremely small feature size. Photolithographic methods are unable to produce true 3-dimensional features. By using a number of layers deposited on top of another, it approximates a 3-D object instead. The capability of micro 3-D objects is useful to many fields such as micro fluidic studies and optics.
- Secondly, photolithography and etching methods are only suitable mostly on a selected few photoresist and silicon based materials, unlike diamond turning which can handle a wide range of materials, from polymers (e.g. acrylic) to metals (e.g. brass).
- Thirdly, many materials that are too hard to be easily machined by conventional machining methods are able to utilize diamond machining

techniques, because diamond is such a hard material that it can abrade most others.

- Etching techniques usually takes a very long time to remove a small volume of material while diamond machining, being a mechanical method, removes material much more efficiently, without compromising precision or surface quality. Seldom are etching methods used to fabricate features of sizes greater than a few tens of microns. In contrast, it is common to diamond turn features that have sizes in the millimeter range or above.
- Another significant edge over photolithography that diamond turning offers is the possibility of fabricating features which sizes are not limited by the diffraction limit. Considering Rayleigh equation, $R = \frac{k\lambda}{NA}$, in which R is the resolution, k a material constant that is dependent on the photoresist material, λ the wavelength of exposure radiation and NA the numerical aperture of the lens system used during photography, it can be seen that the finest dimension resolvable in photolithography improves with the use of radiation of smaller wavelength.

  To obtain feature size of about 500 nm, UV light from an Hg lamp could be used. But to obtain feature size of below 100 nm, expensive advanced lithographic methods that utilize extreme UV, soft x-rays, focused ion beams or electron beams are needed. This leads to increasing production cost.

  On the other hand, diamond turning is a mechanical way of removing material. Considering the precision achievable with feedback control systems and advanced actuators, diamond turning could very probably produce structures with feature size that is comparable or smaller than those achieved in photolithography with relative ease.

- Lastly, the working material needs to be flat during photolithography. However, this is not a requirement in diamond turning, which could handle a curved platform.

Despite the many attractive sides of diamond turning techniques, there are limitations to it, too. Firstly, the diamond tip is brittle and could be damaged if working parameters are not chosen carefully. The low feed rate and depth of cut, required to prolong the usage life of the diamond tool and to preserve the quality of the surface finish, often lead to long machining time. Secondly, since additional sophisticated computational tools are necessary to enable the turning of non-rotationally symmetrical surfaces, many designs to be fabricated on diamond turning lathes are restricted to rotationally symmetrical profiles. Thirdly, tool tip compensation becomes necessary especially when the features are micro sized and when a round tipped diamond insert is used. Tool tip compensation is necessary because a z-translational motion of the tool will result in a different contact point in x and y directions because of the contour of the tool tip. Since the diamond tool tip could wear out after long periods of usage, tool tip compensation needs to be monitored regularly.

Diamond turning technique is often useful in fabricating optical components. For instance, it can turn refractive, reflective and diffractive lenses on various suitable substrates. And to reduce the effective fabrication time for each lens device, high precision diamond turning could be used to manufacture lens molds since the time to make a replica out of a mold is relatively shorter than the time to diamond turn lenses. Furthermore, unconventional mirrors arrays to be used in space studies/telescopes have high demands for curvature accuracy and surface finish and they have been successfully fabricated with diamond turning [21]. Another example of the applications of diamond turning is the fabrication of a special type of aspherical mirror known as Wolter type I mirror [22]. It is an optical element in a soft x-ray microscope,

which is a valuable tool in cell studies due to its high resolution. Naturally, the mirror demands an extremely smooth surface and tight curvature tolerances for it to deliver the expected results. These requirements could be satisfied with the use of high precision diamond turning process.

1.3.2 Shaping Using Diamond Tool

Thus far, the only high precision diamond machining process discussed is the turning process. It is not the only viable process on the diamond machining lathe. Diamond shaping could also be utilized on the same machine. Unlike turning processes, shaping only involves relative translational motion between the diamond cutter and the substrate. During a shaping process, the substrate will not be rotating as the diamond-tip cutter plunges into the substrate and moves across it, thereby removing material. With the proper selection of working parameters, devices with surface quality that is comparable to that produced by diamond turning could be fabricated. This was demonstrated by a research group that used shaping instead of turning to fabricate lens array with aspherical lens elements [23]. Another research group used shaping to produce a profile of two intersecting lens [24]. Like 4-axes diamond turning processes, shaping is another option to fabricate non-rotationally symmetrical profiles. A schematic of diamond shaping is shown in Figure 1.2.

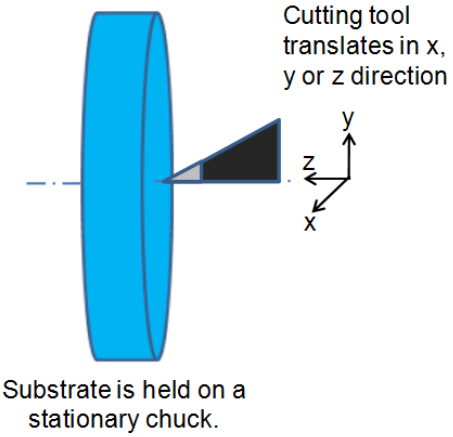

Figure 1.2: A schematic of how diamond shaping is carried out.

1.3.3 Milling Using Diamond Tool

In addition to turning and shaping, diamond milling is another branch of diamond machining that further enhances its versatility to produce a myriad of free form surfaces. In [24], it is reported that diamond milling can fabricate channels of different cross sections, from those with deep and narrow rectangular cross sections to those with V-shaped profiles. Although techniques like deep reactive ion etching (DRIE) and wet etching can also produce these types of channels, the smoothness and straightness of the sidewalls, uniformity of the structures across the substrate and the variability of the V-angle are much more difficult to control with those methods.

1.3.4 Suitable Materials for Diamond Turning

Like all other machining methods, material consideration is important in diamond turning. A set of working parameters should be tailored upon considering the substrate's material characteristics so as to ensure high surface quality and tight dimension tolerances. Careful selection of material could also prevent premature damage to the diamond cutting tool and substrate.

To elaborate on the importance on material considerations, a few concrete examples will be highlighted.

- If a high feed rate and high depth of cut is used on a brittle substrate like silicon, it is likely unsightly pits and cracks will appear on the final product. Instead, they must be kept sufficiently low such that cutting is at the ductile regime of the material [20].
- Soft metals like unalloyed aluminum are often not preferable working materials because of the poor machinability. Soft metals might not be able to withstand the cleaning and handling processes that follows after machining. Thus, alloying is necessary to attain certain degree of hardness. 6061 aluminum alloy, for example, may be a suitable material with good machinability for diamond turning.
- In some other materials like pure nickel are unsuitable for diamond machining because they react chemically with the carbon in the diamond tool tip when the local contact temperature is high during cutting, causing tool damage. Thus, the material has to be modified with suitable alloying metals that can suppress this chemical reaction. NiP, TiN, NiSi and NiTi are some examples of nickel alloys that can prevent that thermally activated chemical reaction [19].

Apart from the materials mentioned above, metals like oxygen free copper (OFC) and brass [24], as well as non-metals like Polymethylmethacrylate (PMMA) [23, 25] have excellent machinability and thus, they are often choice materials to be diamond turned on.

Despite the good machinability of all these materials, it is often impractical to compose entire devices out of those materials, especially if they are bulky structures.

Firstly, a device may need to be composed of lightweight material due to its application. Secondly, it would not make economical sense to have entire devices made of alloys like TiN because they are expensive. Thirdly, since the diamond turned device could be a part of an integrated system, the suitable material of the other parts of the device might differ from that region that is to be diamond-turned. Deposition of machinable metals on selected regions on the device is one plausible solution that addresses those concerns. There have been extensive published work that explored the deposition of Ni-P alloy on various substrates materials and its machinability [26-29]. The Ni-P alloy chemically deposited on structures in baths containing Ni salts and reducing agents is termed as electroless nickel (EN). From these reports, it can be concluded that with the right selection of working parameters, diamond turning on EN can give excellent surface finish. Since EN adheres well only to a few materials such as aluminum, the surface of the device needs processing prior to EN deposition. However, sometimes this might not always be feasible due to material incompatibility.

1.3.5 Alternatives to Diamond Turning

In this work, diamond turning techniques are being employed mainly to produce continuous surface relief that can produce spherical and aspherical profiles of variable radius of curvatures, blazed gratings and perpendicular walls. Thus, it would be good to have a look at alternative fabrication techniques that can produce similar profiles and give a brief assessment on the strengths and weakness of each method.

Staircase phased binary optical components are approximates of those that have smooth parabolic zone profiles, which could theoretically have 100% efficiency if optical absorption is insignificant [30]. The greater the number of staircase steps, n, the better the approximation and the higher the diffraction efficiency. Thus fabrication

methods to produce binary optical components are often useful in realizing diffractive optics. Each time n is doubled, two binary masks must be aligned before exposure. Usually, the efficiency will be close to 80% for n=4.

This might be a very straight forward fabrication method and standard photolithography equipment is sufficient to carry out this process. However, there is likelihood in a loss in dimensional accuracy as alignment error increases with every time the binary masks are aligned. This will lead to a decrease in diffraction efficiency. Thus, it is difficult to obtain a high performance 3-D diffractive optical element with this method.

There is a research team that modified the above-mentioned method to produce various structures with sloping walls. Instead of letting the mask be stationary, the team put the mask in continuous motion during exposure. There are many factors that need to be taken into consideration, including light propagation characteristics and variation in refractive index across the depth of the thick photoresist. The complexity makes it difficult to accurately design a set of working parameters to obtain a certain topology [31].

Another well-established method that has been commonly used to fabricate sloped profiles like blazed gratings is the use of gray scale masks [32, 33]. Instead of using an opaque mask that essentially blocks all radiation from reaching the photoresist, a gray scale mask that has varying opacities to regulate the amount of radiation passing through it. The sloped profiles obtained on the photoresist will be transferred to the substrate after etching.

As compared to the fabrication process to produce staircase phased binary optical components, the use of gray scale masks requires just a single exposure-etching

process. However, there are tedious calibration steps that must be performed prior to the actual etching process. The calibration step is to determine the relationship between optical density of the mask and the thickness of the photoresist required. Only after the calibration can a gray scale mask be custom made. The high cost of the calibration plate and gray scale masks is one of the major drawbacks of this method. A gray scale mask that is less than 20 mm^2 costs about S$2000 while the calibration plate costs about S$5000.

Alternatively, it is possible to use electron beam (e-beam) lithography to create continuous sloped profiles, as reported in [34, 35]. E-beam has high resolution and is able to create a continuous surface relief. However, e-beam writing takes a long time to complete as it writes on the substrate pixel by pixel. Therefore, it will not be an attractive option if large areas and depths need to be processed.

Having discussed about methods to fabricate profiles with slopes, it is also important to look at fabrication techniques to produce vertical walls. Vertical structures with high aspect ratio could conventionally be fabricated using reactive ion etching (RIE) or deep reactive ion etching (DRIE). Structures with 30:1 aspect ratio was reported in [36]. The roughness of the walls increases with the depth of etching, with roughness reaching 1000nm. The presence of undercutting is common too [35]. Despite the high aspect ratio achievable, DRIE is seldom able to cut depths of more than 500 µm.

1.4 Soft Lithography

Diamond turned profiles have very tight dimensional tolerances, with surfaces often of optical quality. Therefore, they could serve as ideal molds for optical components. In many ways, direct replication of optical components from high quality molds is superior to methods which rely heavily on polishing to obtain smooth optical surfaces.

Polishing often requires the use of suitable chemicals coupled with abrasive agents to smoothen a surface. Different material and surface features require a different set of polishing agents, method and duration. To figure what is most suitable, it might take numerous tests, which would incur a significant amount of time and cost. Moreover, it is very likely that these polishing processes alter the dimensions and curvatures of the profiles to a certain extent, even if all the process parameters are optimized. The unpredictability of this alteration due to its process-dependent nature compromises the performance of those optical components. In contrast, diamond machining of optical molds requires no post machining surface processing and the tight dimensional tolerances can be preserved.

There are a number of replication techniques that could be used to obtain equally high quality replicas. Replication is the key to efficient mass fabrication of structures of highly controlled dimensions and surface quality, bringing the effective cost and time of fabrication per device low. The most common techniques can be broadly categorized into two, namely soft lithography and injection molding.

Soft lithography refers to a number of branches of techniques that uses a patterned elastomer as a mold, mask or stamp [37]. Those branches include replica molding [38], micro-transfer molding [39] and micro-contact printing [40], among others. The branch of soft lithography that is most applicable in this work is replica molding. Therefore, the two terms are used interchangeably in this work. In replica molding, a patterned negative master mold will be used to replicate a positive replica, usually with a curable elastomer that will be peeled off once fully cured. It is also common that the end device requires two cycles of soft lithography and in this case, the positive master mold will eventually yield a positive end product.

In [37], it is reported that replication molding through soft lithography could generate features as small as 30 nm. Thus, soft lithography would still be up to task to replicate 3-D topologies that have extremely fine features and there should be no worry that those intricacies might not be faithfully replicated. Because of this high fidelity in transferring fine features on 3-D topologies from the mold to replicas, this working process is highly compatible with diamond turning, which major strength also lies in producing intricate 3-D topologies.

One of the most common materials encountered in replica molding is Polydimethylsiloxane (PDMS). It has a high transmittance over a wide spectral range, especially in the visible range where the optical loss is almost 0 dB/cm [41]. In addition, PDMS is inexpensive, easily accessible, is safe to use without any potential serious health hazards and could be thermally cured at temperatures below 100^0C. This makes PDMS a very suitable material for rapid-prototyping of optical components such as lenses.

Among the components fabricated with PDMS soft lithography is a 2-D lens array that could be stacked to make an optical diffuser [38]. Various types of tunable optical lenses have also used this technique as part of their fabrication process [5-7]. Apart from that, soft lithography has been useful in realizing micro-fluidic systems with active valves and pumps [42] and micro-channels that can be used on lab-on-chips [43]. The variety of devices that has benefited from the development of the technique of soft lithographic underlies its importance and reliability in the field of micro/nano fabrication and precision engineering.

In spite the widespread usage of PDMS in soft lithography, there are a few other materials that have been successfully explored. For one, epoxy was used in the replication of a Woltzer type I mirror [22, 44]. In that process, a layer of gold is

deposited on the surface of the master mold to serve as a parting agent to ease the process of thermal-assisted release of replica. Sol-gel used on a PDMS mold, was also reported to be applicable to nano-replication processes [45]. In the liquid form, sol flows and fills the topologies on PDMS mold easily because both are hydrophobic in nature. Upon drying, the sol transforms to hydrophilic gel. Thus, it can be released from the hydrophobic PDMS mold easily when that occurs. The released gel-like structure turns into glass upon annealing at 600^0C.

Apart from replica molding, injection molding was also developed to realize mass fabrication of micro structures [46, 47]. This method could use plastics that include high density polyethylene (HDPE), PMMA and polypropylene (PP). It is easy to obtain replicas that have high aspect ratio but the down side of this method is that it is not easy to find the optimized injection pressure, mold temperature and injection time, among other working parameters, for each different polymer of a certain aspect ratio. When not optimized, the surface quality of the structures will be seriously undermined. This poses a tricky problem when a structure containing features of different aspect ratios are to be injection molded.

Thus far, a literature study on diamond machining and soft lithography is presented. They are the two fabrication techniques that are used for all the tunable opto-fluidic devices developed in this work. However, it should be noted that the concept of combining those two fabrication techniques for tunable opto-fluidic devices was not conceived in a direct manner. Instead, it was arrived at that idea after numerous explorations numerous alternatives. In the next chapter, some of the important experimental results obtained in the course of exploration shall be detailed before the fabrication methods which are deemed the most viable and suitable for tunable opto-fluidic devices are described. After which, the designs and experimental results

pertaining to the various devices that made use of the fabrication techniques developed will be detailed separately.

Chapter 2. Fabrication Methods

2.1 Motivation Behind Using Diamond Turning and Soft Lithography

It is well established that high precision diamond machining techniques are able to fabricate 3-D free form surface relief that are valuable in the field of optics. One of the initial sources of motivation to explore diamond turning techniques in our work comes from being able to fabricate blazed surfaces of a Fresnel lens to achieve a theoretical 100% optical efficiency. That could provide a much better alternative to lithography and etching techniques which could typically only fabricate low efficiency stepped profiles unless expensive grey scale masks are used. However, diamond turning a diffractive lens with a fixed focal length will not fully demonstrate the value of integrating diamond turning techniques in the making of optical components.

Therefore, as opposed to simply diamond turning a lens on a rigid substrate to produce a fixed-focus lens, a tunable lens, which focal length could be dynamically controlled, would better demonstrate the potential of applying such a technique to a large field of optics engineering. Focal length tunability could be achieved by combining a rigid diamond turned lens with another simple tunable refractive lens. Each time a different type of rigid diamond turned lens is paired with a tunable refractive lens, a different tunable lens system could be produced. The rigid diamond turned lens could be, among many other possible examples, a Fresnel lens, a double focusing lens, an aspherical lens and diffractive toroidal lens.

The subsequent task is to develop fabrication methods to realise such a tunable lens system in a cost and time efficient manner. The most simple and basic single tunable lens is one that uses liquid pressure to deform an elastic film. If the film is bonded to a circular boundary, the deformation will take on a spherical dome shape. The radius

of curvature will depend on the magnitude of the pressure. That, in turn, determines the focal length of the liquid filled lens. This is illustrated in Figure 2.1.

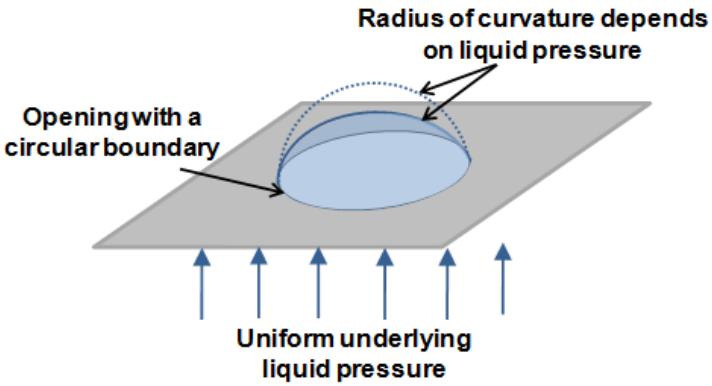

Figure 2.1: The higher the liquid pressure, the smaller the radius of curvature of the deformed film that is bonded to a substrate with a circular opening.

If a rigid fixed-focus lens profile could be integrated on the bottom of a cylindrical well and the opening of the well could be covered with an elastic film, a tunable lens system could be realized with ease. The height of the cylindrical well will be the distance separating the rigid lens and the tunable lens. Since the amount of deformation of the elastic film is to be controlled by liquid pressure, there need to be liquid channels to deliver water to the cylindrical well. In addition, the material of the device has to be transparent to allow light to pass through the lens profile at the bottom of the lens cavity and the water-filled refractive lens. Based on these considerations, we arrive at the general design of liquid tunable lens as shown in Figure 2.2.

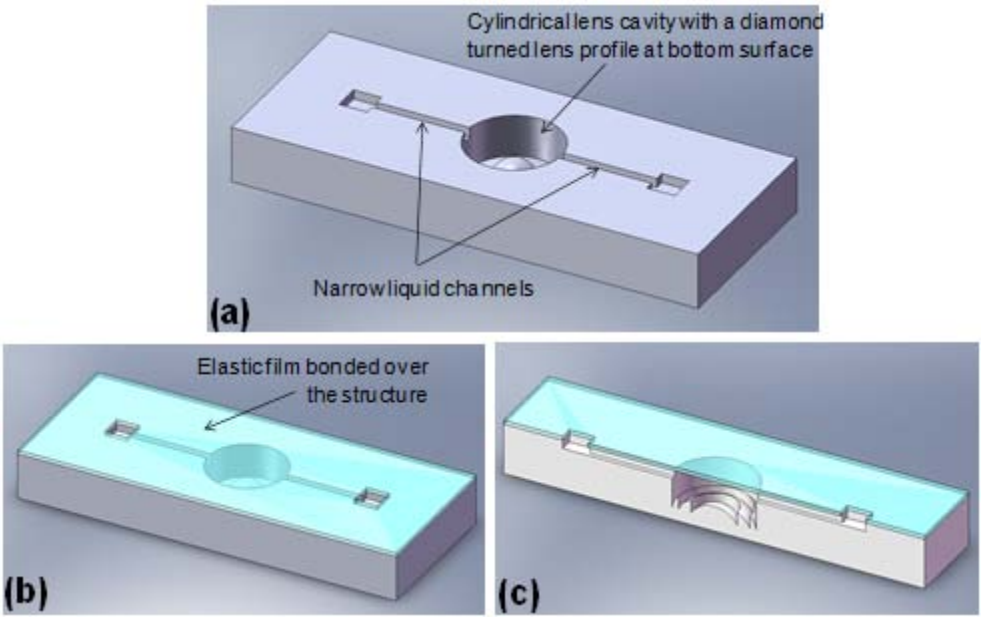

Figure 2.2: General design of the liquid tunable lens device consists of a lens cavity with a lens profile at the bottom surface and a deformable film bonded over it.

One of the most common materials used in opto-fluidic devices that are transparent and elastic is PDMS. Therefore, it is possible to have a thin film of PDMS bonded over a diamond turned PMMA structure to obtain the proposed liquid tunable lens device. However, it is not known how to bond PDMS with PMMA. On the other hand, it is common to use oxygen plasma for PDMS-glass or PDMS-PDMS bonding.

Even if it is assumed that PDMS could bond well with the diamond turned PMMA, every time a new device is needed, a new one has to be diamond turned on PMMA which is a rather time consuming process. Instead, rapid prototyping would be a more attractive option for engineering applications. It has been demonstrated by various research teams that a rapid mold replication process, known as soft lithography, can replicate intricate features down to the nanometre range with high accuracy. Thus, it has become clear that soft lithography has to be applied on diamond turned PMMA structures. This is because by doing so, it would be possible to get the best of both worlds offered by high precision diamond machining to

fabricate 3-D structures with excellent surface quality and the rapid prototyping technique to achieve high fabrication efficiency.

If soft lithography is to be applied to the diamond turned mold once, such that the replica obtained will resemble the structure shown in Figure 2.2(a), an invert of that has to be diamond turned. This means two protruding ridges have to be fabricated on the diamond machining lathe, which is difficult to achieve. Shaping can only produce recessed liquid channels and not protruding ridges. As a result, the fabrication flow process is modified to have two cycles of soft lithography instead of one. In this case, the diamond turned mold will look exactly like the required structure and not the inverted structure.

2.2 Overview of Fabrication Process

Based on the example of a liquid tunable diffractive/refractive hybrid lens that can minimized chromatic aberration, the general fabrication process that has been discussed in the preceding section will be discussed in greater detailed in this section. The exact same fabrication flow can be applied to other liquid tunable lenses developed in this work, which are namely double focusing lens, aspherical lens that can reduce spherical aberration and diffractive toroidal lens that can increase the depth of focus. The only difference is the lens profile that is diamond turned on the bottom surface of each cylindrical lens cavity, which determines the different functionality of each different lens device proposed. A summary of the fabrication flow process is shown in Figure 2.3.

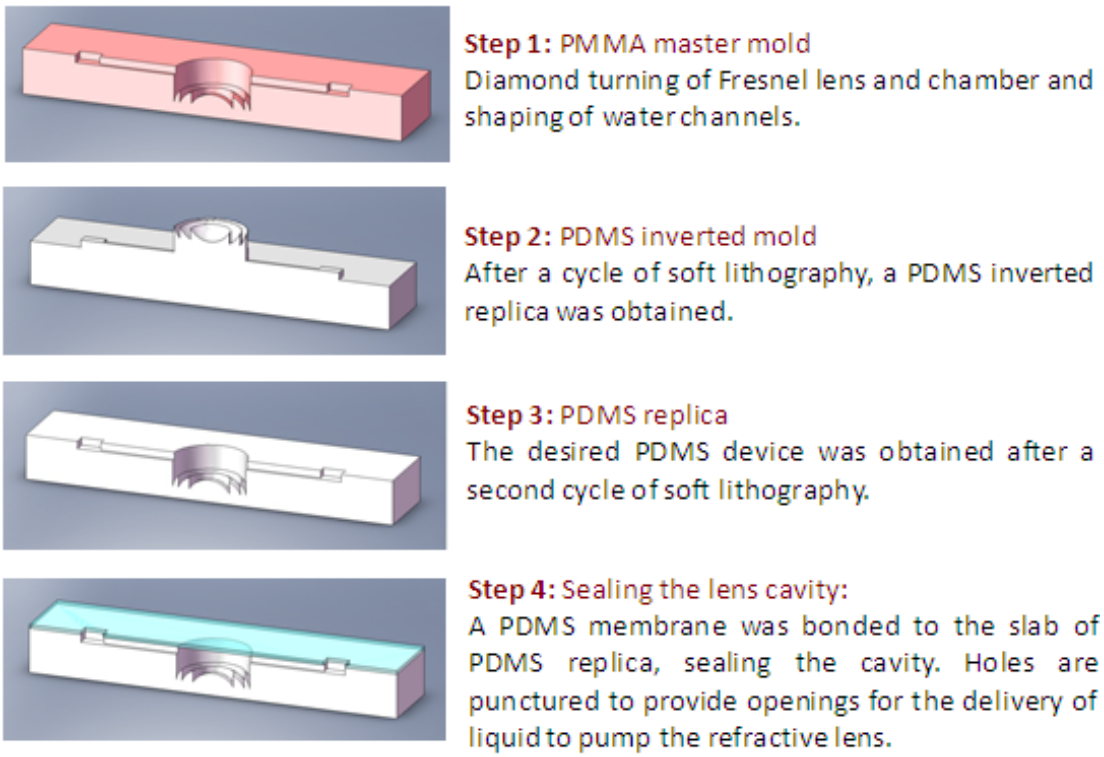

Figure 2.3: With images of the cross sections of the lens device at each stage of fabrication, the steps necessary to fabricate a liquid tunable diffractive/refractive hybrid lens are shown. This fabrication flow is common to all other liquid tunable lens devices developed in this work.

The diffractive/refractive hybrid lens is a structure that consists of parts having dimensions that range from a few microns to a few millimetres. In addition, the annular rings of the Fresnel lens have varying aspect ratios. If this kind of structure is fabricated by etching techniques, the largely varying dimensions may make process optimisation very difficult. Diamond turning easily overcomes this problem. Furthermore, in the context of this work, diamond turning is able to achieve a cutting depth of more than 700 µm and wide diameters easily. The maximum cutting depth is determined by the geometry of the desired profile and the size of the diamond tip on the cutting tool. The capability of removing large amounts of material efficiently while being able preserving high precision and surface quality makes diamond turning techniques more suitable for fabricating micro optical structures. Another notable advantage especially relevant to the hybrid lenses is that all the features to be created on the substrate are machinable consecutively on the diamond turning

machine, which implies that the features share a single machining reference point. As a result of the elimination of multiple reference point, the optical centres of the Fresnel lens and refractive lens, which is defined by the centre of the cylindrical lens cavity, are automatically aligned. This does away the need for tedious manual alignment of the two lenses. It also eliminates human error that would inevitably be introduced during manual alignment of the lenses.

2.3 Diamond Machining of Mold

With reference to Figure 2.3, each fabrication step shall be discussed in greater detail, starting from step 1. One of the most pressing issues to address at the initial stage of the project is deciding the best material to work on to provide a viable way to improve the fabrication process of diffractive optical elements. As the literature survey of the diamond turning work carried out by research teams show, there are a number of substrates that have been explored with diamond machining techniques. Depending on the applications, design and the availability of complementary fabrication tools, there are different substrate materials that can be taken into consideration. The process of arriving at the material of choice of this work shall be described.

2.3.1 Exploration of Diamond Turning on Electroless Nickel

Among the literature reviewed are a number of research works that were performed on the Toshiba-ULG-100A ultra-precision machine available in the Advance Manufacturing Laboratory in the engineering faculty of National University of Singapore. Figure 2.4 shows a photograph of the lathe and Figure 2.5 is a close-up view of the diamond tool insert and vacuum chuck that will hold a workpiece during turning process. The holder which moves the diamond tool inset has a precision of ±10 nm in the three orthogonal directions. Much extensive experimental work with

favourable results has been performed on EN (section 1.2.4). Circular micro-grooves with excellent surface roughness of 4-6 nm were reportedly turned on the EN-coated disks [26]. The material properties of EN, being a Ni-P alloy, could be changed by varying the percentage of P present. Naturally, phosphorous content is important in determining the quality of surface finish of the diamond turned product. 1-5 wt% of P is known as low-P, 5-8 wt% mid-P and above that will be high-P. In a series of experiments performed on EN-coated metal disks as reported in [48], it is suggested that EN with a phosphorous content of 9 – 10 weight % is the most ideal material for obtaining a smooth surface finish with diamond turning. These results suggest that diamond turning is able to satisfy some of the most important requirements of a micro diffractive optical element, which are, namely, a smooth surface and high machining precision to fabricate repeated patterns that have dimensions in the order of a few microns.

Figure 2.4: A photograph of the entire diamond machining lathe. On the left is the computer system where the programming codes are entered while on the right is the part of the machine which handles the cutting. That part is covered with plastic sheets and doors for safety reasons.

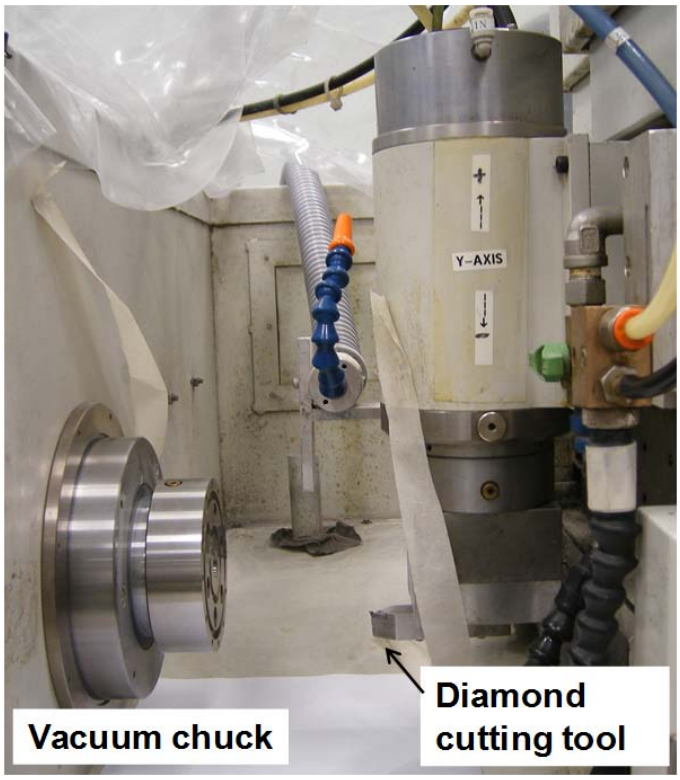

Figure 2.5: A photograph shows the vacuum chuck and the diamond cutting tool on the lathe while not in operation.

These findings led to the search for places where EN plating can be carried out. There was no available resource for such a process in the University at the period of time the work was ongoing. Thus, industrial plating services were employed. It was chosen to do EN-plating on silicon wafers instead of other metallic materials to explore the possibility of combining EN plating with conventional silicon machining processes.

Two different types of wafers were handed to the company for EN plating. One of the wafers is covered with patterned with photoresist as it would be useful to find out if it is possible to EN-coat selective areas on a silicon substrate. The other silicon wafer is clean and new. The plating rate is about 3 µm/h and therefore, it would be impractical to request a thick layer to be plated on those wafers. A 30 µm layer of EN is coated on the wafers instead.

As it turns out, the result of the EN plating was not encouraging. Firstly, the photoresist did not hold up well in the aggressive acidic salt baths. The patterns were destroyed and the plated EN coating peeled off easily, as shown in Figure 2.6. From the layer of EN that was peeled off, it was clear that the plating was not uniform and flaky. It is plain to see that it is not feasible to plate the silicon wafer on selective regions using this method.

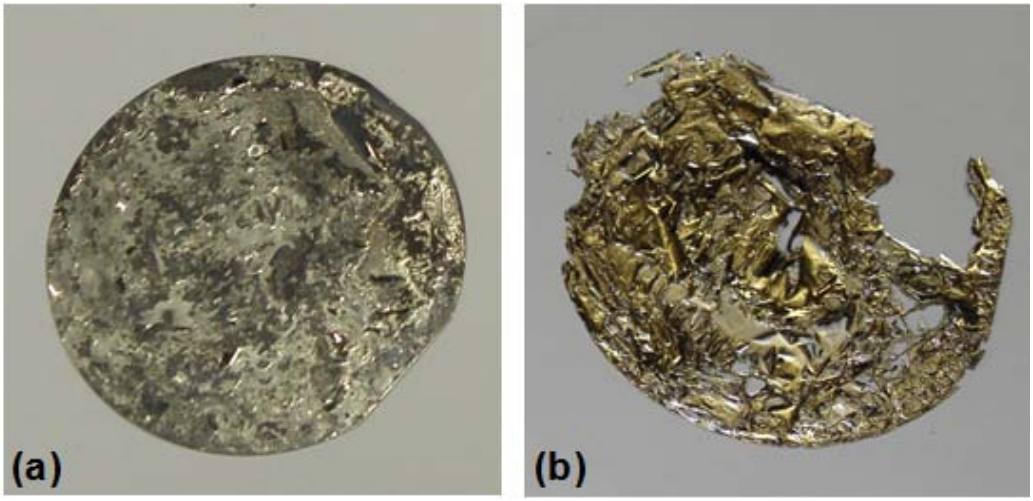

Figure 2.6: (a) A photograph of how the silicon wafter which was layered with patterned photoresist looked like after EN plating. (b) A picture of the uneven and flaky layer of EN that peeled off easily from the wafer.

In contrast, the clean wafer was EN plated much more beautifully. With unaided eyes, the surface appeared rather smooth, uniform and well-adhered to the wafer. However, under an optical microscope, there were many tiny pores on the surface which seem to suggest that the plating process was not optimised and the coating was porous. Nevertheless, a circular well of 10 µm depth was diamond turned on the EN-coated surface. 1000 rpm spindle speed, 0.5 mm/min infeed and crossfeed rate were chosen. A round-tipped diamond tool was used for the test cut and the 10 µm deep cut was done in a single cut. Images under the optical microscope verified that the layer is porous and thus, it would be impossible to obtain an optically smooth surface from such an EN layer, even with different cutting speeds. The conditions of the

surface of the EN layer before and after diamond turning are shown in Figure 2.7 (a) to (d).

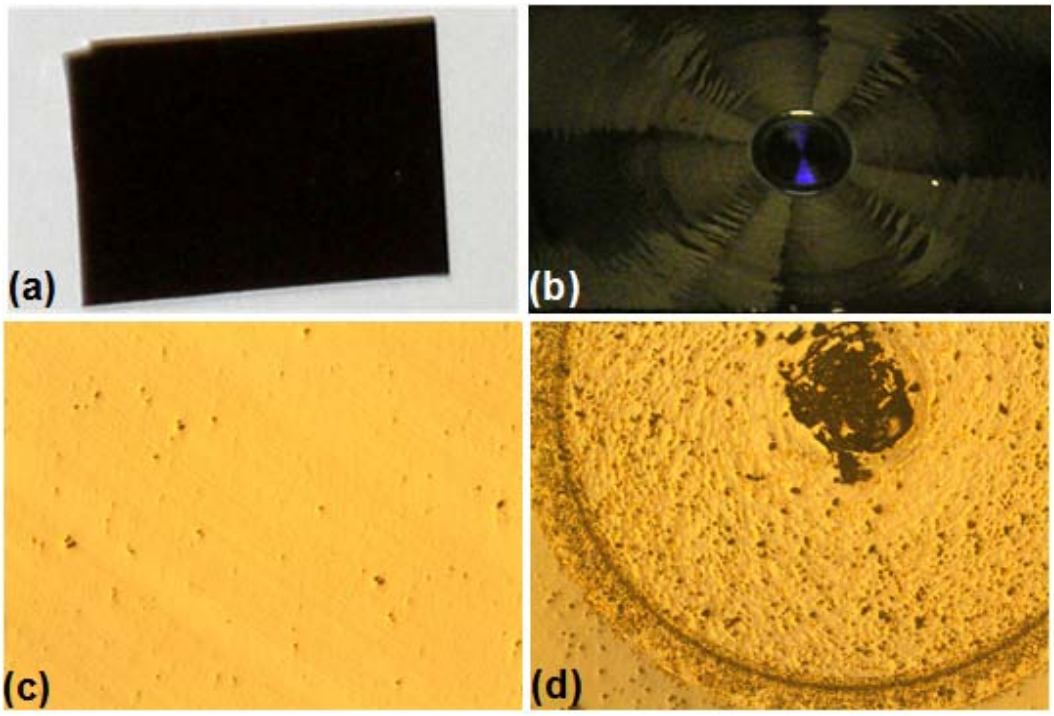

Figure 2.7: (a) The surface of a chip that was cut from an EN-plated wafer appeared rather smooth and even with unaided eyes. (b) A diamond turned surface of the EN-plated silicon chip. (c) Under an optical microscope, the surface of a diamond-trimmed EN layer shows presence of pores. (d) The EN layer is clearly porous as shown on the diamond turned profile.

It is known that the quality of plating can be improved by adding a seed layer to enhance adhesiveness. Aluminium and copper are the most commonly used seed layers for EN plating. Hence, coating the wafers with a thin layer of either metal might help reduce the undesirable porosity. It is also very likely that some of the EN plating process need to be modified to improve the compatibility with silicon material. Unfortunately, because this is an industrial process, it would be difficult to do further tests with modified process parameters or salt bath to improve the quality of EN plating on silicon wafers. Instead, alternative materials have to be explored.

2.3.2 Exploration of Diamond Turning on SU8

The next material that was explored was SU8, which is a type of photoresist that can be spin coated on silicon wafers or glass plates. The thickness of the film can be easily controlled by the spinning speed and time. It is not difficult to reach 100 µm or more of SU8 thickness. Nevertheless, like EN plated substrates, SU8 coated work pieces present their own set of problems.

SU8 is a photoresist and thus, it is sensitive to light, especially UV light. After spin coating a layer of SU8 on a clean glass plate, a UV lamp can be placed above it to expedite the curing process. During this curing process, the layer of SU8 changes from transparent to yellow. A longer exposure time results in deeper shades of yellows. Subsequently, the SU8 coated glass plate will be left overnight in an oven of 65^0C to complete the curing process. It was observed that if UV light was not used to cure the SU8 layer, so as to avoid its colour change, the photoresist takes a very long time to cure, sometimes as long as a few days. Furthermore, when taken out of the oven, the light from the surroundings changes its colour to a dark shade of yellow. At this point, it is evident that SU8 itself will not be suitable to be used as a transmissive optical element, even if diamond turning works beautifully on that substrate. However, it might still be able to act as a reflective lens surface if a reflective metal layer can be deposited on the machined surface.

Apart from the colour change, it was also observed that curing of an initially uniform layer of SU8 in the oven often resulted in the edges to be creased, as shown in Figure 2.8(a). This seems to be due to non-uniform surface tension close to the edges of the glass plates and possibly volume changes that comes from the curing process. This phenomenon is more apparent when thick layers of SU8 of more than 100 µm are spin coated.

After SU8 was fully cured, it is ready to be diamond turned. As the vacuum chuck can only hold a workpiece firmly if the surface in contact with the chuck is trimmed flat and covers the vacuum holes on the chuck completely. This requires the workpiece to be 10 cm in diameter. The glass plate is too small to be directly held by the vacuum chuck. Therefore, it has to be secured on a machined metal disk with industrial wax before being diamond turned. Since the melting point of the wax is 70^0C, the SU8 had to come in contact with the heated metal disk and wax. This triggered another round of material change in the SU8, causing it to darken visibly. After the workpiece was cooled to room temperature, it was secured on the vacuum chuck to proceed with diamond turning. A piece of diamond turned SU8-coated glass plate that is secured on a metal disk is pictured in Figure 2.8 (b).

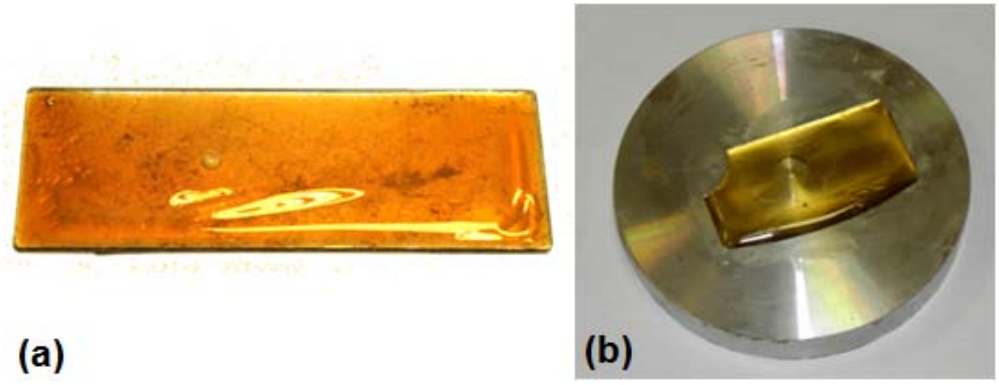

Figure 2.8: (a) Creases are evident at the borders of the cured SU8 layer on a glass plate. (b) A SU8-coated glass plate is secured on a metal disk to enable it to be held by the vacuum chuck on the diamond turning machine.

Because of the creasing on the SU8 surface, trimming has to be done to obtain a flat reference plane before turning the intended features. SU8 is a much softer material, as compared to metals. Because of this reason, a much greater depth of cut could be achieved without chipping the cutting tool. A diffractive lens with 6 µm deep blazed annular rings was turned on the SU8 layer using the same machining speeds as that used on the EN-coated wafers. Optical microscope images of the results are shown in Figure 2.9. The close up view of the blazed rings shows that the surface is far from

smooth. Minute surface tearing probably due to high local temperatures resulted in an uneven surface. It is likely that there will be significant optical loss due to the surface scattering, causing degradation of optical performance.

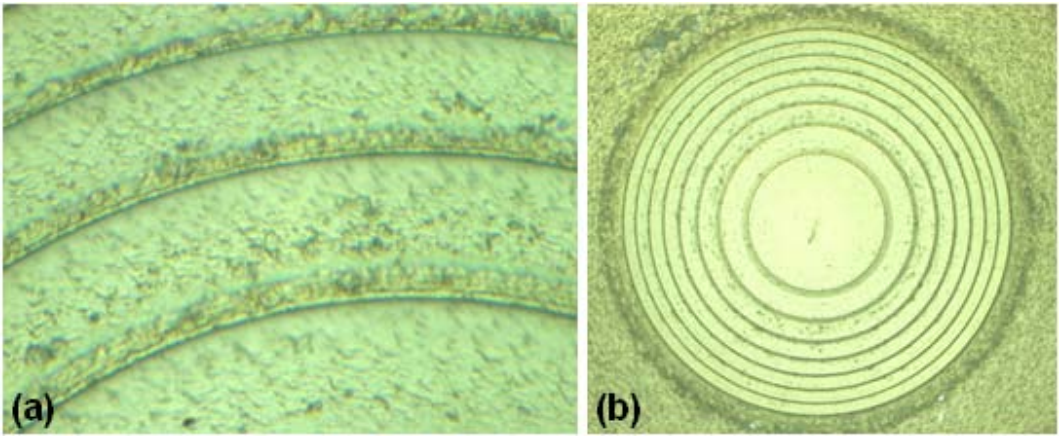

Figure 2.9: (a) A close up view of the surface of blazed annular rings diamond turned on SU8. (b) An overview of the structured which consists of eight rings.

After diamond turning, the glass plate has to be detached from the metal disk by melting the wax it was in contact with. Multiple rounds of heating and cooling, from curing in the oven to detaching of the SU8-coated glass plate on a hotplate, seemed to make SU8 turn into a brittle material. Occasionally, it would peel off from the glass plate. When that happened, the SU8 film appeared warped and it cracks easily. This is apparent in Figure 2.10 which shows SU8 films that were detached from the glass plate.

Because of the poor surface quality produced by diamond turning and the material instability to heat and light, it seems that it is not viable to diamond turning optical lenses on SU8. Its sensitivity to light makes it unsuitable as a material for transmission optical elements while the poor surface quality makes it unsuitable to act as reflective optical elements even if it can be coated with reflective metals. Although different cutting speeds could be experimented to try to improve the surface quality, not much work was continued in that direction as it is clear that the problems

of peeling and developing uneven surfaces after curing are not easy to overcome. Thus, it would be better to explore other materials instead of solely experimenting with SU8.

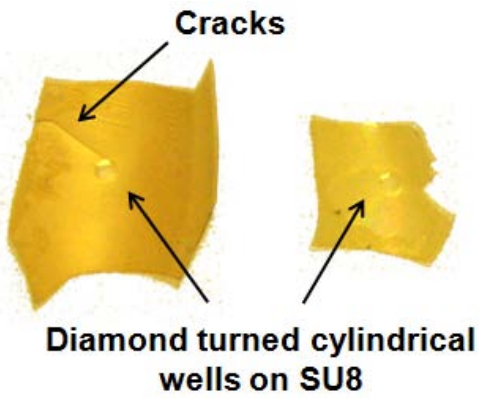

Figure 2.10: Pieces of diamond turned SU8 came detached easily from glass plates. They appear warped, brittle and cracked.

2.3.3 Exploration of Diamond Turning on PMMA

While experiments with SU8 were ongoing, alternatives were being explored as well. As mentioned in the literature review, a few research teams have done diamond turning on PMMA pieces with favourable results achieved. And since PMMA is affordable and accessible, diamond turning was tested on PMMA pieces, too. To avoid having to heat up the PMMA pieces to stick it to a bigger disk with wax and risk warping it, 10 cm diameter, 3 mm thick PMMA plates are purchased. Upon purchase, they are already machined flat and smooth on both sides, making them easy to be held firmly on the vacuum chuck of the diamond turning machine. In this sense, PMMA can be handled much more easily than SU8.

Starting with the machining parameters used for earlier works with EN and SU8, the resulting surface was visibly rough. After trying diamond turning with different work parameters, it was found that a smooth surface was producible with a small feed rate

of 0.1 mm/min, a small depth of cut of 5 μm and a high turning speed of 1000 rpm. The surface that was turned could be so smooth that, with unaided eye, it appeared to be just as transparent as the uncut regions, free of cracks that often give PMMA its white translucent appearance. Due to its high transparency, pictures of the diamond turned PMMA plates were not taken.

After finding out a suitable set of machining parameters could be used to obtain a smooth optical surface on PMMA, the material is selected to be the most suitable mold material for diamond machining to take place on. The same parameters could be used to obtain different types of PMMA molds with different integrated lens profiles.

2.3.4 Discussion of Selection of Tool Tip and Machining Processes

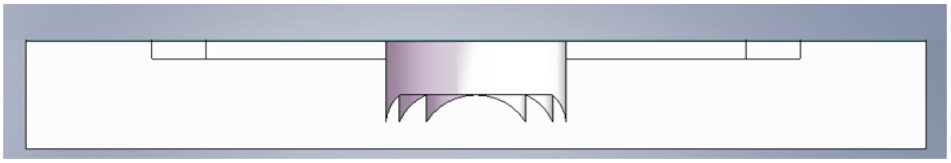

Figure 2.11: The cross-section of the device to be diamond machined on a PMMA substrate.

From Figure 2.11, it is apparent that diamond machining needs to produce vertical walls as well as slopes of varying gradient. Thus, the diamond cutter must be selected to such that its geometry is compatible with the cutting of such a profile. It is known that the efficiency of the Fresnel lens decreases if the edges of the zone rings are not sharp. If round-tipped cutters are used, the rounded corners results in shadowed regions which lowers efficiency [49]. Considering that and the fact that the angles of the slopes on the Fresnel lens are smaller than 45^0, a cutting tool with a 0^0-

45^0 facet-cut single crystalline diamond tip is a suitable choice. It is purchased from Osaka Diamond Industrial Co., Ltd at a price of S$495. An image of the tip of the diamond tool is shown in Figure 2.12. A Toshiba-ULG-100A ultra-precision machine, which has a repeatability of ±10 nm, was used to fabricate all the devices in this work.

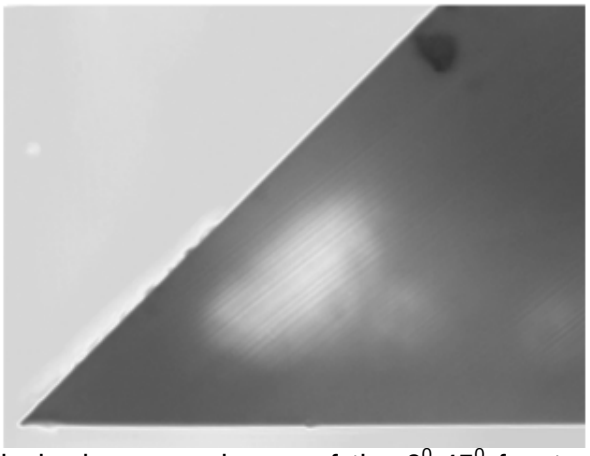

Figure 2.12: An optical microscope image of the 0^0-45^0 facet-cut single crystalline diamond tool tip.

After selecting the suitable workpiece material and the cutting tool, a computer numerical controlled (CNC) program needs to be generated. That requires the generation of data points of the profile which are simply the Cartesian positions of any point on the profile. The cutting tool will move linearly between each data point provided. Although, in principle, these discrete data points could only produce an approximate continuous profile which is a result of many small linear cutting motions, the quality of the device could still be excellent if sufficiently dense data points are entered for non-linear regions of the profile.

In addition to entering programs to define the cutting paths, other machining parameters need to be defined, too. Two different cutting procedures are required to fabricate the lens system on a PMMA plate, namely turning and shaping. The cutting

parameters for each of those procedures have to be chosen with care so as to be able to achieve good surface quality while preserving the tool's life.

The most important parameters include infeed rate, cross feed rate, spindle speed and depth of cut. The chosen parameters are tabulated Table 2.1**.**

Table 2.1: Cutting parameters used for the fabrication of all the devices in this work.

	Infeed rate (mm/min)	**Crossfeed rate (mm/min)**	**Spindle speed (rpm)**	**Depth of cut (µm)**
Turning	5	5.0 (for rough cut) 0.1 (for final cut)	1000	5
Shaping	150	150.0	0	5

Turning process is used to fabricate a deep lens cavity and the Fresnel lens profile at the bottom face of it. The well is approximately 150 µm deep and therefore, it is not possible to cut the entire structure in a single plunge-cut procedure without damaging the diamond tip. Considering that PMMA has a surface Vickers hardness of approximately 280HV and the diamond tip is a 45^0 sharp tip that can chip easily, the depth of cut was maintained at 5 µm. The bigger the depth of cut, the more stress load imposed on the diamond tip and the more likely it is damaged prematurely. To prevent that from happening, the lens cavity is cut in steps, each time removing a layer of 5µm of material. This depth is also referred to as depth of cut. This process repeats itself until the entire lens cavity is cut out. An illustration of the progressive cutting is shown in Figure 2.13.

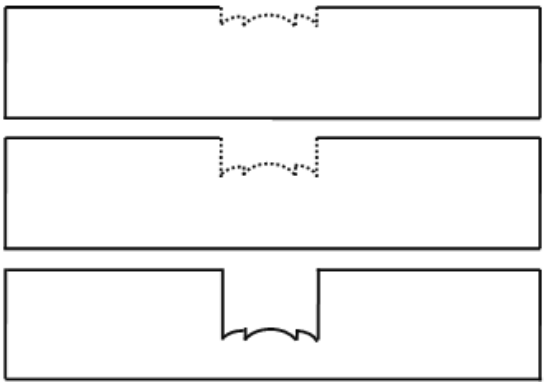

Figure 2.13: The features of the device are cut progressively in steps of 5 µm until the desired depth is reached.

A slow crossfeed rate is necessary to achieve a good surface finish. For optical purposes, a satisfactory surface finish can be obtained when the crossfeed rate of 0.1 mm/min was used to the profiles of the Fresnel lens and the cavity which they were recessed in. However, because the surface finish depends only on the final cutting step of the repetitive cutting cycle, the crossfeed rate was set to be 0.1 mm/min only for the last cut while it could be set at a much higher speed of 5 mm/min for preceding steps. This helped to reduce machining time and to speed up the fabrication process. To ensure good surface quality, a low crossfeed rate has to couple with a high spindle speed as both conditions are essential in producing a glossy and smooth surface finish. For this reason, 1000 rpm spindle speed was used.

In contrast to the lens surface, there was no requirement for the surface finish of the water channels since their sole purpose was to transport fluid to the lens chamber. Therefore, even if the high crossfeed rate of 150 mm/min during shaping process caused the walls of the water channels to be very rough, it was an acceptable speed. Moreover, the high speed did not do perceptible damage to the diamond tool tip, partly because the depth of cut was merely 5 µm.

As opposed to crossfeed rate, the infeed rate does not have a significant effect on the surface finish and they are chosen to be 5 µm/min and 150 µm/min for turning and shaping processes respectively.

Before the diamond machining process commences, precise zero-point referencing of the cutting tool with respect to the workpiece is required because subsequent cutting paths relies on this reference point. Thus, this step is crucial in ensuring the accuracy of the dimensions of the device being machined.

After zero-point referencing, the lens cavity with Fresnel lens profile at the bottom surface is diamond turned using the machining parameters stated in Table 2.1. When that is completed, the chuck stops rotating and the shaping of the liquid channels starts immediately after. It should be noted that since turning and shaping commenced one after the other without releasing of the workpiece from the vacuum chuck, they share the same machining referencing point. Similar to the turning of lens cavity, the two liquid channels are shaped in steps of 5 µm until the desired depths have been reached. Shaping allows non-axis-symmetric rectangular features to be produced on the diamond turning lathe.

When the fabrication of lens cavity and liquid channels on the diamond cutting lathe is completed, the PMMA workpiece is released from the chuck. A photograph of a completed PMMA mold is shown in Figure 2.14. After cleaning with water-diluted alcohol and isopropyl alcohol (IPA), the PMMA plate is ready to be used as the master mold for subsequent soft lithography processes. PDMS is the choice material for soft lithography processes because it has good optical transmission properties over a wide spectral range, from near ultraviolet to near infrared. Soft lithography processes are performed in a 100 k cleanroom. A clean environment prevents impurities from impairing the quality of the lens materials during fabrication.

Figure 2.14: A photograph of a diamond turned lens and two shaped liquid channels on a piece of clear PMMA plate.

2.4 Soft Lithography

To prepare for soft lithography in step 2, PDMS pre-polymer is first prepared using Dow Corning Corp's Sylgard 184 silicone elastomer by mixing the base and curing agent in a 10:1 volume ratio. The curing agent has a Pt based catalyst that adds the SiH bonds across the vinyl groups forming Si-CH2-CH2-Si linkages necessary for solidification. After thorough mixing, the mixture is degassed in a desiccator and poured onto the PMMA master mould that had been cleaned with diluted isopropyl alcohol (IPA) beforehand. The pre-polymer was then placed in an oven for a minimum of 2 hours where it was fully cured at approximately 65 ^{0}C. With the help of a little IPA, the inverse master mould was released from the PMMA substrate.

It is commonly known that PDMS shrinks upon curing. This could lead to distortion of surface profile which is detrimental to the performance of the end product. Although the actual dynamics of this is not thoroughly understood, there are a number of research work done to obtain the empirical relationship between PDMS shrinkage and a number of process parameters during curing of PDMS, such as the thickness of PDMS, mixing ratio of base and curing agent, baking temperature and baking time

[50-52]. Since the PDMS inverted mold has a certain required thickness, what could be controlled to enhance the fidelity of the soft lithography process are the selection of mixing ratio and baking temperature while the baking time has to be selected appropriately according to those two parameters. Generally, a lower baking temperature and mixing ratio would result in minimal shrinkage [50]. Because of this, the baking temperature is set to be 65^0C such that it can be fully cured in a reasonably short period of two hours. Furthermore, the percentage shrinkage for devices with sizes that are in the range of millimetres is typically about 1 to 2%. Thus, with the set of parameters used for this work, soft lithography is expected to be of high reliability and the surface profile would not be significantly degraded. This is verified in the later section of experimental results.

Subsequently in step 3 of the fabrication process, a new volume of pre-polymer that is prepared in the same way as abovementioned is poured onto the fully cured inverse PDMS master mould. However, this pre-polymer was released after curing in the oven for 30 minutes, instead of the minimum 2 hours required for complete curing. Although the pre-polymer has not completely cured after 30 minutes, it has solidified and would retain its shape even after its release from the PDMS mold. The main reason for the early release of the PDMS lens device from the PDMS mold is to prevent the two from forming strong bonds at the contact surface. Not only will that hinder the release, forcefully separating the two would compromise the surface quality. After releasing, the semi-cured PDMS device will be returned to the oven to allow it to cure to completion.

2.5 Oxygen Plasma Bonding

In step 4, a thin PDMS diaphragm has to be bonded to the PDMS structure fabricated in step 3. Since the PDMS film has to deform under a uniform liquid

pressure, the mechanical properties of PDMS prepared in the manner would be of interest. Some important mechanical characteristics of PDMS are tabulated in Table 2.2. The values given in the table are only valid for PDMS that is produced by mixing ratio of 10:1. Other mixing ratios will result in different mechanical characteristics.

Table 2.2: Physical properties of fully cured PDMS that is produced by mixing elastomer and curing agent in a 10:1 volume ratio.

Physical Properties of PDMS		
Young's Modulus (MPa)	**Poisson Ratio**	**Refractive Index**
3	0.49	1.41

The diaphragm has to be prepared separately on a silicon wafer. A small amount of degassed pre-polymer is spin-coated on a silicon wafer at a speed of 1000 rpm for a minute. The spinning speed of 1000 rpm typically produces a film of about 70 µm to be deposited. The higher the spinning speed, the thinner the resulting PDMS film. After making sure the layer of PDMS is free of unevenness or air bubbles, it is transferred to an oven to cure. After complete curing, the film will be ready to be bonded to the PDMS structure fabricated earlier.

Oxygen plasma process replaces the hydrophobic methyl groups (-CH3) on PDMS surface with hydrophilic hydroxyl groups (-OH). Upon contact between two plasma-treated surfaces, condensation reaction results in the formation of –Si-O-Si- bond. That reaction leads to permanent bonding between the processed PDMS surfaces under elevated temperatures. Similarly, oxygen plasma enables bonding between PDMS and glass surfaces. That is the general principle of oxygen plasma which is used to bond the PDMS film and blocks of liquid tubes holders to the PDMS structure, and subsequently, the structure to a thin glass plate. The plasma-bonded structures

need to be kept in the oven for at least two hours to facilitate the chemical reaction and to ensure tight bonding. With this, the fabrication of the tunable Fresnel lens is complete.

Having thoroughly described the fabrication process, the focus now turns to the design and experimental testing of each liquid tunable microlens fabricated.

Chapter 3. Liquid Tunable Diffractive/Refractive Hybrid Lens

3.1 Introduction to Diffractive Optical Elements and Achromatism

Diffractive optical elements (DOE) introduce controlled phase delay on an incoming optical wavefront. By fabricating a surface relief with varying surface height to control the optical path delay introduced at each point on the DOE, the phase distribution across the wavefront that reaches the DOE could be modified. Potentially, it could engineer any arbitrary wavefront from an incoming source with this method. With the engineering of optical wavefronts comes the possibility of transforming light into complex patterns and manipulating optical paths. This has an immense application potential in many fields of technologies. DOE are also valued for their high focal depth. However, as compared to refractive lenses, diffractive lenses have lower diffraction efficiency because a large portion of incident light either goes to the undiffracted 0^{th} order or higher diffraction orders. This leaves little optical power in the first diffraction order, the order that is to be utilized in most applications. Neverthless, DOE are indispensible in modern technologies. The following are few examples of the applications of DOE.

- Diffraction grating is a spectral dispersion element that can be used in spectrometers. There are ruled and holographic diffraction gratings. Ruled diffraction gratings can be fabricated with the use of RIE or DRIE and the resolution depends on the patterned mask used. On the other hand, holographic diffraction gratings are produced by recording the interference patterns of two light beams on a suitable photoresist. Generally, the resolution is superior to RIE/DRIE etching methods.

- Many MEMS-based optical scanners use diffraction gratings as the scanning component. Out-of-plane scanners are limited to low frequency scanning due to mechanical deformation at high speeds while in-plane scanners are able to avoid that problem [53].
- Fresnel zone plates and Fresnel lenses are diffractive focusing optical elements often used on laser light. Among numerous applications, this functionality is important in input/output signal processing devices, x-ray optics integrated in synchrotron light facilities and in medical instruments that are used in micro-surgery [10, 30, 54-56].

The widespread usage of DOE in optical systems that can be integrated in many commercial products indicates its versatility to take a large range of designs that best suit the needs of the applications. However, emphasis will be given to focusing Fresnel lenses because it is part of the design of the liquid tunable diffractive/refractive lens hybrid lens to be discussed in later parts of section 3.1.

Fresnel lens has a unique property of having strong negative dispersion qualities. Dispersion is a wavelength-dependent phenomenon that leads to light of different wavelengths to be refracted at different angles, implying a material's refractive index to be wavelength-dependent as well. Because of this, the focal lengths of light are different for different wavelengths, giving rise to what is known as longitudinal chromatic aberration. This phenomenon impairs an optical system's imaging qualities and thus, achromatic condition, a state where chromatic aberration is cancelled, is desirable.

Qualitatively speaking, an optical element which bends light of a longer wavelength more than light of a shorter wavelength is said to have positive dispersion and vice versa. In both cases of positive and negative dispersion, there is chromatic

aberration due to the different focal spots of light of different wavelength. This phenomenon is illustrated in Figure 3.1. Abbe number is a measure of a material's dispersion properties. Thus, lens made of different material with different Abbe number will have different dispersion strengths.

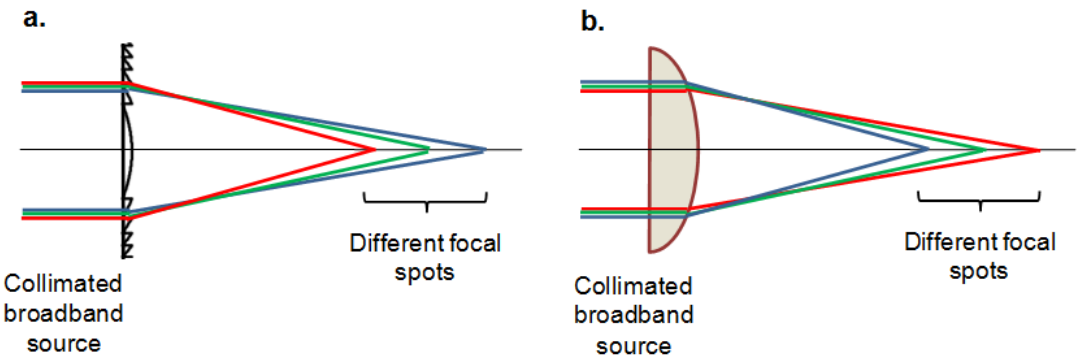

Figure 3.1: (a) Diffractive Fresnel lens has negative dispersion and red light focuses closer to the lens than blue light. (b) Refractive lens has positive dispersion and red light focuses further away from the lens than blue light. The different focal spot of different wavelength along the optical axis constitutes longitudinal chromatic aberration.

To achieve achromatic condition for two designated wavelengths, the following condition must be satisfied [57]:

$$\sum_{i=0}^{n} \frac{1}{f_i V_i} = \sum_{i=0}^{n} \frac{\phi_i}{V_i} = 0 \tag{1}$$

where f is the focal length, Φ is the power, and V is the Abbe number of the lens.

We can infer from the equation that there are basically two properties of lenses which we can exploit to create an achromatic optical system. By noting that conversion and diverging lenses have focal power of opposite signs, appropriate assembly of these

two types of lenses could lead to minimized chromatic aberration at the two wavelengths of interest.

Alternatively, optical elements with opposite signs of Abbe number could be coupled in a system to cancel chromatic aberration. This is when the unique property of Fresnel lens' negative dispersion qualities is useful in negating the positive dispersive power of refractive lenses. It should be noted that the Abbe numbers of refractive lenses are material dependent and it is always positive in the visible wavelength. Contrastingly, the Abbe number of diffractive Fresnel lens is independent of its material and it is negative.

Very often, lenses with different focal power and composed of materials with different Abbe number are used to create an optimised achromatic optical system. For example, a doublet comprising 1.) a high power converging lens with large Abbe number and 2.) a low power diverging lens with small Abbe number is often used to correct chromatic aberration for 2 colors. Crown glass (V ~75) and flint glass (V ~25) could be used for such a purpose. A pictorial representation of an achromatic doublet is shown in Figure 3.2.

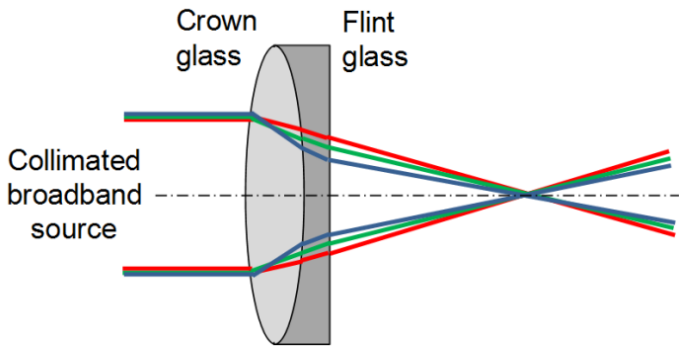

Figure 3.2: An achromatic doublet that comprises a crown glass convex lens and a flint glass plano-concave lens.

Apart from satisfying the achromatic condition, there is another important consideration in a lens design, which is the total power of the lens system. Assuming that (n+1) thin lenses are in contact, the total power of the system can be expressed mathematically as:

$$\sum_{i=0}^{n} \frac{1}{f_i} = \sum_{i=0}^{n} \phi_i \; = \; \phi_{desired} \tag{2}$$

Assuming two lenses are used in a certain achromat and solving equations Eqs. **(1)** and **(2)**,

$$\phi_1 = \frac{V_1}{V_1 - V_2} \, \phi_{desired} \tag{3}$$

$$\phi_2 = \frac{V_2}{V_2 - V_1} \, \phi_{desired} \tag{4}$$

Conventional lens, which is a simple refractive lens, always have a positive Abbe number. Therefore, considering Eq. **(1)**, if only refractive lenses are used, both converging ($\phi > 0$) and diverging ($\phi < 0$) lens are required to form a conventional achromat.

On the other hand, the Abbe number of a diffractive lens is negative. Thus, both the diffractive and refractive lens elements in a hybrid doublet can have positive optical power to cancel chromatic aberration. As a result, considering Eqs. (3) and (4), the

power of the diffractive and refractive lens elements are lower than the total required power of the system. Following that is a reduction in radius of curvatures, size, weight and cost of production. It makes it easier to miniaturize optical systems and put to commercial use.

What has been outlined is a simplified methodology in designing an achromat that is able to cancel chromatic aberration at two different wavelengths. This means, theoretically, the focuses of the two designated wavelengths is at an exact spot while the focus of nearby wavelengths differs slightly. Nevertheless, the chromatic aberration within that range is reduced as a result.

It is not possible to completely cancel chromatic aberration for the entire spectrum. However, the achromatism could be improved with designs that cancel chromatic aberration at three or more wavelengths. This would require a triplet achromat or more complex optical systems. Those designs are not within the scope of discussion in this work.

3.2 Calculations and Design of Liquid Tunable Diffractive/Refractive Hybrid Lens

The main objective of the design of the proposed liquid tunable diffractive/refractive lens is to produce a compact achromat that can cancel longitudinal chromatic aberration at two different wavelengths at a certain focal point. It should also be easily tunable over a large focusing range.

An overview of the device is shown in Figure 3.3(a). The tunable double lens consists of two parts, namely 1.) a thick PDMS substrate which houses a cavity with a double lens profile at the bottom surface and two liquid channels and 2.) a thin PDMS

diaphragm bonded on top of the substrate that seals the lens cavity. As distilled water, the chosen working liquid in this work, is delivered through the liquid inlet, it fills the lens cavity and exits through the liquid outlet. After the lens cavity is fully filled with no trapped air bubbles, the liquid outlet will be closed and subsequent injection or extraction of water will be done through the inlet. As water is injected, it will eventually cause the diaphragm to deform elastically into a spherical dome shape. This constitutes the tunable refractive lens. Its diameter is defined by the circumference of the lens cavity and the degree of deformation is dependent on the amount of liquid pressure exerted. As the curvature of the refractive lens changes, the focuses of the hybrid lens changes simultaneously. This design of liquid tunable lenses enables achromatization with only a single liquid. This greatly reduces the complexity of the lens setup and fluid control system, thereby offering significant cost savings. The entire lens device, apart from the liquid tubes, is made of PDMS because of its excellent optical transmission properties. Thus, light can be transmitted easily, even if the PDMS substrate is thick. The approximate dimensions of the lens device are given in a cross-sectional diagram in Figure 3.3 (b).

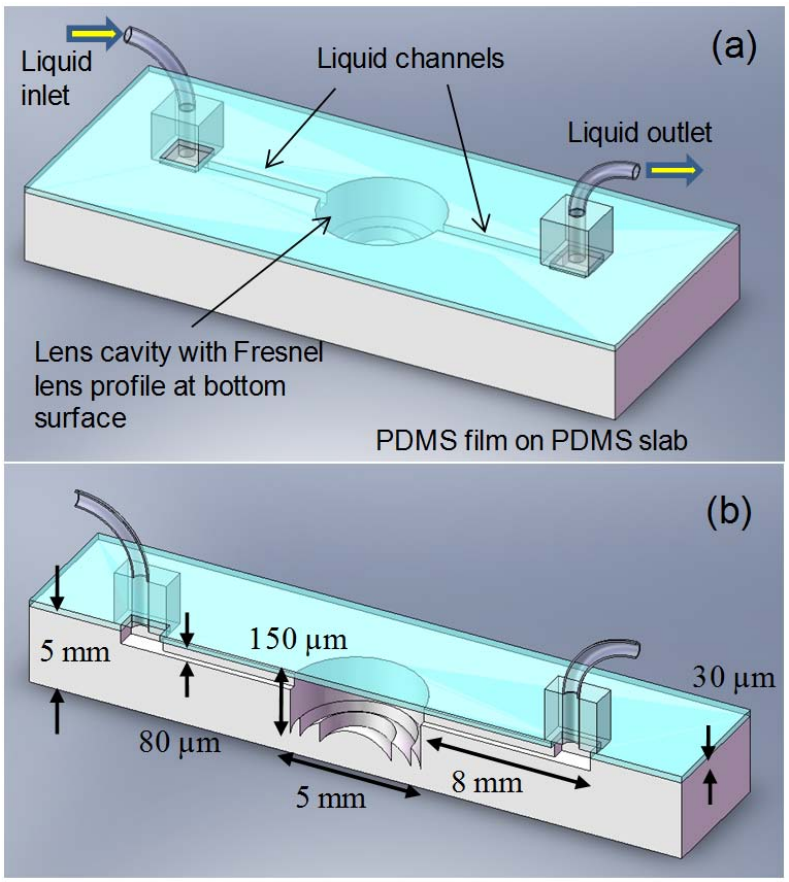

Figure 3.3: (a) An overview of the liquid tunable diffractive/refractive hybrid lens device at non-operating state. (b) General dimensions of the device are given on the mid cross-sectional view.

In the initial step of designing the hybrid lens, the dispersion characteristics of distilled water, which is the material of the refractive lens, have to be studied.

The dispersion characteristic of distilled water could be describe by the empirical Sellmeier equation [58],

$$n^2 = 1 + \frac{C_1\lambda^2}{\lambda^2 - C_2} + \frac{C_3\lambda^2}{\lambda^2 - C_4} + \frac{C_5\lambda^2}{\lambda^2 - C_6} + \frac{C_7\lambda^2}{\lambda^2 - C_8} \quad (5)$$

where λ is the wavelength of light, *n* the refractive index and C the various constants.

At a temperature of 20 ^{0}C, the constants are as follow,

C_1 = 5.684027565 E-1

C_2 = 5.101829712 E-3

C_3 = 1.726177391 E-1

C_4 = 1.821153936 E-2

C_5 = 2.086189578 E-2

C_6 = 2.620722293 E-2

C_7 = 1.130748688 E-1

C_8 = 1.069792721 E1

With these figures, the dispersion graph can be plotted.

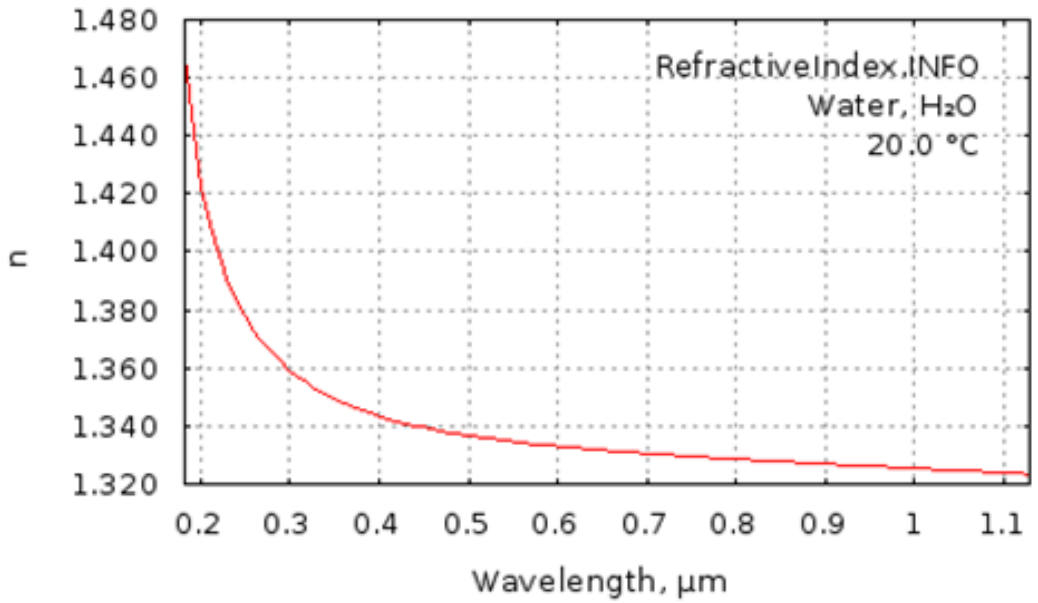

Figure 3.4: Graph of refractive index against wavelength shows the dispersion characteristics of distilled water at 20^{0}C.

Next, the most suitable overall Fraunhofer D line (λ = 589.2 nm) focal length of the hybrid lens has to be determined by looking at how the focal lengths vary within the range of wavelengths during operation of the hybrid lens. The visible spectrum (λ = 400 nm to λ = 700 nm), will be the spectrum of interest.

Let the overall D line focal length of the hybrid lens be denoted as $f_{desired}$.

[58] Abbe number of Fresnel lens, $V_{diff} = -3.452$.

[58] Abbe number of distilled water, $V_{refracti\ ve} = 55.74$.

From Eqs. (3) and (4), the focal lengths of the diffractive and refractive lens element of the hybrid lens at D line could be calculated as follow:

$$f_{diff\ ,D\ line} = \left(1 - \frac{V_{refractive}}{V_{diff}}\right) f_{desired} \tag{6}$$

$$f_{refractive\ ,D\ line} = \left(1 - \frac{V_{diff}}{V_{refractive}}\right) f_{desired} \tag{7}$$

Subsequently, using Sellmeier equation given in (5), the focal lengths of the diffractive and refractive lens element of the hybrid lens at any wavelength could be calculated.

$$f_{diff\ ,\lambda} = \left(\frac{\lambda_{D\ line}}{\lambda}\right) f_{diff\ ,D\ line} \tag{8}$$

$$f_{refractive\ ,\lambda} = \left(\frac{n_{water\ ,D\ line} - 1}{n_{water\ ,\lambda} - 1}\right) f_{refractive\ ,D\ line} \tag{9}$$

Since the thicknesses of the lenses are small compared to the focal length, thin lens approximation can be used to calculate the resultant focal length of the hybrid lens at a certain wavelength.

$$\frac{1}{f_{hybrid\ ,\lambda}} = \frac{1}{f_{diff\ ,\lambda}} + \frac{1}{f_{refractive\ ,\lambda}} \tag{10}$$

Having established the mathematical relationship between focal length of the hybrid lens and wavelength, the next step would be to do a similar calculation for the focal length of a conventional single refractive lens.

$$f_{single\ \ lens\ ,\lambda} = \left(\frac{n_{water\ ,D\ line} - 1}{n_{water\ ,\lambda} - 1}\right) f_{desired} \tag{11}$$

After comparing the wavelength-dependence characteristics of a hybrid lens and a conventional refractive lens, it is found that the design is optimal if the overall D line focal length of the hybrid lens is at 15 mm. The graphical representations of the results are given in Figure 3.5.

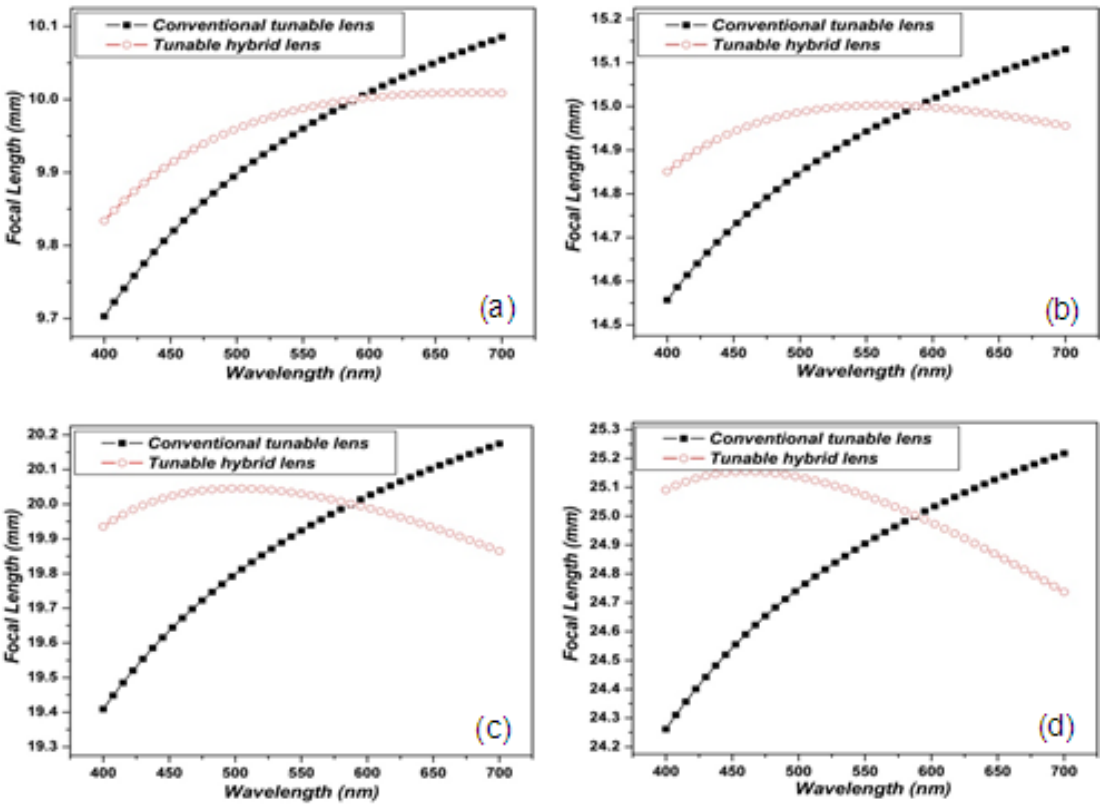

Figure 3.5: A graph of focal length against wavelength for a hybrid lens and a conventional single refractive lens at (a) 10 mm, (b) 15 mm, (c) 20 mm, (d) 25 mm D line focal length.

Based on the calculations above, some of the parameters of the hybrid lens are set.

- Overall D line focal length of the hybrid lens, $\frac{1}{\phi_{desired}} = 15.0\ \text{mm}.$
- $f_{diff} = \frac{1}{\phi_{diff}} = 257\ mm$
- $f_{refractive} = \frac{1}{\phi_{refractive}} = 15.9\ mm$

This means that if the Fresnel lens is designed to have a focal length of 257 mm and when distilled water is pumped in to obtain a refractive lens of focal length 15.9 mm,

the hybrid lens will be able to cancel out chromatic aberration at two wavelengths, namely 486.1 nm and 656.3 nm, which are the Fraunhofer F and C lines respectively.

Subsequently, the dimensions of zone rings of the Fresnel lens have to be calculated based on the selected focal length of 257 mm and source wavelength of 589.2 nm (Fraunhofer D line).

In the calculations, the following symbols are used:

λ = source wavelength

n_{pdms} = refractive index of PDMS = 1.41

n_w = refractive index of distilled water = 1.33

n_{air} = refractive index of air = 1

h_o = height of the edges of the zone rings of the Fresnel lens

h = profile height within the zone rings

m = Fresnel zone number

f = focal length of diffractive lens

r = distance from a point of the surface relief of the diffractive lens to the focal point

R_m = radius of the zone ring of a certain zone number

For constructive interference, the optical path lengths (OPL) of light that crosses the diffractive element must have a difference of 2π. Therefore, to calculate the height of the Fresnel rings, the aforementioned principle about OPL is applied at the edge of each zone rings and the center of the lens.

$$\frac{2\pi}{\lambda}\left(n_{pdms} - n_w\right)h_o = 2\pi \tag{12}$$

➔ $h_o = \frac{\lambda}{n_{pdms} - n_w} = 7.365\,\mu m$

The width of the zone rings of the Fresnel lens varies across the diameter and the radius of those zone rings have to be calculated. Since the optical path difference of the optical rays from the outer edges of adjacent annular rings to the focal point has to be a multiple of the wavelength to enable constructive interference, we obtain the following equations.

$$\left[\left({R_m}^2 + f^2\right)^{1/2} - f\right] n_{air} = m\lambda$$

➔ $R_m = \left(\frac{2mf\lambda}{n_{air}}\right)^{1/2} = (2mf\lambda)^{1/2}$ (13)

The radius of curvatures of the annular rings of the diffractive Fresnel lens within each annular ring is calculated by the radius of curvature of an equivalent spherical lens that has a focal length of 257 mm. The mathematical relationship between the radius of curvature of the spherical lens, R, and the required focal length can be expressed as

$$f = \frac{n_{air}}{n_{pdms} - n_{air}}\, R \quad (14)$$

A representative zoom-in view of the resultant Fresnel lens showing just the first 4 zone rings are shown in Figure 3.6.

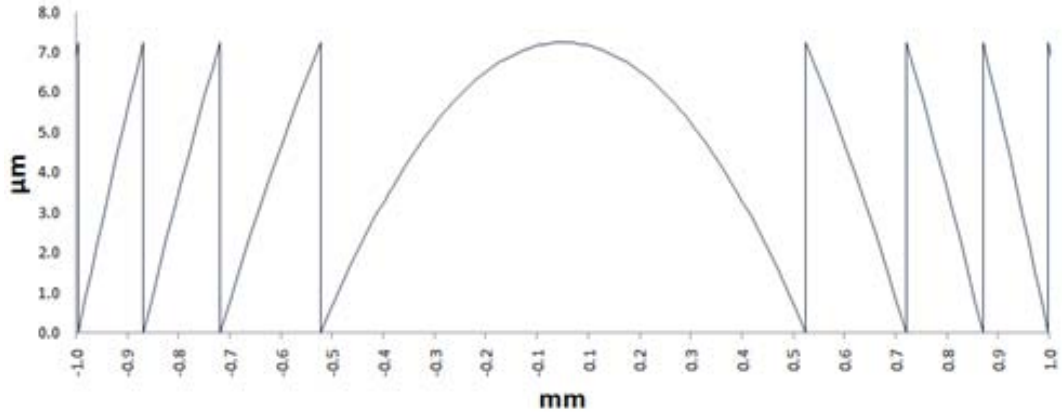

Figure 3.6: An enlarged view of the first four zone rings.

The lens cavity determines the number of Fresnel zone rings that can be accommodated and the diameter of the refractive lens. The separation between the Fresnel lens and the refractive lens is about 150 µm, which is the depth of the lens cavity. The water channels are 80 µm wide. They have to be kept sufficiently narrow to minimize the effect they have on the boundary conditions of the refractive lens and ensure the elastic deformation of the PDMS film remains spherical.

3.3 Experiments and Results: Testing of Surface Quality with AFM and White Light Interferometry

The surface condition of the tunable hybrid lens is a big factor in determining its optical performance. When an optical component has a surface roughness that is comparable to the wavelength of the incident light which it operates with, the optical performance will be significantly impaired as the surface variations interferes with the propagation of light in an undesirable way. Therefore, it is important to investigate the surface conditions of the diamond turned PMMA master mold and the PDMS devices, especially after two cycles of soft lithography. Atomic force microscopy (AFM) is used to obtain local surface roughness for a small area that spans only 10 x 10 μm^2 while white light interferometry is used to obtain an accurate surface profile of more than half the area of the Fresnel lens.

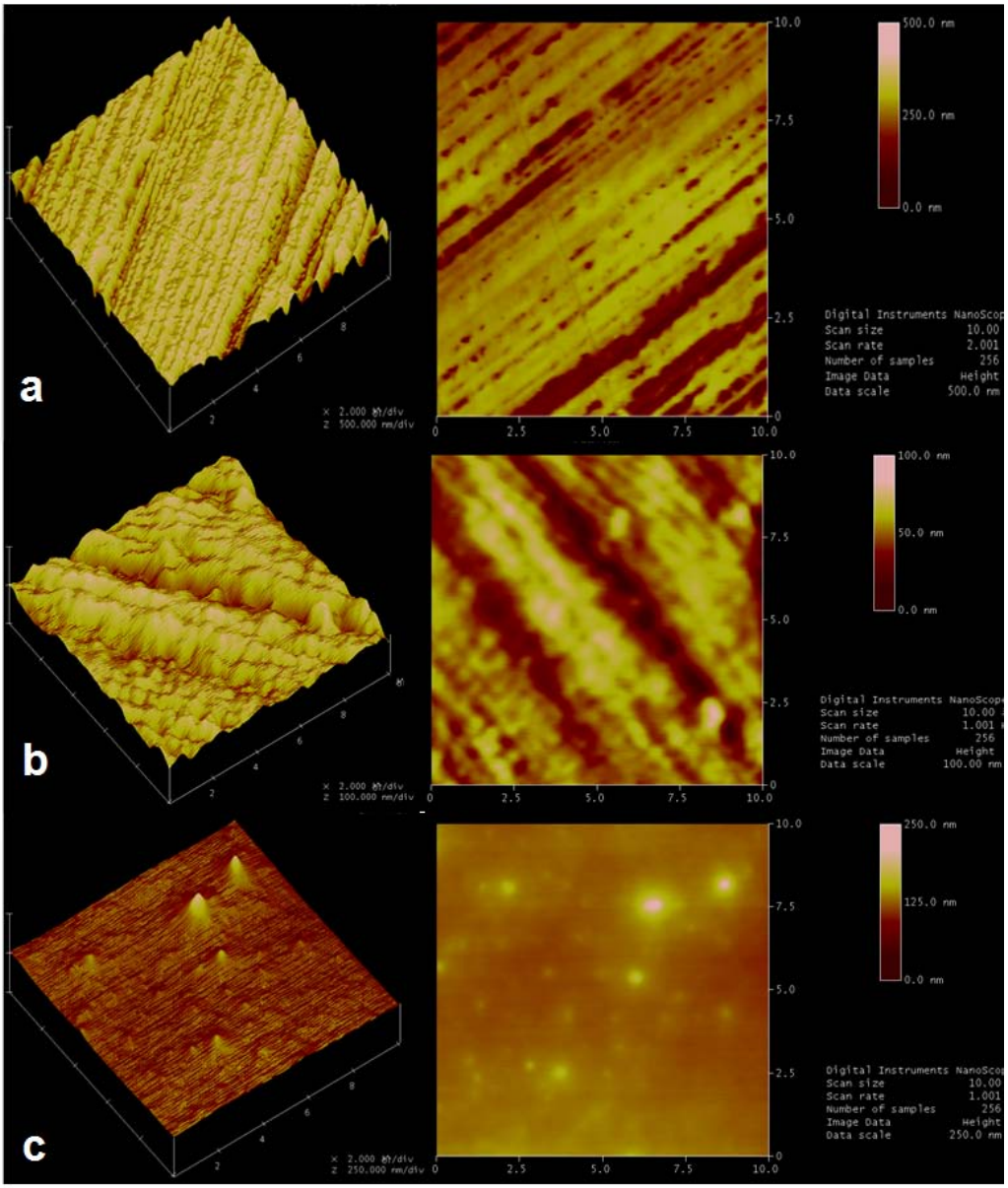

Figure 3.7: 3- and 2-D AFM images of the surfaces of a (a) diamond turned PMMA master mold, (b) a PDMS mold obtained after one cycle of soft lithography and (c) a PDMS device obtained after two cycles of soft lithography are displayed.

Table 3.1: Values of mean surface roughness of various components obtained from AFM tests.

Object	Diamond turned PMMA	PDMS mold after 1 cycle of soft lithography	PDMS mold after 2 cycles of soft lithography
Mean surface roughness, Ra (nm)	36.5	5.8	13.1

3-D images of AFM results are displayed at the left of their corresponding 2-D images in Figure 3.7 while values of their average surface roughness are tabulated in Table 3.1. Using the turning speeds listed in Table 2.1, the resulting surface of diamond turned PMMA substrate has a mean surface roughness of 36.5 nm, much better than what could be achieved by lithography and etching methods. This surface finish is considered very good as the surface irregularities have dimensions that are on average smaller than 10% of the shortest wavelength to be used during operation. Thus, it is deemed suitable for optical use, even by the stringent standards demanded of optical components. However, the surface is still less smooth than surfaces reportedly achieved in other published work [48]. However, as discuss earlier, the surface finish is simultaneously dependent on many factors including the substrate material, turning speeds and geometry of the cutting tool. It is possible that the working parameters are not adjusted to optimal values that need to take into account the unique combination of the facet cut geometry of the cutting tool and non-crystalline PMMA material structure. To the best of the author's knowledge, most of the published work limits the discussion to the trends different aspects of surface qualities pertaining to certain geometry of the diamond tool and the empirical results are obtained from experimental work on metallic substrates. Thus, there is no published result which could be used as a reference to the combination of tool tip and substrate material required in this work. Carrying out experiments to find out the

optimal machining parameters on PMMA substrate with the 45^0 facet-cut tool tip takes a great amount of work and would be beyond the scope of this work. Instead, the general trends of the working parameters derived on experiments performed on metallic substrates are considered. For example, with reference to [48], it is known that within the range of 0 – 10 µm cutting depth, the surface roughness of the metallic surface does not vary much. In addition, it is also established that the higher the feedrate, the higher the surface roughness. The relationship between surface roughness and spindle speed is less straightforward as the trend is not mono-directional. Surface finish improves dramatically only beyond a certain spindle speed of approximately 500 rpm. Guided by these results, experiments are carried out to find out a set of machining parameters that give a reasonably good optical surface finish, assuming those general trends stand true for plastic materials and metal alike. Since a sharp facet-cut tool tip is substantially more vulnerable to damage than one with a round-tip and PMMA is more brittle due to its amorphous nature, the required machining parameters tend to be much more extreme than what was tested in [48].

Another interesting observation is that surface roughness values of the PDMS mold and PDMS lens device are both substantially smaller than that of the diamond turned PMMA structure. That could be partly due to the different modes used to test rigid PMMA structures and soft PDMS replicas. Contact mode is used to test PMMA surfaces since it is rigid and it is not likely that the material has stiction forces that can significantly impede the AFM cantilever from traversing the surface. On the other hand, PDMS is a polymer that is rather elastic and sticky which gives rise to stick-slip motions when the cantilever tip moves across the surface. This phenomenon will result in patchy extraction of data. To overcome this problem, tapping mode is used on both of the PDMS pieces instead.

In addition, it is observed that the surface roughness of the second PDMS mold is lower than the first, and both are tested using contact mode. The reason for this decrease in surface roughness is believed to be associated with the fabrication method during the second cycle of soft lithography. As it is mentioned that the second cycle of soft lithography is performed by pouring pre-cured PDMS on a fully cured PDMS mold, there are concerns regarding if the two would bond to each other permanently since they are of the same material. If that happens, the replica would not be able to be released from the PDMS mold. To avoid such a problem, the PDMS replica is released from the mold after 30 minutes of heating when it starts to solidify but before it is thoroughly cured. This helped in easing the release process but it also allowed the possibility of minute surface reflow on the partially cured replica when it is returned to the oven to cure. Although this would not alter the crucial dimensions such as those associated with the zone rings of the Fresnel lens, it might result in a slightly smoother surface.

After testing the local surface roughness with AFM, it is also important to look at the overall surface profile. This would help to determine if the blazed surfaces of the diffractive lens are smooth and if the annular zone rings are accurately spaced and have a uniform height throughout the entire lens structure. These have a direct effect on the efficiency and optical performance of the lens.

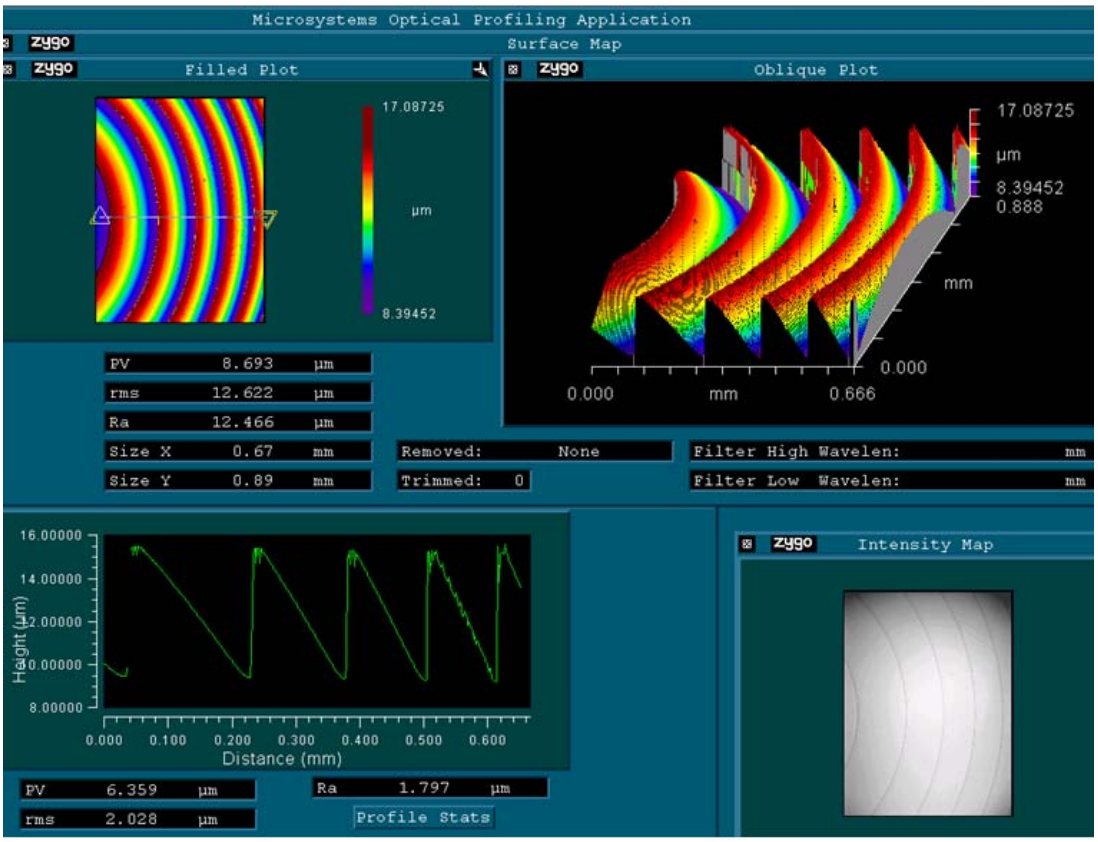

Figure 3.8: A screen shot of the data captured by a Zygo white light interferometer. It contains representative information of the profile of a section of five Fresnel rings.

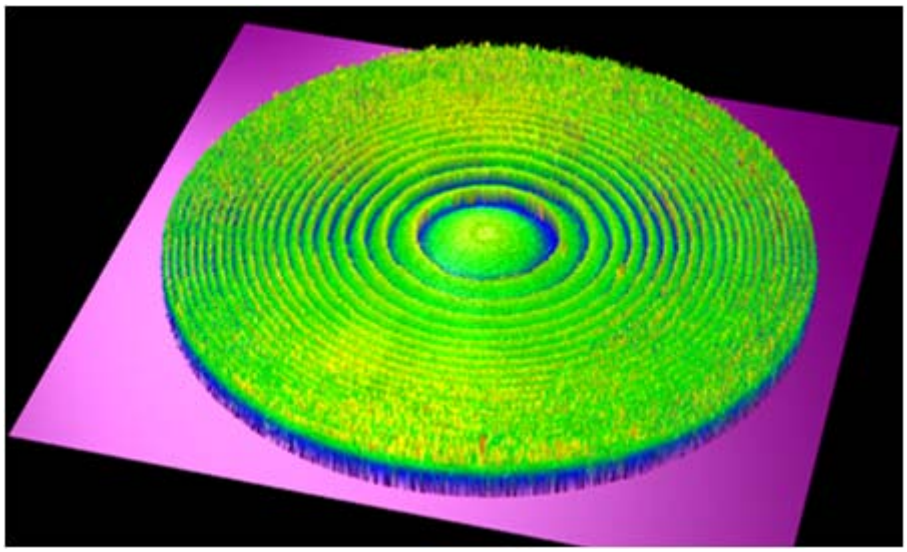

Figure 3.9: Extracted information from white light interferometer gives this 3-D plot of a quarter section of the Fresnel lens, showing all 21 zone rings.

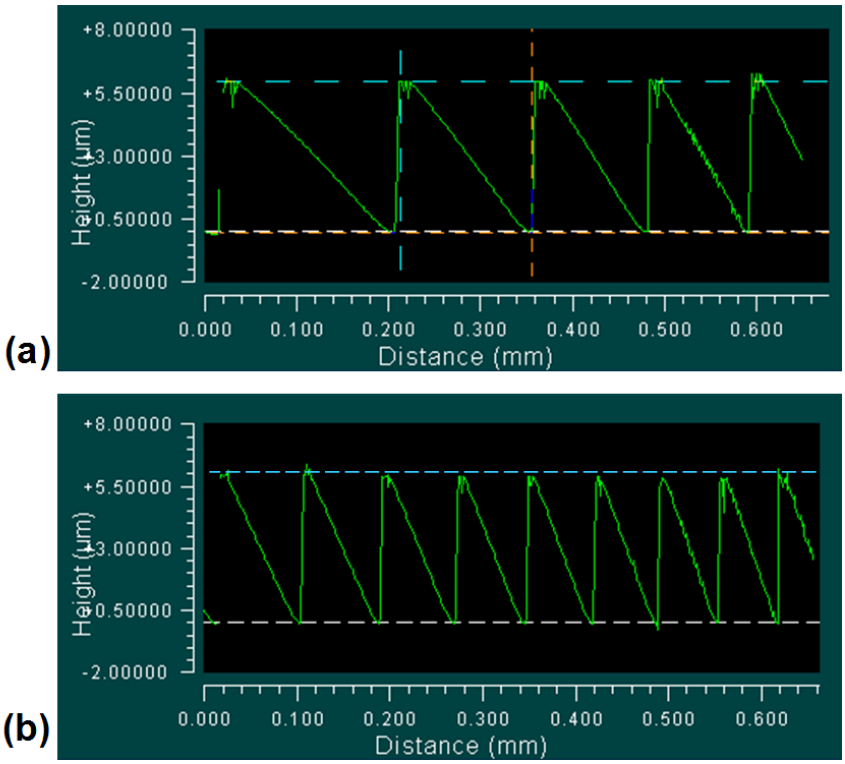

Figure 3.10: (a) and (b) shows the cross-sectional profile of the zone rings at inner and outer regions of the Fresnel lens respectively. The varying spacing between annular rings and uniform height shows that the features on the lens device adhere well to design.

Non-contact and swift white light interferometry is carried out on a PDMS Zygo White-Light 3D Surface Profiler. Because PDMS are extremely transparent, it is difficult to test the surface with white light interferometry if there is no additional reflective coating on the PDMS structures. Thus, a thin layer of gold is evaporated on the top surfaces of the PDMS structure before testing. Figure 3.8 shows a screen shot of the information generated by the program used to process the data captured by the surface profiler. The results in Figure 3.8 are associated with a representative portion of the surface of the diamond turned Fresnel lens on PMMA substrate. Apart from 3-D surface plots, the cross-sectional view associated with the straight line drawn on the 3-D surface plot is obtained. It gives a clearer graphical representation of the surface quality on the blazed surfaces of the zone rings. Overall, it is verified

that the diamond turning produces intricate features accurately with good surface qualities, despite having gone through two cycles of soft lithography. A 3-D plot of the entire Fresnel lens that has 21 annular rings is given in Figure 3.9

Further tests are carried out to compare the zone rings at the central and peripheral regions of the lens the results are shown in Figure 3.10 (a) and (b) respectively. Firstly, it is apparent that the heights of the Fresnel rings are remarkable uniform across the large diameter of the lens. Secondly, the spacings of the rings are increasingly closely spaced towards the peripheral regions, demonstrating the reliability of diamond cutting once again.

3.4 Experiments and Results: Focal Length Tunability

To test the usability of the fabricated tunable hybrid lens, the variation of focal length with injected volume of water was studied using a position sensitive detector (PSD) and lasers of two different colors, namely, green (λ = 532 nm) and red (λ = 632.8 nm). A schematic of the experimental setup is shown in Figure 3.11.

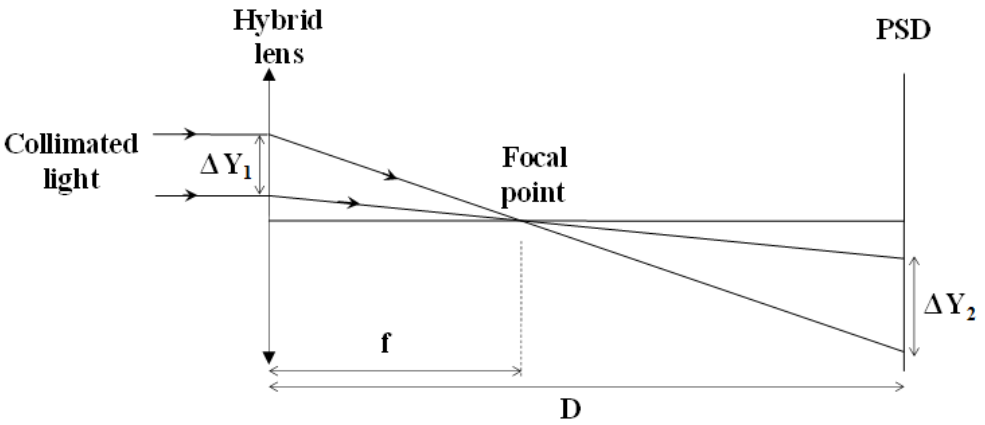

Figure 3.11: Schematic of experimental setup which uses PSD to measure focal length.

Using simple geometry, the focal length of the hybrid lens is derived as follows:

$$f = \frac{D}{\frac{\Delta Y_2}{\Delta Y_1} + 1} \tag{15}$$

For each focal length measurement, D is fixed and a beam of collimated light is passed through the hybrid lens near the centre. Subsequently, the beam of light is shifted a fixed distance of ΔY_1, which is set to be 200 μm. Taking the difference in PSD readings for these two positions and converting them to the equivalent distance shifted on the PSD, the focal length could be derived using Eq. (15). Experimental results for green light are shown in Figure 3.12. It can be seen that the focal lengths of the hybrid lens are tunable to a minimum of 10mm, with approximately 20 mm change in focal length achieved.

Similar experiments are performed on a tunable conventional lens. It is structured exactly like the tunable hybrid lens except a flat surface replaces the Fresnel lens profile at the bottom of the lens cavity. The results are shown in Figure 3.13.

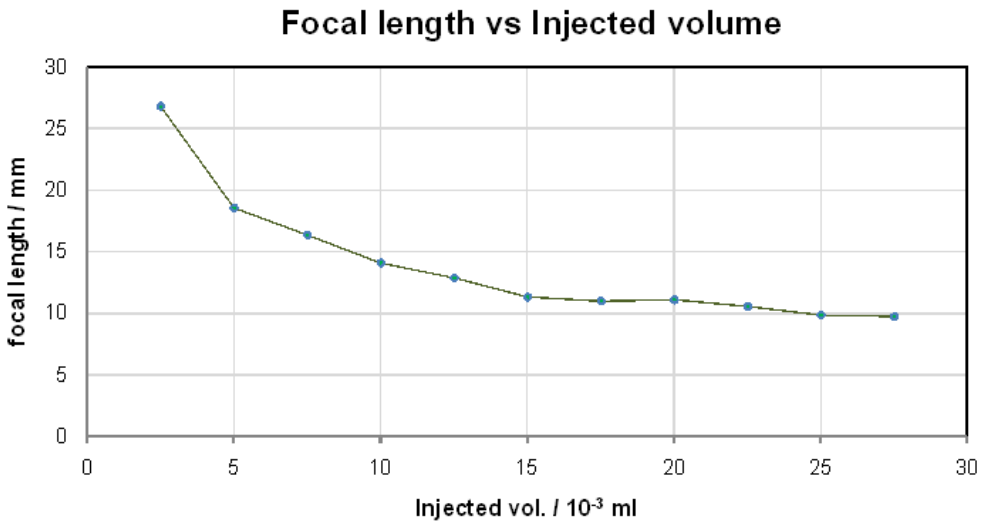

Figure 3.12: Graph of green light focal length of hybrid lens against injected water volume.

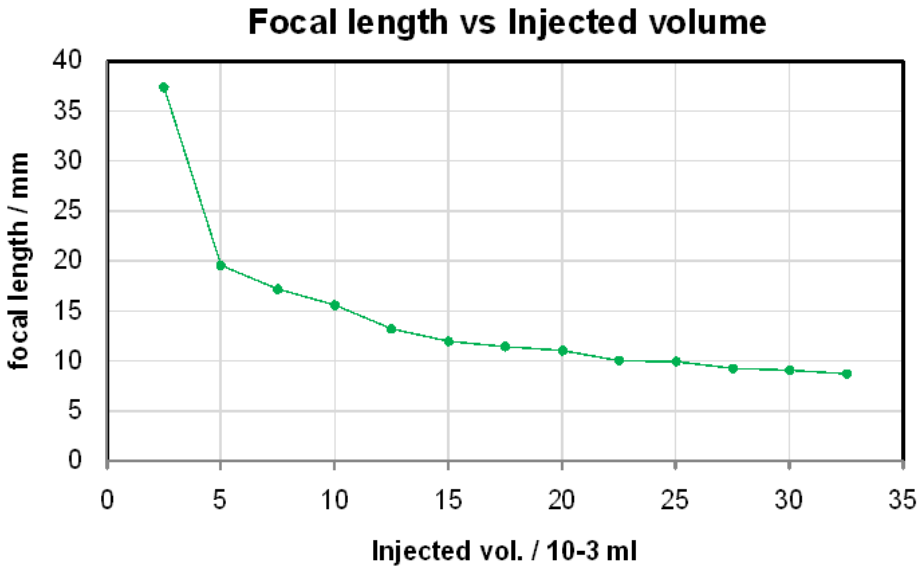

Figure 3.13: Graph of green light focal length of conventional lens against injected water volume.

Comparing the four graphs, it can be seen that there are discrepancies between the two sets of results for injected volumes of water corresponding to certain focal lengths. As chromatic aberration is not able to account for the systematic error of approximately 7 mm, the error is likely to be caused by inaccurate judgement of the point where there is no deformation of the diaphragm. This could be the result of difficulties in detecting slight deformation on the refractive lens.

Although the focal lengths of the conventional and hybrid lens using green and red light are measured, the setup using PSD is not precise enough to detect the chromatic aberration, much less to determine if the hybrid lens is able to minimize the chromatic aberration. Therefore, another method needs to be used to measure changes in focal lengths that are in the range of a few tens to a few hundreds of microns. When such precision is needed, interferometric techniques are often up to task. Because of the ease of setup and resistance to external environmental disturbances, cyclic lateral shear interferometer is used for the purpose of measuring the small distances between green and red light focuses.

3.5 Introduction to Lateral Shear Interferometry

Lateral shearing interferometry has been used in the testing of optical components and the study of flow and diffusion phenomena in gases and liquids, among other fields. It is possible to obtain a number of useful information about the incident wavefront in a single lateral shear interferogram. For instance, the extent of defocus, tilt and various aberrations, such as coma, astigmatism, spherical aberrations could be qualitatively inferred from a lateral shear interferogram. Quantitative evaluation is also possible with suitable mathematical models and signal processing instruments. Besides that, interferometers are very sensitive instruments and they are able to detect even minute variations in the wavefront. It is mainly because of these two reasons, lateral shear interferograms are used in the investigation of chromatic aberration in this work.

There are many types of lateral shear interferometers and they vary in the arrangements used to obtain interferences patterns. For example, there are configurations based on Mach-Zehnder interferometer, Michelson interferometer and

cyclic interferometer. They all make use of beam-dividing surfaces that splits an incoming light source into beams of different amplitudes before interfering with each other as they converge. Beam dividers divide the amplitude of the incident wavefront but they do not affect the shape of the wavefront. Therefore, information about the incident wavefront will be preserved and observed after interference. Alternatively, there are types of lateral shearing interferometers that make use of interference between different orders, usually the zeroth and the first order, of a diffracted beam as aberrations of the original wavefront are preserved as long as the diffraction angle is not too big.

Next, the principle of lateral shear interferometry shall be briefly explained. Generally, what is taking place in a lateral shear interferometer is that an incoming defective wavefront is split into two different paths. One of the beams is then displaced by a small amount with respect to the other beam. Subsequently, these two beams of light will be directed to converge and interfere, producing an interferogram. How the lateral shear is obtained depends largely on the shape of the wavefront. If the original wave has a planar wavefront, lateral shear can be obtained by lateral displacement in its own plane. How the incident wavefront deviates from a planar wavefront will be observed in the interferogram.

At this point, it will be useful to introduce some mathematical expressions that can be used to obtain a better appreciation of the information that can be extracted from the interferograms. The incoming light is assumed to be collimated which implies the wavefront is planar.

First and foremost, the wavefront error can be denoted as W(x, y). If the wavefront is sheared in a certain direction i.e. x-direction, by a small amount, S, then it can be

approximated that $\left(\frac{\delta W}{\delta x}\right) S = \Delta W = n\lambda$ [59]. Because accuracy increases while sensitivity decreases as S decreases, the amount of shear to be used must balance the need for both.

Some commonly faced errors that can be present in an optical system, even before the incident ray hits the sample to be tested, include defocus and tilt. This could occur if the light is not well collimated and it did not hit the interferometer perpendicularly. These should be eliminated before inserting the test lens into the optical system, so that the interferogram will only contain information that is of interest, which is the performance of the test lens. One of the most often encountered errors that is introduced by the test lens is spherical aberration. Primary spherical aberration can be expressed as $W(x, y) = A(x^2 + y^2)^2$. Thus the equation corresponding to the shearing interferogram is $\Delta W = 4A(x^2 + y^2)xS = n\lambda$, if defocus and tilt are ignored.

Figure 3.14, Figure 3.15 and Figure 3.16 are pictures of lateral shear interferograms at various positions in the vicinity of the focal spots without the presence of tilt, in the presence of tilt and in the presence of spherical aberration respectively [59]. Without spherical aberrations, the interferograms are composed of straight lines. Without tilt, the focus is detected when the overlapping region of the two circles is uniformly illuminated. Sometimes this is difficult to detect, especially when shear is introduced manually, because any slight offset from the focus, either towards the inside or outside the focus, will result in similar interferograms that consist of vertical straight lines. Therefore, sometimes a small amount of tilt is introduced as it is easier to track when the tilted lines of the interferogram have become horizontal at the focal point. In the presence of spherical aberrations, curved lines and even rings will be observed in the interferograms. Inside the focus, the lines are closely packed with a slight bulge

at the centre region. As it approaches the focal point, the central fringe extends to its widest. Beyond the focal point, rings start to appear within the central fringe. The greater the spherical aberration, the greater the density of the rings for a certain offset from the focus, assuming the shearing remains constant. Increasing the shear, too, results in greater density of interferometric lines.

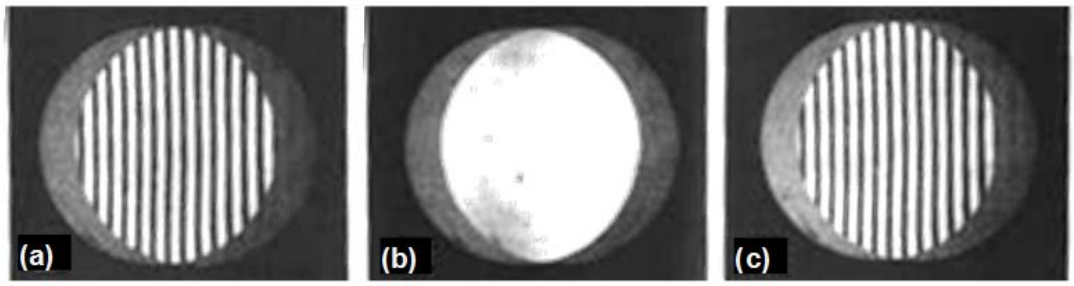

Figure 3.14: Pictures of lateral shear interferograms for (a) inside the focus, (b) at the focus and (c) outside the focus.

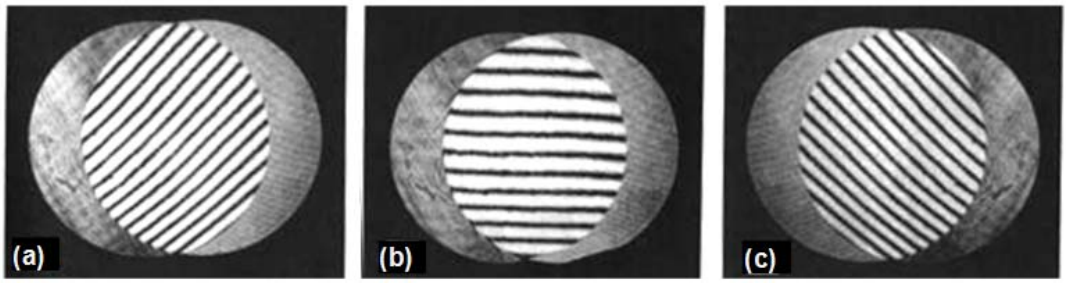

Figure 3.15: Pictures of lateral shear interferogram for inside, at and outside the focus in the presence of tilt.

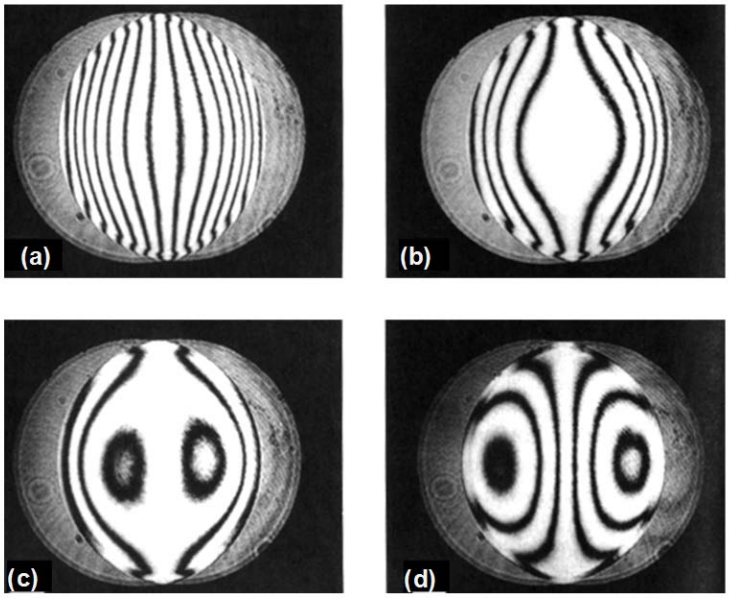

Figure 3.16: Pictures of lateral shear interferograms for (a) inside the focus, (b) at the focus and (c), (d) outside the focus in the presence of primary spherical aberration.

3.6 Experiments and Results: Application of Lateral Shear Interferometry to the Study Chromatic Aberration in the Tunable Lenses

Having discussed the general theory of lateral shearing interferometry and how certain relevant interferograms could be interpreted, the experimental results applying lateral shearing interferometry to study chromatic aberration in the tunable hybrid lens and tunable conventional lens shall be presented.

Lateral shear interferometry is useful in measuring longitudinal chromatic aberration, a phenomenon that results in light of different wavelengths to focus at slightly different distances. Since the distance away from the focal point can be inferred from the closeness of fringes or number of fringes captured in an interferogram, chromatic aberration can be evaluated by noting the difference in number of fringes which appeared in two interferograms obtained when two different wavelengths of light are

used while keeping other conditions like amount of shear, aperture size and amount of elastic deformation of the PDMS membrane constant. However, this requires signal processing instruments that can capture the interferograms in high definition and the boundaries of the beams, the overlapping regions and the interferometric lines must be precisely identifiable.

Alternatively, the relative positions between the two focal lengths of two colors can be measured, since the interferogram at the focus can be easily recognised as the one with the widest central fringe as compared to other interferograms captured at positions away from the focus.

For this purpose, a typical cyclic interferometer such a triangular-path interferometer can be used with collimated light. In this type of interferometer, two coherent light beams travel in opposite directions and they would emerge to interfere with each other. One advantage of this configuration is its insensitivity to vibration and other environmental effects in a controlled laboratory. The stability is required for the observation and capturing of the interferograms. Moreover, it is relative easy to construct as opposed to other configurations. A schematic is shown in Figure 3.17 while a photograph of the setup is shown in Figure 3.18. The steps to performing the experiment on the tunable hybrid lens and tunable conventional lens are as follow:

1. Pump in water to completely fill the lens cavity and water channels of a tunable hybrid lens device. Ensure no trapped air bubble is present and the membrane is as flat as possible before closing the inlet and outlet valves.
2. Align the optical elements in the setup to ensure that the green laser light hits the tunable lens perpendicularly and enters the lateral shear interferometer setup collimated.
3. Adjust the configuration of the cyclic lateral shear interferometer to make sure there is appropriate interference of the beams of light. The interferometer can

be observed on a diffuser plate that is placed at the light exit of the lateral shear interferometer.

4. One of the plane mirrors in the cyclic lateral shear interferometer is displaced in the plane of the beam direction and this will result in a certain amount of lateral shear. This shear is adjusted until the fringes in the interferogram are well-spaced.
5. Search the focal spot by moving the collimating lens below the tunable lens vertically until the central fringe shows the widest width in the interferogram.
6. The distance between the tunable lens under test and the collimating lens below it is measured. Subtracting that measured value with the focal length of the collimating lens, the focal length for green laser, f, is known.
7. After measuring f, the green laser could be detached from the connecting head and be replaced by a red laser through the same connecting head. This prevents disturbances to other elements of the optical system, thereby minimizing the further introduction of errors to the setup. Once again, the focal spot for the red laser is searched for by adjusting the collimating lens till the interferogram shows the widest central fringe. The position of the collimating lens is noted.
8. Subsequently, the red laser is replaced by a blue laser. The amount of distance needed to move the collimating lens before the new focal spot is reached is then noted. The distance separating the focal spots of the red and blue laser spots are denoted as Δf. This value serves to quantify the amount of chromatic aberration. If there is no chromatic aberration, the focuses of both colors will coincide.
9. To get more sample data, steps 7 and 8 could be repeated a few times.
10. When a set of data points is obtained for this configuration, the inlet valve is opened and a small amount of water is pumped in to further deform the membrane. This essentially shortens the focal length of the tunable lens.

11. Repeat steps 5 to 10 to obtain data points at various f values for the tunable hybrid lens device.
12. Repeat steps 1 to 11 to obtain data points at various f values for the tunable conventional lens device.

=

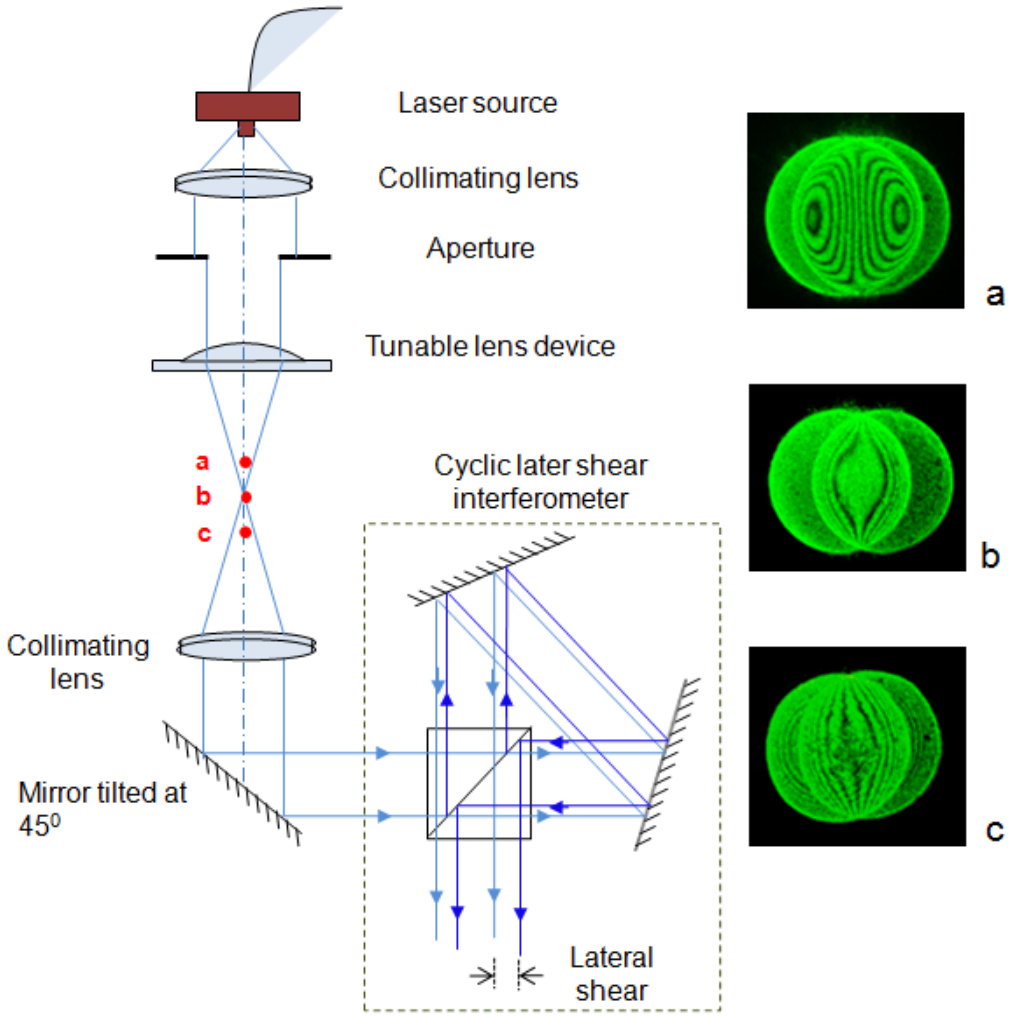

Figure 3.17: A schematic of the experimental setup that uses a triangular path cyclic lateral shear interferometer in the testing of tunable lenses. On the right are three interferograms corresponding to the points inside the focus, at the focus and outside the focus, denoted by a, b and c respectively.

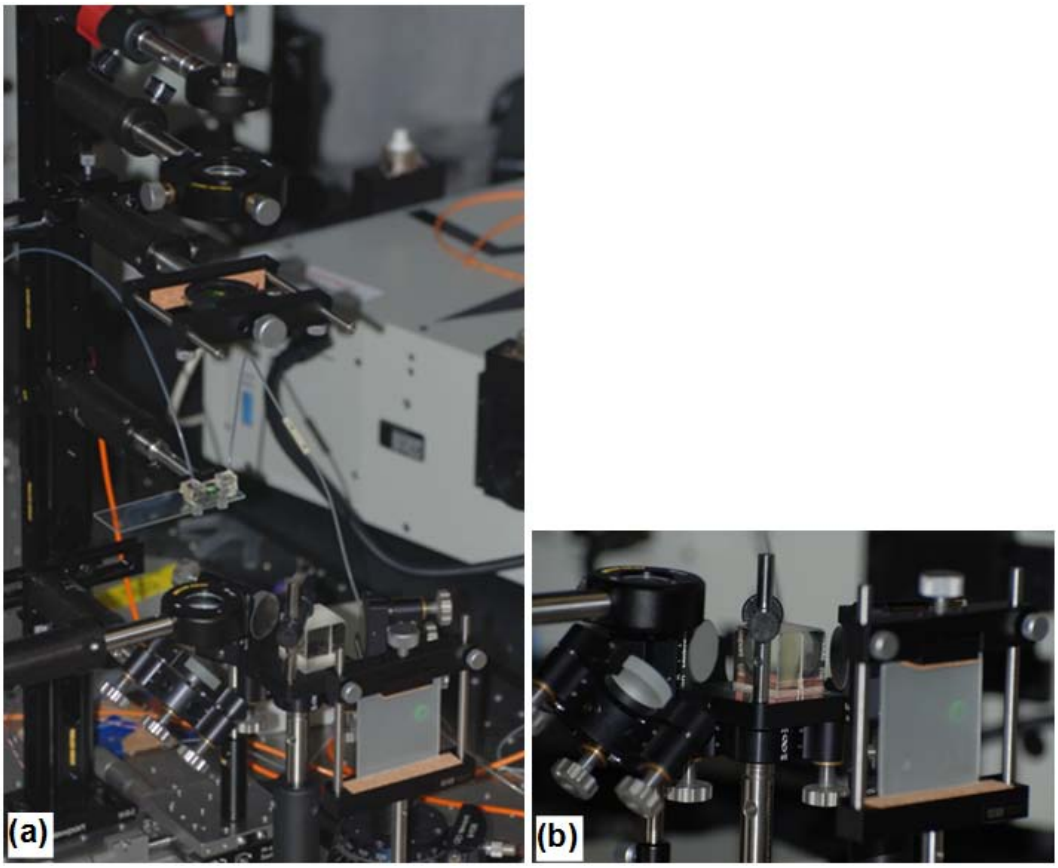

Figure 3.18: (a) A photograph of the lateral shear experiment setup. (b) A zoom-in view on the lateral shear interferometer with a diffuse plate capturing an interferogram.

To find out if the fabricated lenses behave as predicted in theory, theoretical curves are plotted together with the experiment results for both lenses in a graph as shown in Figure 3.19. The theoretical calculations used to obtain the theoretical curves are outlined in the section below.

Calculations for the theoretical curve for conventional tunable lens start with the lens maker equation, which is given by

$$\phi = \frac{1}{f} = (n-1)\left[\frac{1}{R_1} - \frac{1}{R_2} + \frac{t(n-1)}{nR_1R_2}\right] \tag{16}$$

where R_1 and R_2 are the radius of curvatures of the front and back of the lens respectively while t is the thickness of the lens.

Since R_2 for plana-convex lens is infinity and assuming thin lens conditions hold, the lens maker equation reduces to

$$f = \frac{R_1}{n_{w,ave} - 1} \tag{17}$$

Using the equation, the difference in focal lengths when red and blue lasers are used can be expressed as

$$\Delta f_{conventional} = \frac{R_1}{n_{w,red} - 1} - \frac{R_1}{n_{w,blue} - 1} \tag{18}$$

The values of the refractive indices $n_{w,red}$ and $n_{w,blue}$ are 1.33205 and 1.33910 respectively. They are obtained by using Sellmeier equation, assuming the ambient temperature is 20^0C. Substituting these values into the equation, the following expression is obtained.

$$\Delta f_{conventional} = 0.062612\, R_1 \tag{19}$$

Once again, applying Sellmeier equation at the wavelength of a green laser, 0.532 μm, the value of $n_{w,green}$ is found to be 1.33538. Using that value and substituting Eq. (17) to Eq. (19), the theoretical relationship between Δf and f is derived.

$$\Delta f_{conventional} = 2.10 \times 10^{-2} f \tag{20}$$

Subsequently, the theoretical relationship between Δf and f is derived for the tunable hybrid lens. Substituting (13) and (17) into **(2)**, the following expression is obtained.

$$f_{hybrid} = \frac{1}{\frac{n_w - 1}{R} + \frac{2m\lambda}{n_{air} R_m^2}} \tag{21}$$

For the design of Fresnel lens used in this work, the ratio $\frac{R_m^2}{m}$ is a constant.

$$\frac{R_m^2}{2m} = 1.51382 \times 10^5 \tag{22}$$

Substituting Eq. (22) and the values of the refractive indices of water at red and blue wavelengths into (21), the following relationship between Δf_{hybrid} and f_{hybrid} is obtained.

$$\Delta f_{hybrid} = \left[\left(\frac{9.901\times10^{-4}}{f_{hybrid}}\right) + (1.386 \times 10^{-5})\right]^{-1} - \left[\left(\frac{1.011\times10^{-3}}{f_{hybrid}}\right) + (1.931 \times 10^{-5})\right]^{-1}$$

(1)

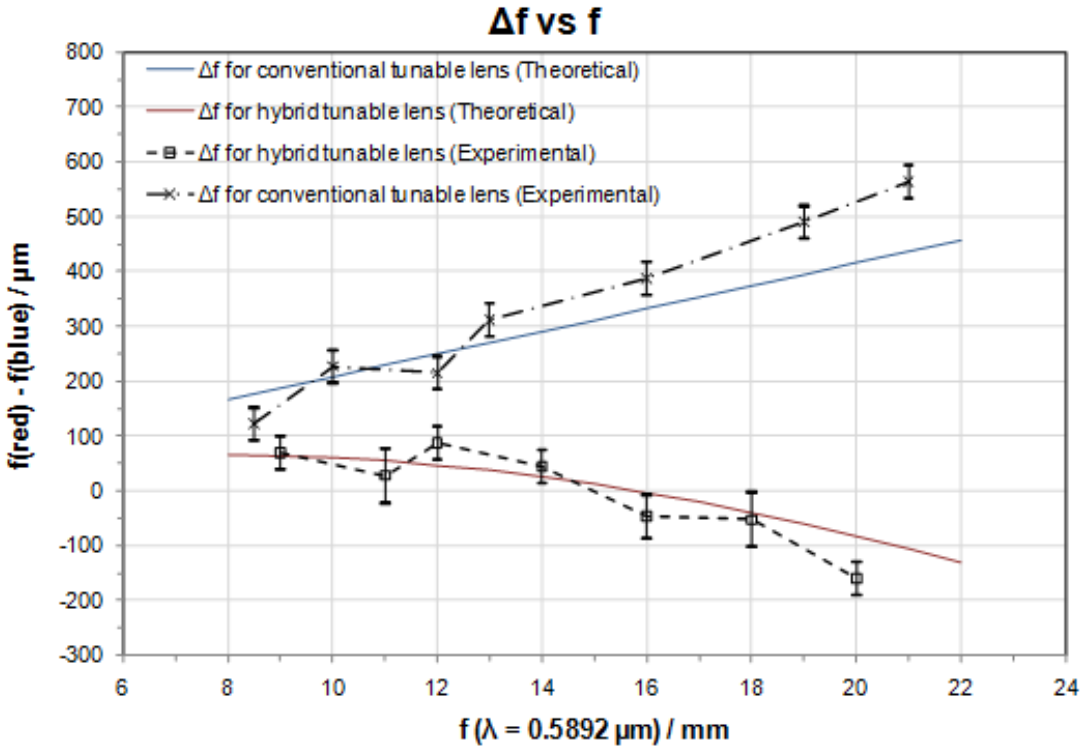

Figure 3.19: The results of Δf against f is plotted in this graph. The theoretical curve is superimposed on the experimental results for easy comparison.

From Figure 3.19, it is verified that the performance of the tunable lens behaves closely to the model which the design of the lens was based on. Both the theoretical and experimental results show that the magnitude of the chromatic aberration of the tunable hybrid lens is consistently higher than that of the hybrid lens. The positive dispersion of the refractive conventional lens is manifested by its positive values of (f_{red} – f_{blue}) for the entire operating focal range. In contrast, the hybrid lens shows positive dispersion in the lower range of the focal lengths tested while this trend reverses at higher focal lengths. This can be explained by the fact that the dispersive power of refractive lens dominates over that of the Fresnel lens when the effective focal length is short. As the power of the refractive lens decreases, the dispersive power of the Fresnel lens dominates instead, hence the reverse in trend. Theoretically, the magnitude of the average chromatic aberration remains within 150 µm for the operating range of 8 to 22 mm, which is much smaller than that of

conventional lens. The aberration of conventional lens ranges from approximately 150 to 450 μm. The smaller the aberration, the smaller the spot size will be. With smaller spot size, higher resolution is then possible. Thus, the improvement in imaging quality even for a decrease of a few tens of microns in spot size is immense.

3.7 Experiments and Results: Diffraction Efficiency

Lastly, the diffraction efficiency of the diffractive/refractive hybrid lens has to be measured. Diffraction efficiency is the ratio of the power of incident light and the power of the light within the central zone of the focussed light spot. The measured diffraction efficiencies of red, green and blue light are 88%, 92% and 73% respectively. For comparison, the theoretical calculation of diffraction efficiency can be calculated by the following equation [60]:

$$\eta(\lambda) = sinc^2\left[\frac{\lambda_o}{\lambda}\frac{n_2(\lambda) - n_1(\lambda)}{n_2(\lambda_0) - n_1(\lambda_0)} - 1\right] \tag{23}$$

Using that equation, the theoretical diffraction efficiency is 98%, 96% and 76%. Compared the theoretical values, the measured values are smaller possibly due to one or combination of the following reasons. Firstly, there may be partial absorption of light by PDMS and water. Secondly, the diamond-tip cutting tool may be slightly blunted due to long periods of machining, resulting in the Fresnel lens having shadowed regions at the edges of the annular rings. This could also undermine the diffraction efficiency. Thirdly, it is possible that the PDMS could have impurities that could scatter some of the incoming light. Nevertheless, the diffraction efficiency is higher than what is typically achieved by etching and lithography methods.

Diamond cutting combined with multiple cycles of soft lithography has been demonstrated to be a reliable, efficient and cost-effective fabrication method to produce multiple liquid tunable diffractive/refractive lens replicas from a single PMMA master mold. The compact hybrid lens device exhibit good surface qualities and optical performances. As compared to a single tunable refractive lens, the designed diffractive Fresnel lens was verified to decrease the chromatic aberration of the hybrid lens in the visible spectrum over a large effective focal range from 8 to 21 mm. The mechanism to achieve the large range of focal lengths is simple and requires no complicated or expensive equipment.

Chapter 4. Liquid Tunable Double Focus Lens

4.1 Introduction to Multiple Focus Lenses

Most of the designs of variable focusing lens in the literature only allow the lens to have a single focus at a particular configuration. Simultaneously processing information from object points with a single lens is not possible, especially if the points are displaced far apart from each other. Instead, it requires a change in configuration of the lens using various actuation methods discussed in section 3.1. Those methods are often cumbersome and require a certain amount of time for mechanical displacement of optical components, making it difficult for real-time data acquisition. Therefore, it is desirable to reduce information processing time by having lenses that are capable of focusing at various points simultaneously.

A double focusing lens remains the most widely researched multi focusing lens. They are based on a number of different working principles and fabrication methods. One type of double focusing lens which is available commercially is a triplet composed for a calcite crystal bi-convex lens sandwiched between two glass bi-concave lenses. Due to the birefringence of the calcite lens, it has two different refractive indices towards an incident ray, depending on its polarizing state. The double focus lens can be designed such that ordinary rays of an incident light pass through without refraction while extraordinary rays refract. Combined with the use of a quarter wavelength phase plate, the double focusing lens could be integrated into a common-path interferometer [61]. This type of interferometer is designed to provide increased signal stability in spite of external disturbances such as platform vibration and irregular air currents. Such interferometer has been successfully implemented in scanning force microscopes [62]. The focuses of the double lens in the system are

fixed but by moving the stage which holds the lens, they are brought to coincide with the varying surface height of the test samples.

There is another type of double focus lens that is not based on birefringence effect. Instead, it works by having a lens surface that has different radiuses of curvatures at the central and peripheral regions. As a result, when a beam of light is incident on this type of lens, light that falls on the centre of the lens will focus at a different spot as the outer ring of light. This type of double focus lens can be integrated in DVD/CD pick-up heads whereby the aspherical surfaces of the central and peripheral can each be tailored to work best on the different materials that DVDs and CDs are made of [63]. Compared to optical systems that use two separate lenses with two corresponding objective lenses, the use of a single lens that combines two radiuses of curvatures reduces the number of optical components required. In that work, the solid PMMA double focus lens is fabricated by diamond turning.

Using a mirror plate and a double lens that is structured similarly to that presented in [63], a research team has developed a compact optical system that offers telescopic and wide-angle view on a single lens [64]. The switch in views does not require any movement of the lens but just a simple opening or closing of a hinged-shutter which serves to block or transmit light through the central region. However, it should be noted that a permanent magnet has to move between the front and side of the metal-coated shutter to open and close it. The double lens is fabricated by first end-milling a mold on an aluminium workpiece before curing a volume of PDMS within the cavity of the mold. The PDMS which takes on the shape of the mold is the double lens device.

Thus far, the double focus lenses that are discussed have fixed focal lengths. In many applications, focal lengths have to be brought to different surface heights.

Therefore, the stage holds the fixed-focal length lens needs to be dynamically moving. In most circumstances, large, complex and expensive electro-mechanical systems are required to move the bulky groups of optical components and that makes miniaturizing of the system difficult. Because of this, variable focusing double lenses with simple actuating mechanisms will has enhanced usability and even commercial appeal.

In [65], a liquid tunable double lens is developed. With a simple calibrated syringe pump, liquid pressure is applied to deform an elastic PDMS film with different thickness at the central and peripheral region. As depicted in Figure 4.1, the thicker parts of the film have a larger radius of curvature than the thinner parts of the film. The non-uniformity in deformation produces two distinct focuses at different distances away from the lens.

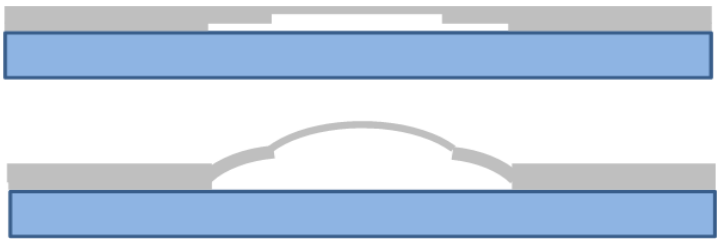

Figure 4.1: A schematic of a liquid tunable double lens that is based on the varying amounts of deformation of a PDMS film with different thickness.

4.2 Calculations and Design of a Liquid Tunable Double Lens

Having discussed the importance and applications of double focusing lenses, a liquid tunable double lens that is fabricated with the use of diamond cutting and soft lithography shall be presented. The structure and material used is similar to that of the liquid tunable diffractive/refractive hybrid lens discussed in chapter 3 and it is shown in Figure 4.2.

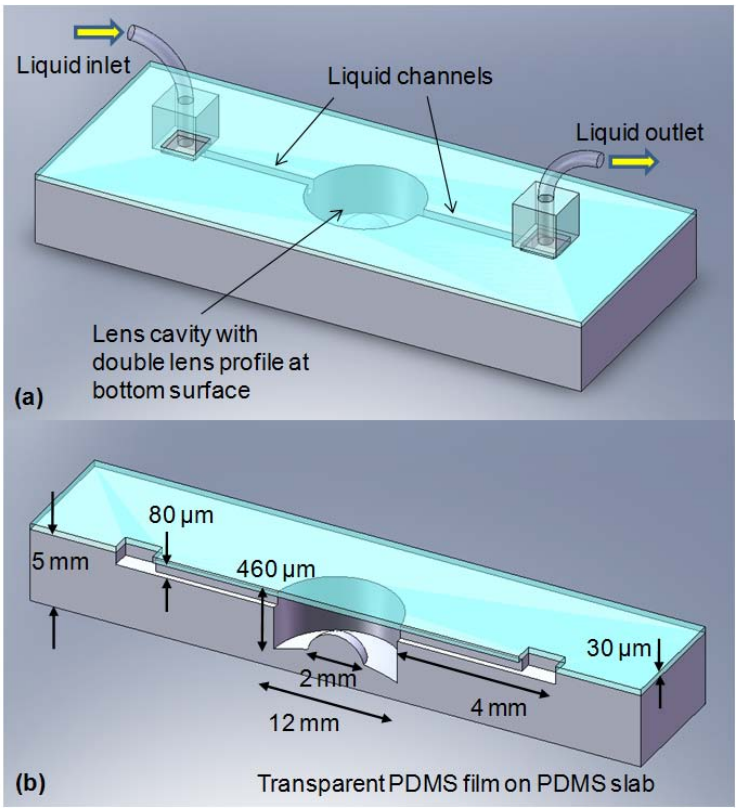

Figure 4.2: (a) A diagram that shows the main features of the liquid tunable double lens device. (b) The dimensions of the features are given on the diagram.

Next, the calculations that led to the design of the double lens shall be discussed in the following section. First, let's take a look at the general scenario given in Figure 4.3 which a beam of light passes through a single spherical interface to be brought to focus.

Symbols used in the following figures include:

n_1: refractive index of surrounding medium of the lens

n_2: refractive index of lens material

S_o: object distance

S_i: image distance

R: radius of curvature of lens

R_{CL} : radius of curvature of central lens of the double lens

R_{PL} : radius of curvature of peripheral lens of the double lens

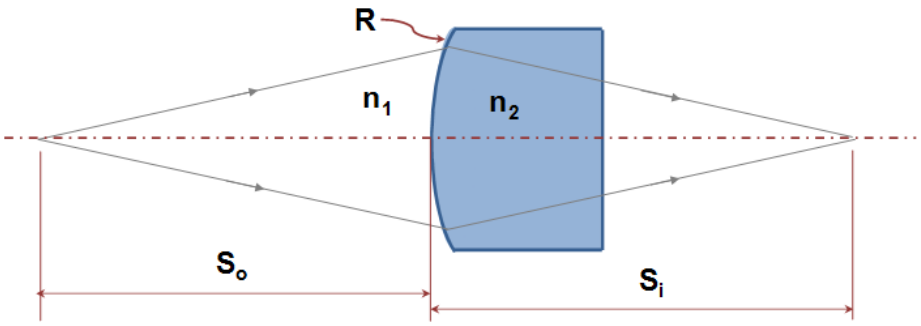

Figure 4.3: The diagram shows the ray paths that pass from the object point to the image point via the refractive lens.

Applying Fermat's Principle which maintains that the optical path lengths from the object point to the image point is constant, the following equation could be derived [57],

$$\frac{n_1}{S_o} + \frac{n_2}{S_i} = \frac{n_2 - n_1}{R} \tag{24}$$

Assuming distilled water is used as the working liquid in the tunable hybrid double lens, (24) shall be applied at the air-water and water-PDMS interface sequentially. This would allow the effective focal lengths of the central and peripheral regions of the device to be derived. Although the derivation ignores the presence of aberrations that might be present in the lens device, the derivation gives a reasonably good approximation to the actual scenario.

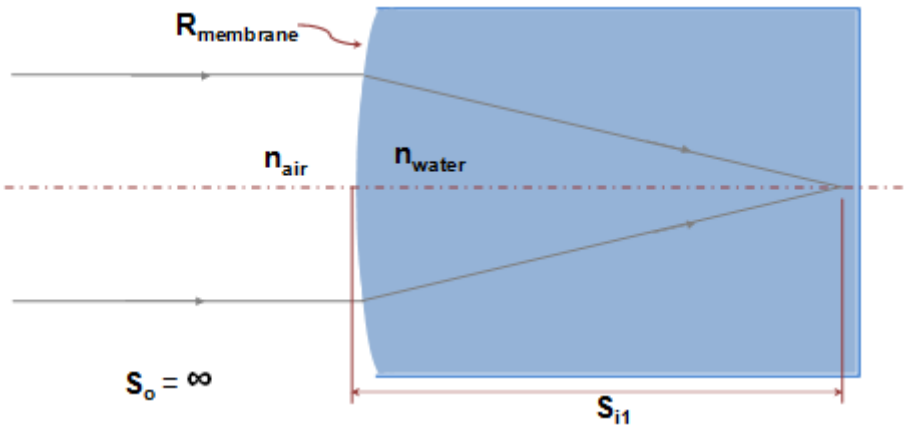

Figure 4.4: The ray paths at the air-water interface of the deformable membrane section of the double lens device.

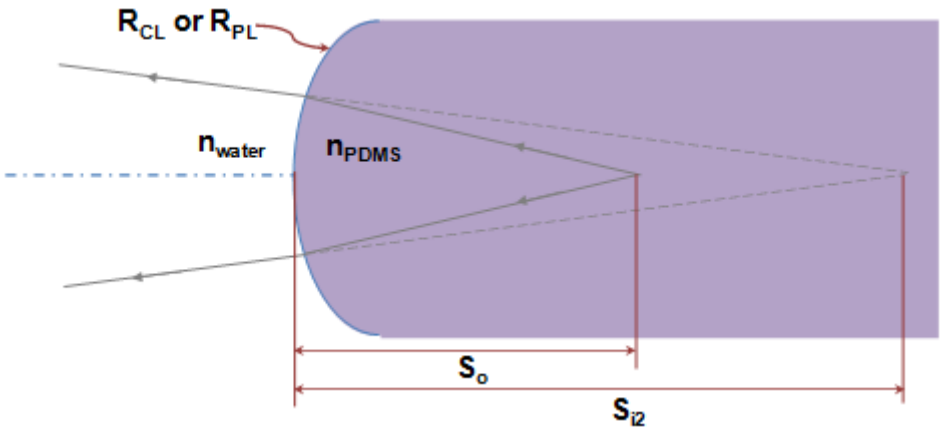

Figure 4.5: The ray paths at the water-PDMS interface in the lens cavity of the double lens.

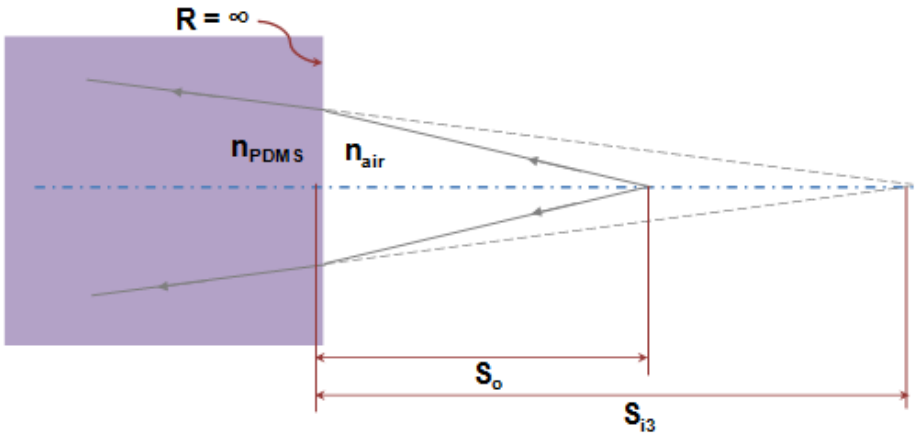

Figure 4.6: The ray paths at the PDMS-air interface where light exits the double lens device.

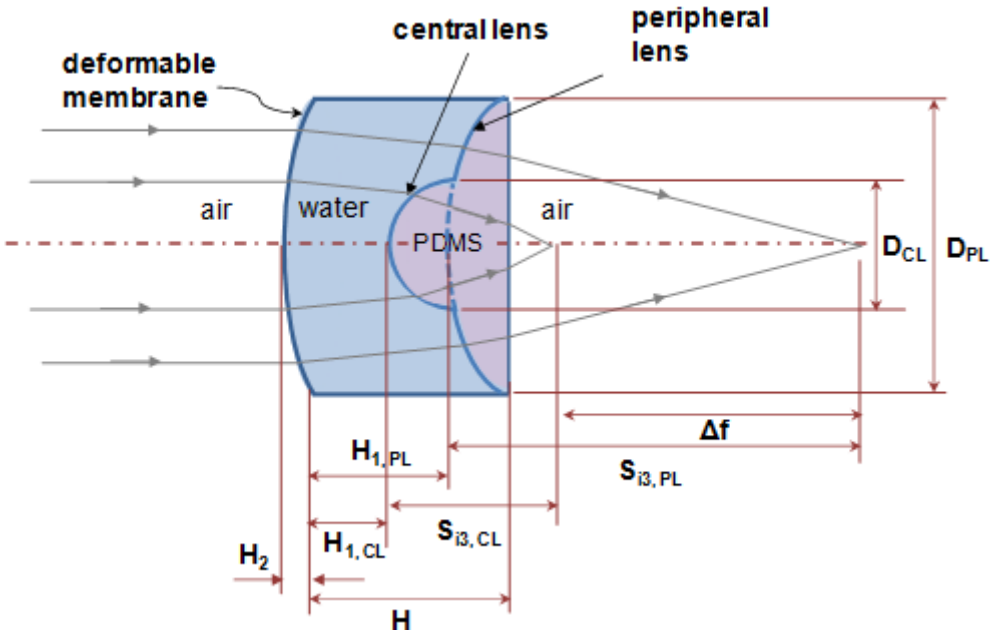

Figure 4. 7: Ray paths that pass through central and peripheral lenses are depicted in this diagram. The symbols used to denote the distances between various points are indicated in the figure.

In the air-water interface as shown in Figure 4.4, applying the formula given in Eq.

(24) results in the following,

$$\frac{1}{\infty} + \frac{1.33}{S_{i1}} = \frac{1.33 - 1}{R_{membrane}} \tag{25}$$

The resulting image point at this interface then acts as the object point for the PDMS lens at the water-PDMS interface, as illustrated in Figure 4.5. Since this double lens is a combination of two distinct lens curvatures, they have to be processed separately. The calculation involving the central lens shall be discussed first. Taking into the account of the deformation of the deformed membrane and clearance of the lens cavity, Eq. (24) can be applied again to yield the following,

$$\frac{1.33}{-(S_{i1} - H_2 - H_{1,CL})} + \frac{1.41}{S_{i2,CL}} = \frac{1.41 - 1.33}{R_{CL}} \tag{26}$$

$$R_{membrane} = \frac{D_{PL}^2 + 4H_2^2}{8H_2} \tag{27}$$

Likewise, the image point of the peripheral lens can be calculated following the same methodology by replacing R_{CL} with R_{PL} and $H_{1,CL}$ with $H_{1,PL}$ in Eq.(26).

$$\frac{1.33}{-(S_{i1} - H_2 - H_{1,PL})} + \frac{1.41}{S_{i2,PL}} = \frac{1.41 - 1.33}{R_{PL}} \tag{28}$$

Lastly, considering the exit of the light at the PDMS-air interface, applying Eq. (24) to the central and peripheral part of the lens yields the following,

$$\frac{1.41}{-\left(S_{i2,Cl} - H + H_{1,CL}\right)} + \frac{1}{S_{i3,CL}} = \frac{1.41 - 1}{\infty} \tag{29}$$

$$\frac{1.41}{-\left(S_{i2,Pl} - H + H_{1,PL}\right)} + \frac{1}{S_{i3,PL}} = \frac{1.41 - 1}{\infty} \tag{30}$$

$$\Delta f = S_{i3,PL} - S_{i3,CL} \tag{31}$$

To demonstrate that combining diamond turning and soft lithography is a viable way of fabricating a tunable double-focusing lens suitable, the focal points of the two lenses have to be suitably spaced to allow easy verification of its functionality through experiments. They cannot be too close to each other as that would make identification of the distinct focuses difficult. Neither can they be too far apart due to the space limitations on the optical table where experiments are carried out. Thus, the difference between the focal lengths of the central and peripheral lenses should at least be approximately 15 mm when the membrane is pumped almost to a hemispherical shape. In another words, H_2 is expected to vary between 0 and ~6 mm.

With these considerations, the dimensions of the designed geometry relevant to the calculations outlined earlier are listed below.

R_{CL} : 3 mm

R_{PL} : 100 mm

$H_{1,PL}$: 280 µm

$H_{1,CL}$: 110 µm

D_{CL}: 2 mm

D_{PL}: 12 mm

A large peripheral lens diameter is necessary to avoid light signal coming through that region from being obscured. The width and depth of the water channels remain the same as that used in the tunable diffractive/refractive hybrid lens, which is 80 μm. This is to ensure the boundary condition of the lens cavity remains as close to circular as possible and the deformation of the PDMS film could be spherical.

4.3 Experiments and Results: Focal Lengths Tunability

Next, the ability of the lens to simultaneously focus at two different points is demonstrated. The schematic of the experimental setup is shown in Figure 4.8. A beam of collimated light is made incident perpendicularly on the lens device. Subsequently, with various volumes of water pumped in to change the curvature of the PDMS diaphragm, the various focal points of the central and outer lenses are detected with a charge-coupled device (CCD). The distance between the CCD and the focusing lens in front of it is fixed at twice the focal length of the focusing lens. When locating one of the focal lengths of the lens device, the pair is moved while maintaining the same distance apart from each other until a clear bright focal spot is captured on the CCD. Noting the position of the CCD, the pair is moved again in search of the other focal spot. The 2f distance between the CCD and focusing lens, the object-image ratio is 1:1. This allows for easy conversion because the distance moved by the pair from one focal spot to the other, d, would be exactly the distance separating the two focuses. In addition to noting the distance between the two focuses, the actual focal length has to be measure as well. This is done by intercepting the ray path between the lens device and the angled mirror below it with a thin sheet of paper when the CCD captures the focal spot of the central lens. By finding the point which shows the smallest spot on it, the distance between that spot and the water-pumped lens is then the focal length, f_c. The focal length of the

peripheral lens, f_p, is then the sum of that value and the distance traversed by the CCD.

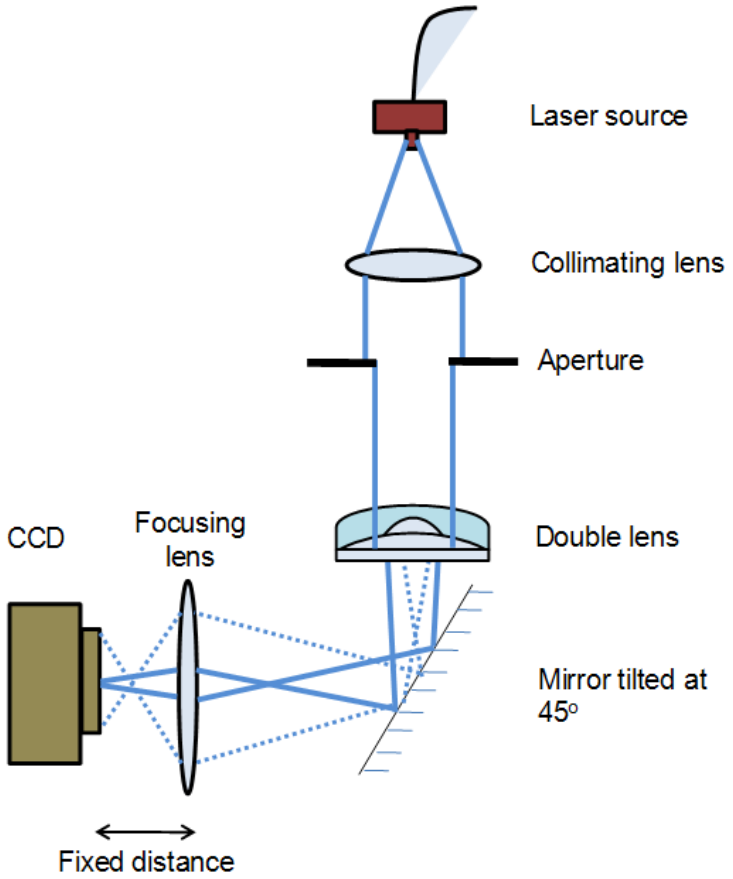

Figure 4.8: A schematic of the experiment setup used measure the focal points of the central and peripheral lens. The CCD and the focusing lens before it is moved together, while maintaining the distance between them, until CCD captures a distinct focal point of either lens on the screen.

Because of the design, the difference in focal lengths for the central and peripheral lens is in the order of centimetres. It would be difficult to use lateral shear interferometry to locate the focal spots at a certain lens configuration due to the limitation of the micrometer travel range. The lateral shearing technique would be more suitable in locating focal spots spaced apart less than a millimetre apart. Therefore, unlike the experiment setup to locate the focal spots of different colour on the diffractive/refractive hybrid lens using the lateral shear interferometer, a meter

rule that is attached adjacent to the grill the CCD moves along is used to track the distance moved by the CCD. The human error that might arise is conceivably greater. Nevertheless, it is within reasonable range considering the focuses are spaced rather wide apart.

In summary, the order which the experiment is carried out is summarized below.

1. Inject water until lens cavity is fully filled while keeping PDMS film as flat as possible.
2. Move CCD and focusing lens together to search for central lens focus. Measure f_c and note position of CCD from rule.
3. Move CCD and focusing lens together to search for peripheral lens focus. Note new position of CCD on rule and calculate d.
4. $f_p = f_c + d$
5. Pump in an additional amount of water and repeat steps 2 to 5.

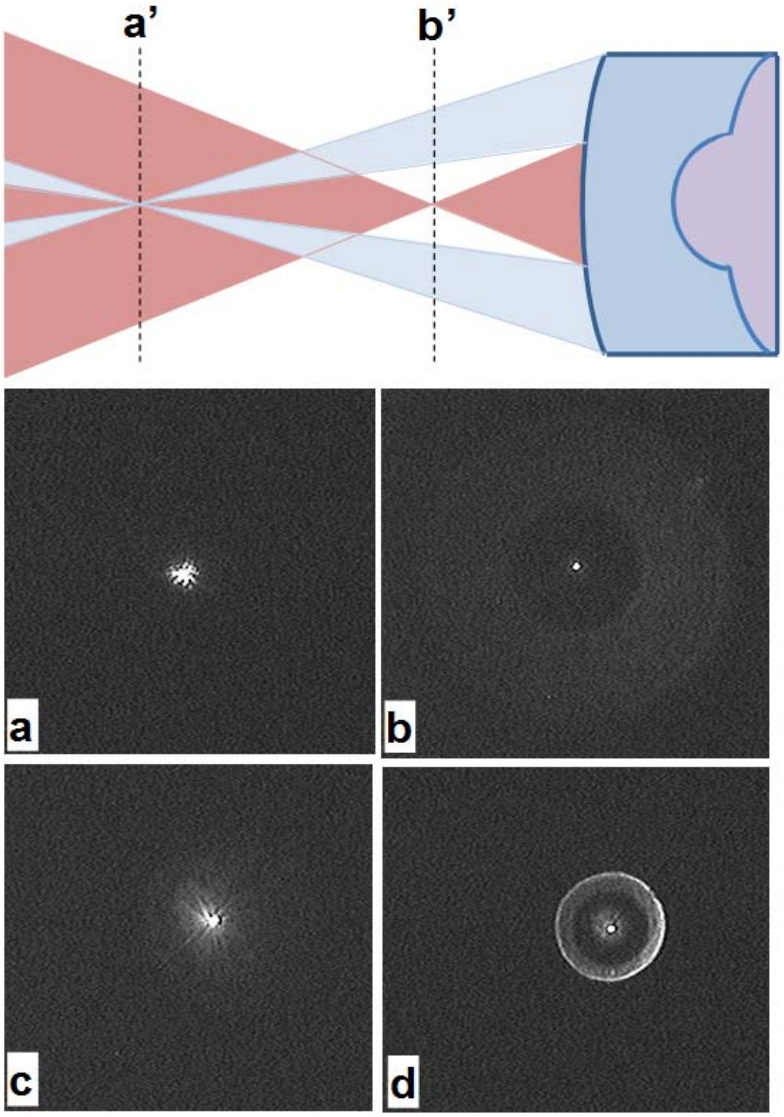

Figure 4.9: At the top is a ray diagram for the double lens. Images captured by the CCD are shown below it. (a) and (b) are images corresponding to planes a' and b' respectively, as indicated in the ray diagram. At even greater deformation of the PDMS film, (c) and (d) are captured at planes a' and b' respectively.

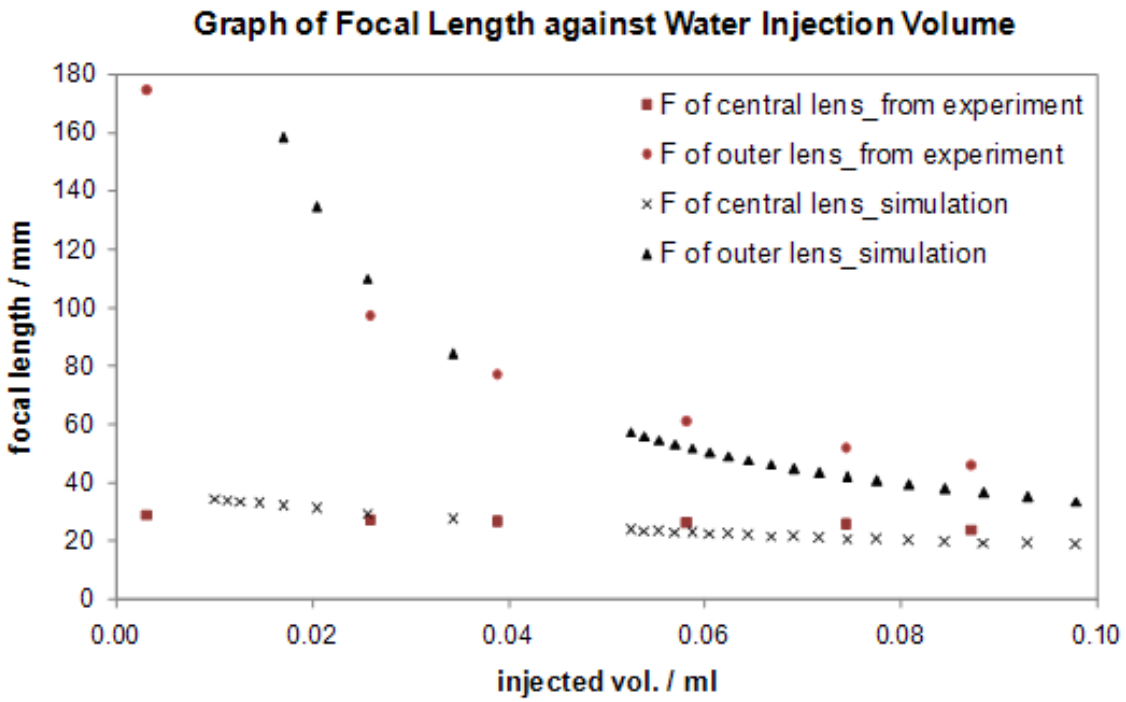

Figure 4. 10: Experimental results demonstrating the central and peripheral lenses' tunability are superimposed on the simulation results.

Figure 4.9 shows a ray diagram of a tunable double lens. It can be seen that at plane a' where the focus of the central lens is, the focal spot will be surrounded by a ring of light which is contributed by light that passed through the peripheral lens. This is captured by the CCD as shown in Figure 4.9(a). In contrast, further away from the lens device, the focus of the peripheral lens is within the cone of light belongs to the central lens. But since the light from the central lens must have attenuated at such a big distance from the lens device, the intensity is comparatively much lower than that of the focal spot of the peripheral lens. Thus, it is expected that a bright focal spot will be observed within a dim disk of light in plane b'. Again, this is verified by Figure 4.9(b) although the disk of light could be difficult to observe due to its low intensity.

When additional water is pumped in to decrease the radius of curvature of the PDMS film, the focal lengths of the central and peripheral lens are decreased and closer to each other. This is evident in the graph shown in Figure 4. 10. Because of this effect,

the smaller ring of light surrounding the focal spot at plane a' is intensified and this is manifested in Figure 4.9(d). However, the extremely dim disk of light which the focus of the peripheral lens lies in is still difficult to identify in Figure 4.9(c).

Figure 4. 10 is a graph that summarizes the experimental results of the tunability of the double lens. The focal lengths of the outer and central lens are able to be tuned from 174 mm to 36 mm and 29 mm to 23 mm respectively. This means the difference in focal lengths between the two lenses can be varied from 145 mm to 13 mm.

Simulation results using a ray-tracing program known as ZEMAX is superimposed on the experimental data. The designed dimensions associated with the lens device and the optical properties of the materials that made up the lens are keyed into the program to derive the simulation results. The proximity between the two is strong evidence that the combination of diamond turning and soft lithography is capable of producing a functional device that performs close to designed values.

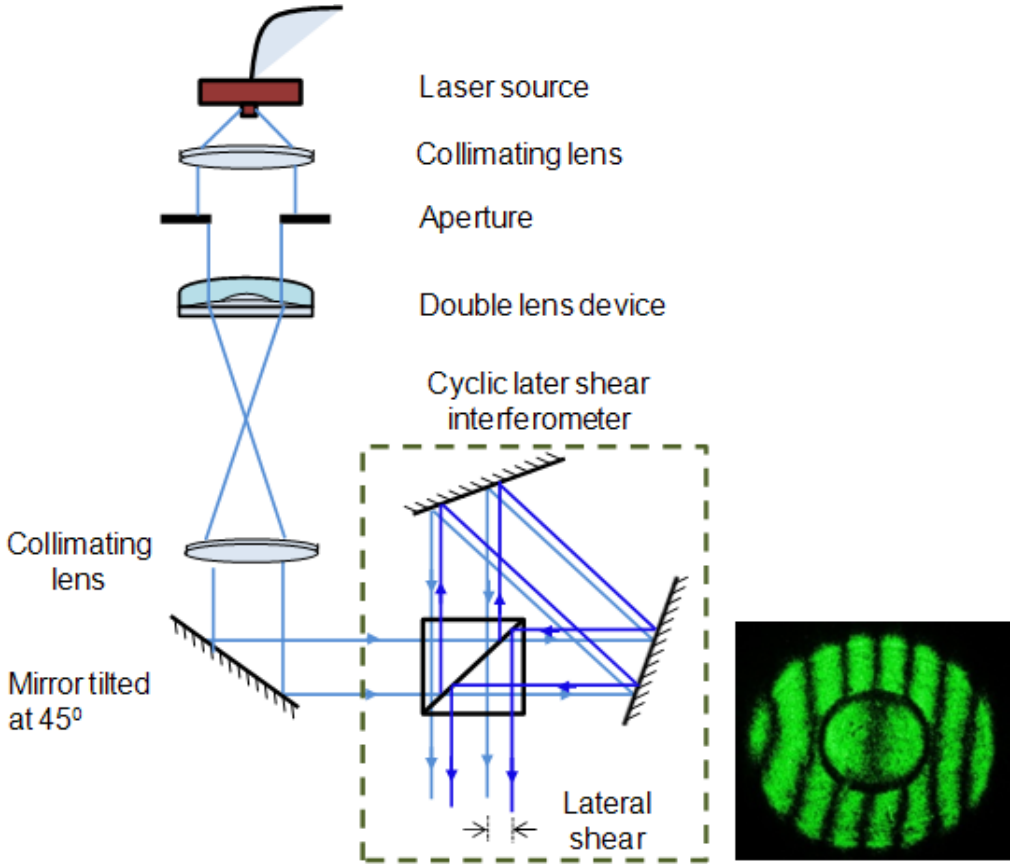

Figure 4.11: Lateral shear interferometer used to demonstrate the focal length difference between the central and peripheral lens.

To have a better idea of the characteristics of the wavefront, lateral shear interferograms of the double lens at a point close to the focal length of the central lens is shown in Figure 4.11. It can be clearly observed that the density of fringes of the peripheral regions is greater than that at the central region. This corresponds to the fact that the position where the interferogram is obtained is closer to the focus of the central lens than that of the outer lens.

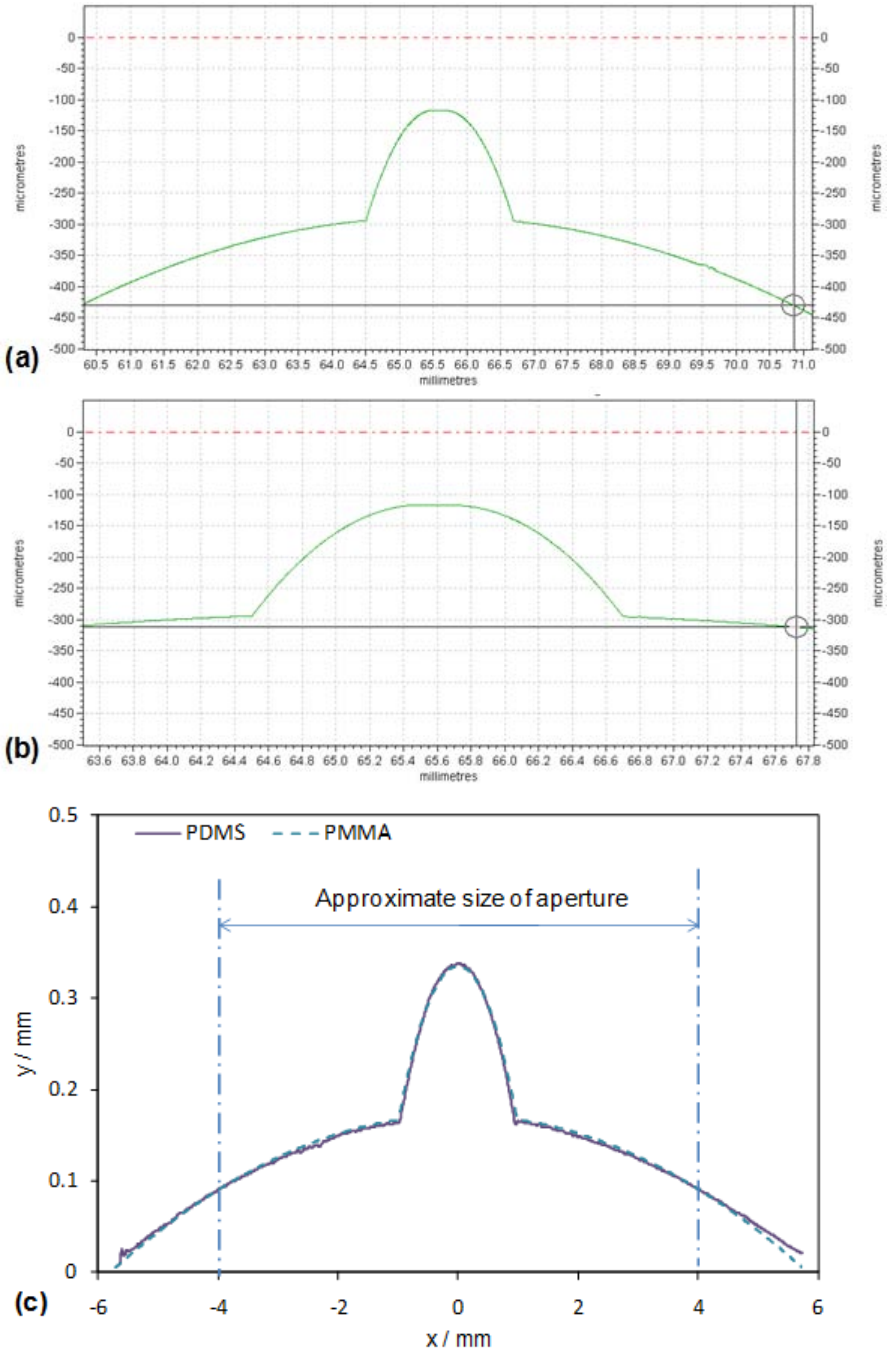

Figure 4.12: (a) A surface profile of the double lens is obtained with a mechanical tip profiler. (b) Zooming in, it is clear that the boundary which the two lenses meet is clearly defined. (c) A comparison of the profiles of a PMMA mould and a PDMS lens device shows that soft lithography is a reliable replication process.

Because the diameter of the double focus lens is 12mm, it is too large to be captured by the white light interferometer. Instead, the lens profile of the diamond turned structure is measured by using Taylor Hobson Form Talysurf contact profilometer and the results are shown in Figure 4.12. It is apparent in the plot that the surface of

the double lens is smooth and the dimensions adhere closely to designed values. In addition, the boundary where the central and outer lenses meet is clearly defined, despite the large differences in curvatures. This is something that is difficult to realize with those more common methods such as grey scale photolithography or thermal reflow techniques.

Taking a step further, the profiles of the diamond turned PMMA mould and the PDMS lens device obtained after two cycles of soft lithography are compared. Because raw data is not able to be exported from Taylor Hobson for further processing, a Mitutoyo Form Tracer CS5000 is used instead. The profiles of the PMMA mould and PMDS lens device are measured and superimposed on the same graph for easy comparison. From Figure 4.12 (c) it is apparent that the two profiles are highly similar, other than a portion of the peripheral regions the deviation from the profile of the mould is more significant. However, that would not affect the experimental results because the aperture used limits the working area to be approximately within 8 mm diameter where the profile follows the designed values very closely. Thus, it is verified that the two cycles of soft lithography will not compromise the profile and optical performance of the PDMS lens device. In fact, the rapid prototyping technique is a reliable fabrication method of reducing the effective cost and time of fabrication per lens device.

Chapter 5. Liquid Tunable Lens to Minimize Spherical Aberration

5.1 Introduction to Spherical Aberration

First order optics is mathematically simple to process and it would be useful tool to get a quick assessment of how an optical system would behave. However, as compared to first order optics, higher order optics provides a better approximation to an optical system and it would be an indispensable tool when developing better imaging systems. The difference between first order optics and higher order optics is that the former typically assumes that the emerging wavefront segment from the paraxial rays is perfectly spherical. This does not hold true when the periphery of an imaging lens is taken into account.

Usually, third order optics is sufficiently capable of handling the most commonly encountered aberrations, referred to as Seidel aberrations. They include spherical aberrations, coma, astigmatism, distortion and curvature of field. Unlike chromatic aberration, these Seidel aberrations occur even when monochromatic illumination is used. Different Seidel aberrations result in different forms of imaging imperfections but in this section, the focus will be on spherical aberration.

Spherical aberration refers to the phenomenon that occurs when peripheral optical rays that make large angles with respect to the optical axis of the imaging lens have focal lengths that differ from the paraxial rays. This is illustrated in Figure 5.1. Spherical aberration is present even if the lens is a perfect sphere. It will be less apparent if an aperture is small enough to just allow paraxial rays to pass through the system. However, by blocking out light from the peripheral regions, the image formed will be much dimmer.

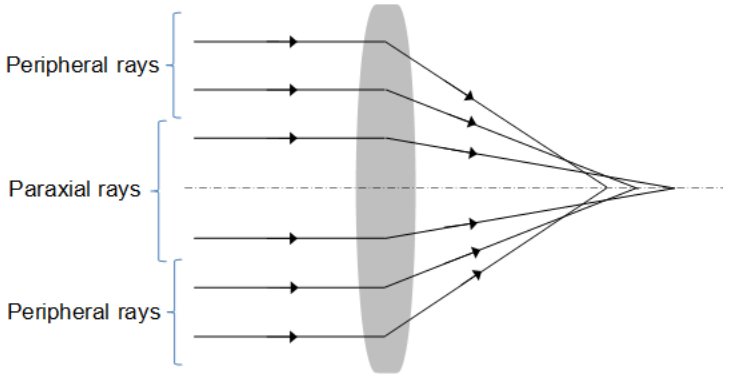

Figure 5.1: The central rays focus at different points from peripheral rays.

The most common and conventional way of achieving that is through proper lens design. For a certain focal length, the radius of curvatures of the front and back surfaces of a lens can be varied. Different combinations of the radius of curvatures can result in varying spherical aberration. Computer simulations and ray tracing programs could help determine the lens design that gives minimal spherical aberration. Alternatively, aspherical lenses could be designed to bring the peripheral rays to the same focal spot as the paraxial rays. However, since aspherical lenses are more difficult to produce, they are generally more expensive than lenses that consist of spherical surfaces.

In the published literature, there are a number of relatively less common ways that have been developed to reduce spherical aberrations. Through the use of transfer functions computations, it has been demonstrated that annular apertures could be designed to reduce spherical aberrations [66]. As annular apertures tend to block out a large portion of the light, a variation of annular apertures known as annular apodizers was proposed [67]. Instead of having an opaque central region, apodizers use shade masks that partially blocks out light instead. Using similar transfer function computation techniques and computer simulations, these apodizers also show that they are capable of reducing spherical aberrations. Apart from these, a research

team that published a work about the design of diffractive/refractive hybrid lens revealed another way to counter spherical aberration. In that work, the diffractive lens was holographically recorded by interfering two spherical wavefronts. With proper selection of the radiuses of curvatures of those two spherical wavefronts, it is possible to reduce spherical aberration [68].

Since spherical aberration is essentially the result of a non-spherical wavefront that could not produce a perfect image point, theoretically, it can be minimized by correcting the imperfect wavefront. The modification of wavefront could be achieved by passing the wavefront through a certain medium with a carefully crafted topology of varying surface height. As the incoming light passes through it, different segments of the light will experience different phase delays due to the varying thickness. As a result, the parts of wavefront that deviated from spherical shape will be eventually corrected. Thus, it should be apparent that the surface profile required to correct a wavefront depends on the wavefront itself. Generally, aspherical lenses have been commonly used to correct spherical aberration [69].

Bulk aspherical lens are usually given smooth surface finish by grinding, lapping and polishing on a CNC machine. These systems usually incorporate computer algorithms that can take surface profile measurements locally before performing corrective grinding and lapping in cycles until a satisfactory surface is obtained. Because grinding could easily result in surface cracks if not well controlled, there are different types of grinding developed to suit the needs of different kinds of materials and lenses. They include diamond grinding, ductile grinding and semi-ductile grinding [70]. These methods may not work as well with small lenses due to little contact surface. Thus, ultra precision diamond turning would be a much better option to fabricate miniature lenses as they generally produce good surface quality that does not require further polishing.

5.2 Design of Aspherical Surface to Minimize Spherical Aberration

Referring to Figure 3.16, it is known that spherical aberration is present if rings and lobes appear in the lateral shear interferograms obtained instead of straight lines. Looking at the inset interferograms of Figure 3.17, spherical aberration is clearly present in the liquid tunable lens device. The deformation of the PDMS film is likely to have played a large part in causing the spherical aberration.

Thus, in this work, an aspherical surface that serves to cancel the spherical aberration caused by a liquid tunable conventional spherical lens is developed. Although it is reasonable to assume that the PDMS film deforms spherically due to the uniform liquid pressure applies, the boundary condition, which is a result of the film being bonded to the slab, makes it non-spherical near the boundary. At the circumference, the boundary condition resembles a clamped boundary condition. Therefore, instead of being at the angle that is tangential to the spherical deformation, the film is horizontal at the immediate vicinity of the boundary. This implies that despite the uniform liquid pressure, the deformation of the PDMS film deviates from a spherical shape near the boundary. Typically, the spherical shape occupies about 70 to 80% across the diameter. This is illustrated in Figure 5.2.

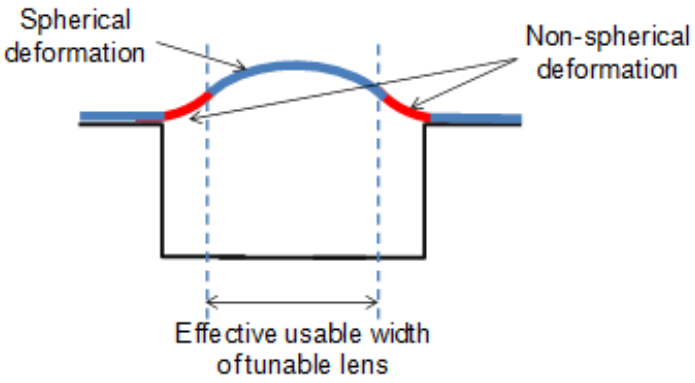

Figure 5.2: The spherical deformation of the PDMS film occupies about 70 to 80% across its diameter.

The designed aspherical lens profile works best at a certain focal length of the liquid lens. At focal length shorter than the designed value, the spherical aberration could only be partially compensated. On the other hand, the resulting spherical aberration of the tunable aspherical lens is greater than that of the conventional lens at focal lengths longer than the designed values. Qualitative speaking, the spherical lens itself has a fixed spherical aberration that is opposite in sign to that of the PDMS film. At small focal lengths, the spherical aberration of the PDMS film is large and is partially cancelled by the aspherical lens. At the design focal length, the magnitude of the spherical aberration of the PDMS film and the aspherical lens is equal. Thus, they cancelled out exactly. As the focal length reduces further, the spherical aberration of the PDMS film is very small but the aspherical lens still contributes a fixed aberration to the lens device. Hence, there is a detectable deterioration in optical performance at this focal range. Figure 5.3 gives a graphical comparison of an uncorrected and corrected liquid tunable lens structure.

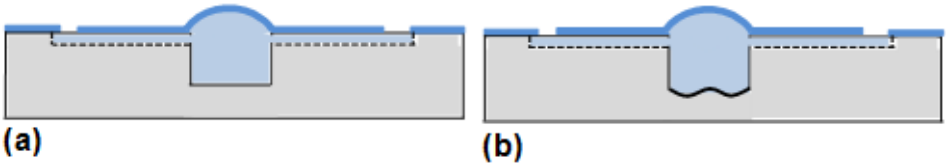

Figure 5.3: (a) A conventional tunable lens has spherical aberration that is mainly contributed by the spherical deformation of the PDMS film. (b) The aspherical lens profile on the lens cavity could counter the spherical aberration.

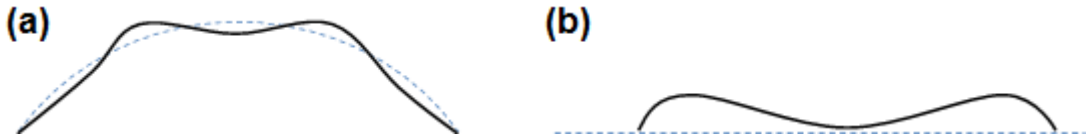

Figure 5.4: (a) A single aspheric lens profile that can be described as a polynomial superimposed on a spherical shape. (b) The profile required for the device in this work is simply a polynomial as the deformable PDMS film serves as the spherical shape.

Having given a qualitative description of the working principles of the tunable aspherical lens device, the method to calculate the aspherical lens profile will be described.

The standard equation of an aspherical lens is given as follows:

$$y(x) = \frac{C_1 x^2}{1 + \sqrt{1 + C_2 x^2}} + \sum_{0}^{\infty} A_n x^{2n} \tag{32}$$

The equation gives a single profile that is essentially a polynomial profile (described by the summation term) superimposed on a spherical one (described by the first term), as illustrated in Figure 5.4(a). The equation has to be modified to be applicable to our device because instead of a single aspheric, the tunable lens device is separated into a spherical PDMS film deformation and a polynomial profile at the

bottom surface of the lens cavity. For comparison, the aspherical surface required is given in Figure 5.4(b). Because of this, C_1 is set to be zero. Ignoring the higher order terms that are insignificantly small, the modified equation required is given as follows.

$$y(x) = A_o + A_1 x^2 + A_2 x^4 + A_3 x^6 \tag{33}$$

Based on the geometry and material properties of the lens device, a commercially available ray tracing software package, ZEMAX^{TM}, is able to calculate the optimised aspherical lens profile that is required. The fixed parameters that have to be entered into a ray tracing program are listed below.

- Material and refractive index of lens device: PDMS (1.41) and distilled water (1.33)
- Thickness of PDMS below the lens cavity: 5 mm
- Height of lens cavity: 150.7 µm
- Diameter of lens cavity: 10 mm
- Design focal length: 20 mm

Using iteration method, the ray tracing program finds the optimized coefficient A_1 while the other coefficients are initially set to arbitrary values. When the optimized A_1 is calculated, the calculation is repeated for A_2 and so on until the complete polynomial is calculated. The final equation that is derived is given as follows.

$$y(x) = 0.061769x^2 - 3.22566 \times 10^{-3}x^4 + 5.376492 \times 10^{-6}x^6 + 0.387805 \tag{34}$$

Diamond turning is used to produce this lens profile on PMMA and the similar fabrication process used for earlier devices is again utilized to fabricate this tunable aspherical lens. Next, the experimental results will be presented.

5.3 Experiments and Results: Spherical Aberration

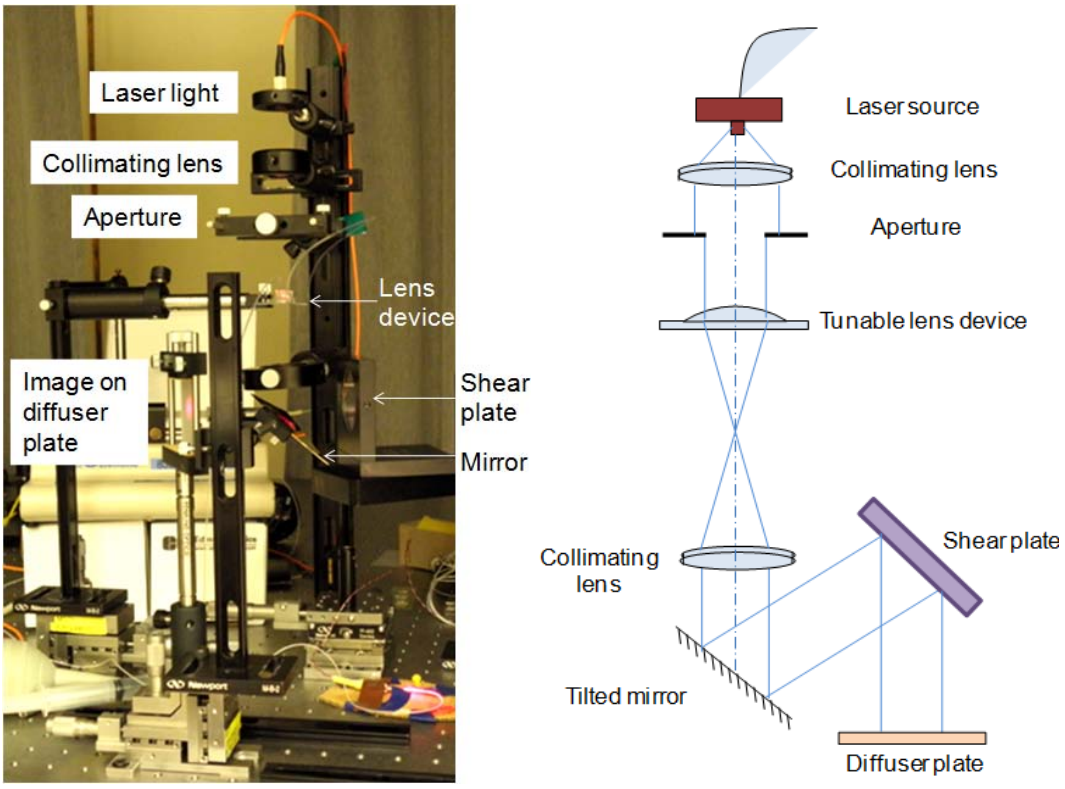

Figure 5.5: A photograph and a schematic of the experimental setup used to test the tunable aspherical lens.

In the previous chapters, a cyclic lateral shear interferometer is used to test the tunable lens devices that have 5mm diameter. However, it is found that it is not as easy to observe the fringes of the shear interferogram of a 5mm aspherical lens. Thus, the diameter of this aspherical lens is made to be 10mm. This results in the interferogram to be too big to be captured by the mirrors used to build the cyclic lateral shear interferometer. To overcome this problem, an off-the-shelf lateral shear plate with a large working area is used instead. The working principles of the shear

plate, as well as the interpretation of the interferograms obtained are similar to that of the cyclic shear interferometer. A photograph and a schematic of the experimental setup are shown in Figure 5.5.

The interferograms captured at different working focal lengths are shown in Figure 5.6. It can be observed that the fringes of the interferograms are comparatively straight at focal lengths of 24mm and 23 mm. As the focal length of the lens devices decreases, the lobes become increasingly obvious. The central fringes of the interferogram are also increasingly curved. These observations verified that the aspherical lens has significantly reduced spherical aberration at focal lengths of approximately 23 mm while the aberration compensation was not as complete at shorter wavelengths. This agrees well with the optical model which the design of the lens is based on.

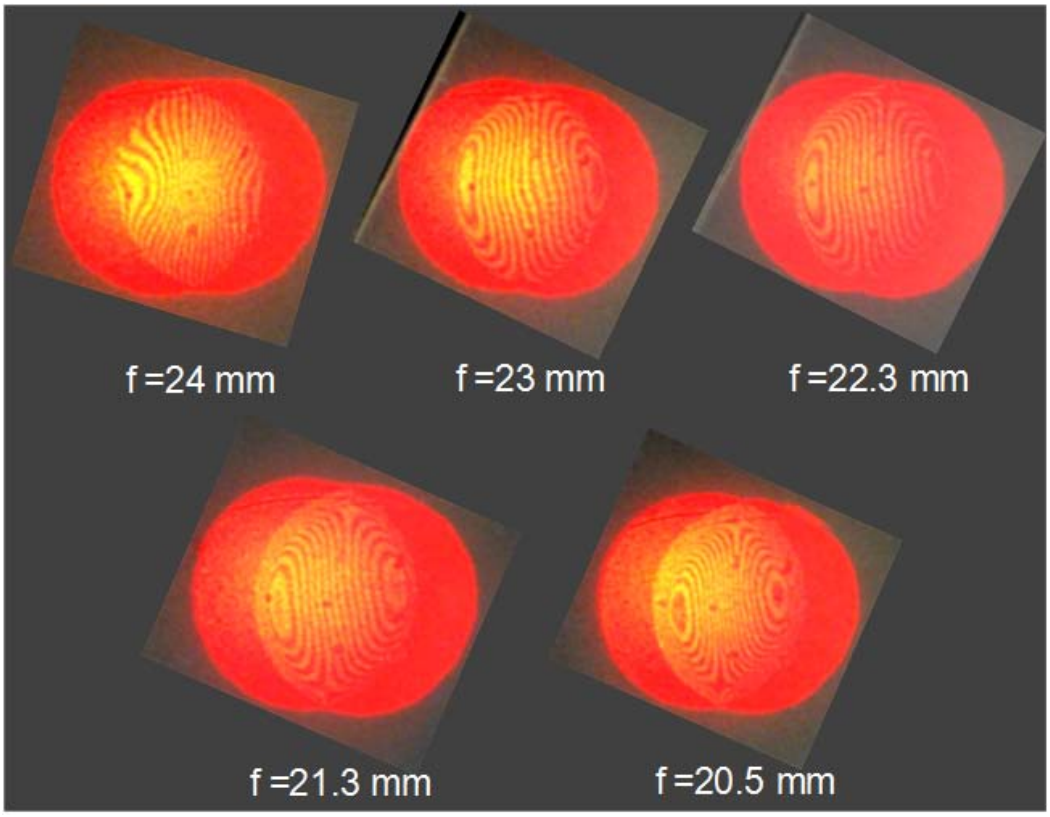

Figure 5.6: Lateral shear interferograms of the tunable aspherical lens at different wavelengths.

Chapter 6. Liquid Tunable Toroidal Lens

6.1 Introduction to Depth of focus

Based on different criteria use to resolve image points, depth of focus (DOF) can be defined differently. Using Rayleigh's criterion, two image points are considered resolvable if the highest intensity of light between them remains below $8/\pi^2$ of the maximum intensity found at the center of the airy disk of each spot. If Sparrow condition is used instead, the closest that two resolvable image point can come to each other is when the resulting intensity between them is not higher than the maximum intensity of their airy disks. Despite the different definitions, DOF of a lens can be loosely understood as the traverse range which an image remains clear. Conventional lenses often have to trade off DOF for a higher resolution or vice versa. The higher the resolution, the smaller the minimum resolvable feature size and the bigger the required numerical aperture. On the other hand, a higher DOF will require a smaller numerical aperture and hence the trade off.

There are a number of ways to overcome this problem. Axicons which are known to be capable of produce non-diffracting beams that could propagate in free space for long distances without significant attenuation [71]. Because this beam of light is very narrow, the DOF and resolution are very much enhanced too. One shortcoming of axicons is they have low light efficiency. Secondly, it is generally difficult to fabricate axicons, which can be conical or logarithm in shape, using standard fabrication methods.

Similarly, computer generated holograms capable of producing pseudo non-diffracting Bessel beams are capable of increasing DOF [72]. However, they are

susceptible to chromatic aberration as their performance is sensitive to the wavelength of the light source.

Annular apertures and annular lenses have also been reported to be able to extend the DOF. However, they suffer from low optical power and decreased contrast at the edges of the images due to brighter outer diffraction rings [73]. Optical apodizers that have multiple rings spaced apart at π phase variations to increase the focal depths have also been reported. However, like annular apertures, the rings which obstruct portion of the illumination often results in decreased transverse resolution and low optical power [74].

There are also works that exploited the Sparrow condition for resolving image points to enhance focal depth by constructing a quasi-bifocus lens. The lens has two different focuses at close proximity on the same optical axis. Because they are positioned so close together, the two are practically non-resolvable. Therefore, the lens is termed as a quasi-bifocus lens. By having two non-resolvable focuses on the same optical axis, it would appear as if the DOF is increased [75].

High DOF is important for many industries and research studies. For instance, biologist who needs to study mobile micro-organisms often face the problem of poor imaging qualities because the mobile objects are constantly moving in and out of focus. A microscope with extended DOF could allow a certain amount of mobility while preserving imaging clarity. In optical data storage applications, focal spots are continually becoming smaller as bigger numerical aperture are needed to achieve higher storage density, As a result, the DOF is also continually being compromised. A short DOF leads to greater difficulty in tracking data. Similarly, the quality of lithography could be compromised when the DOF limits the smallest feature size that

can be fabricated accurately. Thus, it is pertinent to find methods to keep a sufficient DOF for various applications.

6.2 Design of Diffractive Toroidal Lens

In this work, the working principle of the toroidal lens device is somewhat similar to the quasi-bifocus lens. Instead of having two focuses along the same optical axis, the toroidal lens focuses to a ring. If the diameter of the ring is brought to within the Rayleigh's limit, it will appear to be a focal spot since the separation will be optically unresolvable. The design of this toroidal lens is modified from the Fresnel lens design discussed earlier in chapter 3. The focusing capabilities are provided by those blazed annular rings for maximum efficiency and compactness. The diameter of the ring of focus, regardless if it is resolvable or not, is determined by the distance the original optical axis of Fresnel lens is offset from the center. A comparison between a toroidal lens and a Fresnel lens is shown in Figure 6.1.

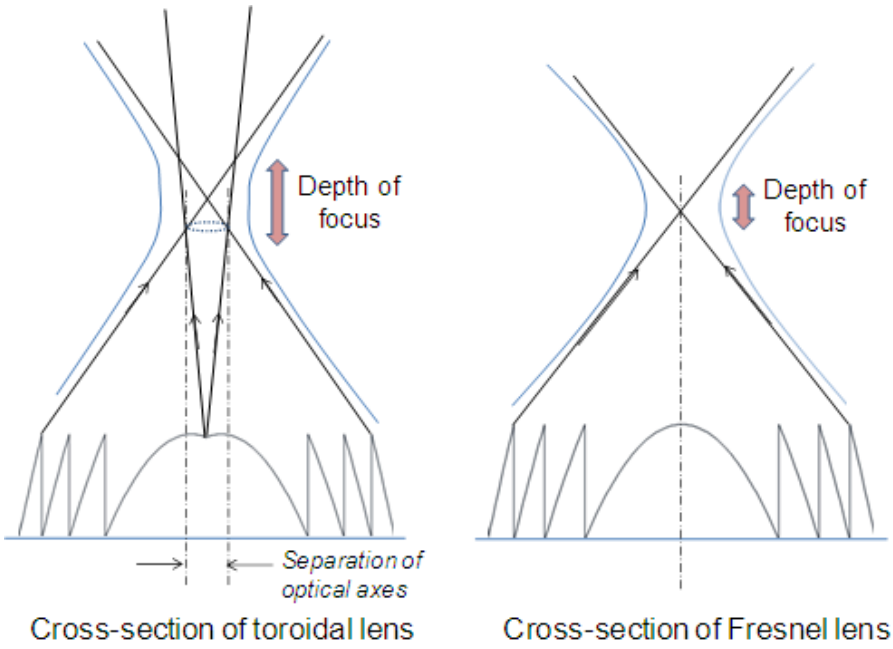

Figure 6.1: The toroidal lens is a Fresnel lens with an off-centred optical axis. Toroidal lens could focus to a ring while the Fresnel lens focus to a spot.

Maximum diameter of the ring before it becomes resolvable = $1.22\,\lambda/NA$

$\approx 1.22\,f\lambda/D$

Where f is the focal length, D is the diameter of the lens aperture.

Referring to the design parameters used for Fresnel lens as described in chapter 3,

f = 15 mm

λ = 0.5892 μm

D = 4 mm

⇨ Max. diameter = $(1.22 \times 15 \times 0.5892)/4$

= 2.696 μm

Since the focal length, f, is variable, the above value is used could only be used to gauge the range which the optical axis of the toroidal lens should be separated. Moreover, the slope at the central region of the Fresnel lens is so gentle that it is horizontal for a few microns. Therefore, the separation of the optical axis might need to be greater than the calculated value before the focal ring could be detectable. Based on these reasons, a toroidal lens with its optical axis separated by a distance of 5 μm is fabricated and tested.

6.2 Experiments and Results: Measurement of Spot Sizes

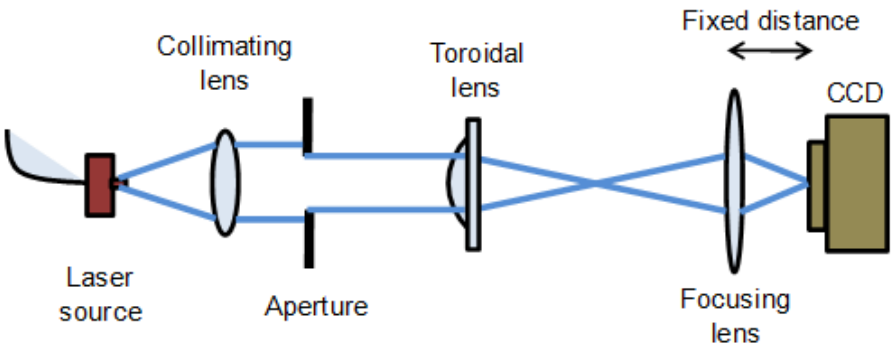

Figure 6.2: Schematic of the experiment setup used to test the toroidal lens.

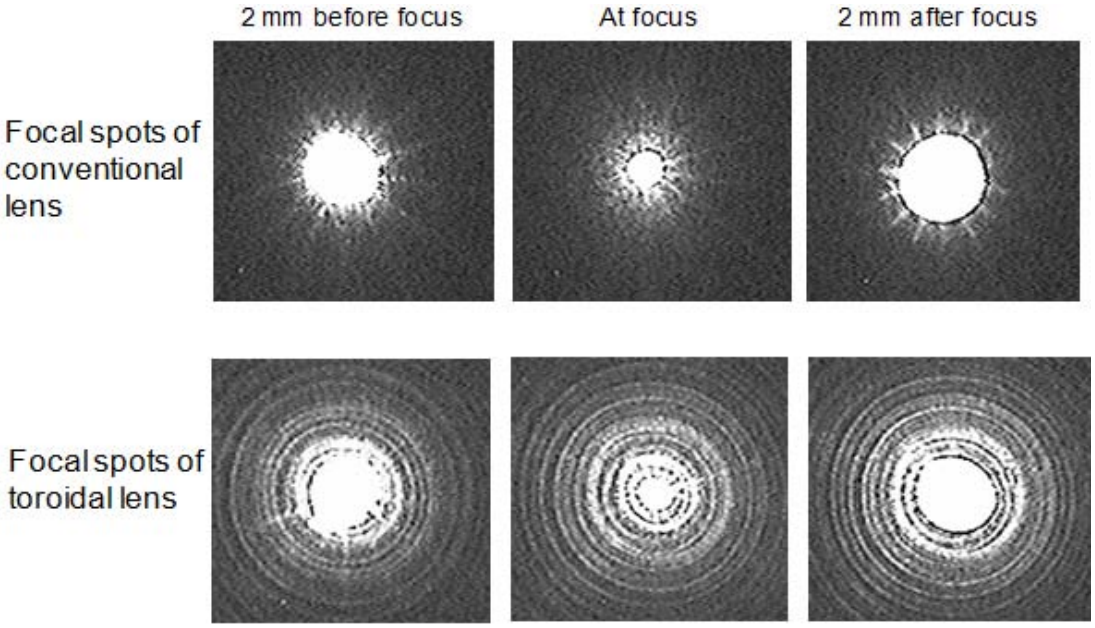

Figure 6.3: The representative light spots outside focus, at focus and inside focus of the conventional and toroidal lenses are shown here.

Figure 6.4: Intensity map of a spot image captured by the CCD. The corresponding spot size is identified easily on this graph.

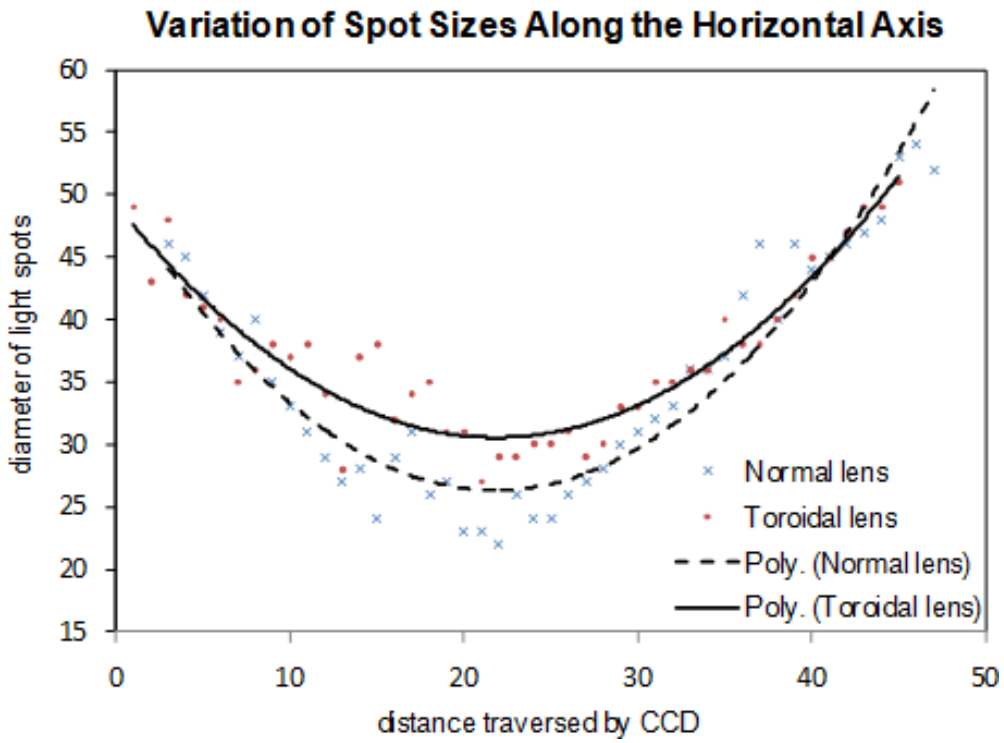

Figure 6.5: Graph shows the variation of spot sizes of the normal and toroidal lenses along the horizontal which the CCD traversed. Both the vertical and horizontal axis are in arbitrary units.

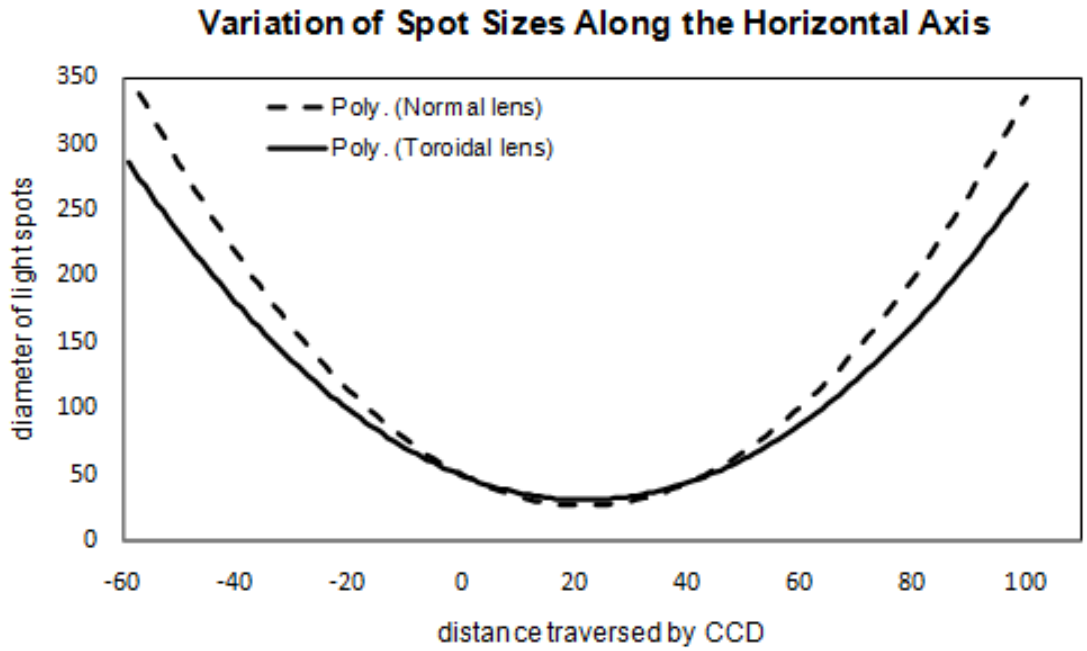

Figure 6.6: Extending the polynomial lines derived from the experimental results, it can be seen that the spot sizes of the normal lens are much bigger than that of toroidal lens at positions away from the minimum beam waist.

Figure 6.2 is a schematic of the experiment setup used to test the toroidal lens. It is similar to the one used to test the double focusing lens. The CCD is placed at a distance that is twice the focal length of the focusing lens before it to obtain a 1:1 image ratio. By moving horizontally, the CCD captures the light spots at various positions near the vicinity of the focus, from 2 mm before the focus to 2 mm after the focus. Each image is captured at 100 µm intervals.

Figure 6.3 shows representative CCD images of the light spots of the conventional lens and toroidal lens at three positions, namely 2 mm before reaching the focus, at the focus and 2mm away from the focus. The relative spot sizes are unchanged and it is clear that the light spots that are far from the focus are very much larger than at the focus for both lenses. Based on the captured grey scale images as shown in Figure 6.4, the spot size of each image is easily obtained. Tabulating the spot sizes of all the images captured, the change in sizes of the light spots along the 4 mm

traversed is computed. As a comparison, the change in spot sizes for a conventional tunable lens is tested with the same methodology as well.

The graph that summarizes the results of the spot size variances is shown in Figure 6.5. Two-degree polynomials are used to approximate the trend in the data sets for both lenses. As compared to the curve of the normal lens, the slope of the toroidal lens is clearly gentler. At the region near the minimum beam waist, the diameters of the focus spots of toroidal lens are generally larger than that of the normal lens. However, if the polynomials are extended to regions further away from the beam waist as shown in Figure 6.6, it can be seen that the diameters of the focus spots of the normal lens at those regions are much greater than that of toroidal lens. Thus, the slight decrease in resolution near the beam waist when toroidal lens is used is a worthwhile trade off for an increase in depth of focus and superior resolution at regions away from the beam waist. With reference to the schematic shown in Figure 6.1, the experimental results verified that toroidal lens indeed is capable of exhibiting extended depth of focus.

The graph shown in Figure 6.5 displayed a large variation within the data points. This could be caused by the bright outer rings that interfered with the central maximum spots. Therefore, modifications may have to be made to the experimental setup to avoid that. In addition, the design could be further improved and optimized by varying the separation of optical axes of the toroidal lens. The design of the current toroidal lens did not take into the account of the various aberrations present in the liquid toroidal lens, such as spherical aberration. Therefore, Rayleigh's condition might not be sufficient for the optimization of the geometry of the toroidal lens. Upon optimizing the separation of the optical axes of the toroidal lens, the curvature of the polynomial graph in Figure 6.6 will be much smaller. This would imply that the beam diameter of

the toroidal lens will stay small for a longer distance, giving a further increase in depth of focus with much lesser trade off in imaging resolution.

Chapter 7. Conclusion and Future Work

7.1 Conclusion

- Combining ultra-precision single point diamond turning and soft lithography, various types of liquid tunable lenses have been successfully fabricated and tested. This fabrication process allows the fabrication of 3-D optical components that have a wide range of aspect ratios and order of dimensions, while preserving the excellent surface quality required of optical components. This is something that is difficult to achieve with lithography and etching techniques.
- The fabricated liquid tunable diffractive/refractive hybrid lens is able to minimize chromatic aberration within the visible spectrum, while achieving a high tunability of approximately 20 mm.
- A liquid tunable double-focusing lens was fabricated. As it could focus to two different depths simultaneously, it could be used to increase the speed which data could be retrieved or recorded optically.
- A liquid tunable aspherical lens that can reduce spherical aberration further demonstrates the versatility of diamond turning in producing rotationally symmetrical 3-D surface relief for optical purposes.
- A liquid tunable toroidal lens has been fabricated and experimentally verified to be capable of extending the depth of focus.
- Characterisation of the optical surfaces using white light interferometry, AFM and mechanical profiler has been carried out. Results show that the surface quality of the PMMA mold and the PDMS lens device are excellent and suitable for optical usage.
- Soft lithography, being a rapid prototyping process, has been shown to be useful in decreasing the average time and cost of fabricating a liquid tunable

lens device. The advantages of combining soft lithography with diamond turning have been clearly demonstrated through the ease of replicating multiple optical components from a single diamond-turned mold with high reliability.

7.2 Future Work

In the future, it is possible to build on this work to fabricate further improved optical components using the fabrication process developed. For instance, currently, the diffractive/refractive hybrid lens displayed significant spherical aberration despite being able to cancel chromatic aberration. Likewise, the aspherical lens is only able to improve on the spherical aberration but not chromatic aberration. Thus, future work could be done on fabricating a single aspherical diffractive lens profile to simultaneously reduce chromatic and spherical aberration. This would no doubt enhance the versatility and functionality of the lenses.

More extensive experimentation with the diffractive toroidal lens could also be performed. In addition to fabricating toroidal lens that focuses to an unresolvable to achieve extended DOF, as was done in this work, toroidal lenses that have much larger separation in optical axes could be experimented as well. Since this kind of lens could produce an optical effect that is similar to an annular aperture which has been extensively studied to show promising abilities to reduce spherical aberration and extend DOF, it is possible that the toroidal lens could have these benefits. Apart from those benefits, the blazed diffractive surfaces of the toroidal lens enabled high efficiency and the entire beam of incoming light could be utilized. Therefore, it is also possible that these toroidal lenses will be able to avoid the well known problems brought on by annular apertures such as poor light efficiency. Due to the unique

transfer function associated with the diffractive toroidal lens, it might be useful for special optical purposes such as being able to give edges of images enhanced clarity.

Lastly, a more comprehensive study on the relationship between the resolution and depth of focus of toroidal lenses could be carried out. An addition of a quantitative analysis would complement the qualitative observation of the general characteristics of toroidal lens.

List of Publications

[1] **H.M. Leung**, H.B. Yu, G.Y. Zhou, A.S. Kumar, and F.S. Chau, Development of Liquid Tunable Diffractive/Refractive Hybrid Lens Based on Combination of Diamond Turning and Soft Lithography. Advanced Materials Research 74, NEMS/MEMS Technology and Devices (2009) 85-88.

[2] H.B. Yu, G.Y. Zhou, F.K. Chau, F.W. Lee, S.H. Wang, and **H.M. Leung**, A liquid-filled tunable double-focus microlens. Optics Express 17 (2009) 4782-4790.

[3] G. Zhou, **H.M. Leung**, H.B. Yu, A.S. Kumar, F.S. Chau, Liquid tunable diffractive/refractive hybrid lens. Optics Letters 34 (2009) 2793-2795.

[4] **H.M. Leung**, G. Zhou, H. Yu, F.S. Chau, and K. A. Senthil, Liquid Tunable Double Focus Lens Fabricated with Diamond Cutting and Soft lithography. Applied Optics 48 (2009) 5733-5740

[5] **H.M. Leung**, G. Zhou, H. Yu, F.S. Chau, and K. A. Senthil, Diamond turning and soft lithography processes for liquid tunable lenses. Journal of Micromechanics and Microengineering 20 (2009) *025021*

[6] H. Yu, G. Zhou, **H.M. Leung**, F. S. Chau, and A. S. Kumar, "Tunable liquid-filled lens integrated with aspherical surface for spherical aberration compensation," Optics Express (2009). *(Paper accepted)*

References

[1] S. Sato, A. Sugiyama, and R. Sato, "Variable-focus liquid-crystal Fresnel lens," *Japanese Journal of Applied Physics, Part 2 (Letters),* vol. 24, pp. 626-8, 1985.

[2] S. Kuiper and B. H. W. Hendriks, "Variable-focus liquid lens for miniature cameras," *Applied Physics Letters,* vol. 85, pp. 1128-30, 2004.

[3] F. Krogmann, W. Monch, and H. Zappe, "A MEMS-based variable micro-lens system," *Journal of Optics A: Pure and Applied Optics,* vol. 8, pp. 330-6, 2006.

[4] H. Suz-Kai and L. Gwo-Bin, "A controllable micro-lens structure for bio-analytical applications," in *2007 20th IEEE International Conference on Micro Electro Mechanical Systems - MEMS '07, 21-25 Jan. 2007*, Piscataway, NJ, USA, 2007, pp. 763-6.

[5] H. Yu, G. Zhou, S. Chau Fook, F. Lee, and S. Wang, "A tunable Shack-Hartmann wavefront sensor based on a liquid-filled microlens array," *Journal of Micromechanics and Microengineering,* vol. 18, p. 105017 (8 pp.), 2008.

[6] Z. De-Ying, V. Lien, Y. Berdichevsky, C. Jaehyuck, and L. Yu-Hwa, "Fluidic adaptive lens with high focal length tunability," *Applied Physics Letters,* vol. 82, pp. 3171-2, 2003.

[7] J. Chen, W. Weisong, F. Ji, and K. Varahramyan, "Variable-focusing microlens with microfluidic chip," *Journal of Micromechanics and Microengineering,* vol. 14, pp. 675-80, 2004.

[8] R. Hongwen and W. Shin-Tson, "Variable-focus liquid lens by changing aperture," *Applied Physics Letters,* vol. 86, pp. 211107-1, 2005.

[9] L. Choon-Sup and H. Chul-Hi, "A novel refractive silicon microlens array using bulk micromachining technology," Piscataway, NJ, USA, 2000, pp. 87-8.

[10] J. Vila-Comamala, X. Borrise, F. Perez-Murano, J. Campos, and S. Ferrer, "Nanofabrication of Fresnel zone plate lenses for X-ray optics," *Microelectronic Engineering,* vol. 83, pp. 1355-9, 2006.

[11] J. D. J. Stigliani, R. A. J. Mittra, and R. G. SemOnin, "Resolving Power of a Zone Plate," *J. Opt. Soc. Am.,* vol. 57, pp. 610-611, 1967.

[12] H. Shih-Yu, L. Che-Ping, H. Yang, and C. Ying-Pin, "Optimal design using thermal reflow and caulking for fabrication of gapless microlens array mold inserts," *Optical Engineering,* vol. 46, pp. 43402-1, 2007.

[13] W. Moench and H. Zappe, "Fabrication and testing of micro-lens arrays by all-liquid techniques," *Journal of Optics A: Pure and Applied Optics,* vol. 6, pp. 330-7, 2004.

[14] C. J. Li and S. Y. Li, "To improve workpiece roundness in precision diamond turning by in situ measurement and repetitive control," *Mechatronics,* vol. 6, pp. 523-535, 1996.

[15] Y. Okazaki, "Micro-positioning tool post using a piezoelectric actuator for diamond turning machines," *Precision Engineering,* vol. 12, pp. 151-156, 1990.

[16] J. D. Rasmussen, T. C. Tsao, R. D. Hanson, and S. G. Kapoor, "Dynamic variable depth of cut machining using piezoelectric actuators," *International Journal of Machine Tools & Manufacture,* vol. 34, pp. 379-392, 1994.

[17] A. Y. Yi, H. Chunning, F. Klocke, C. Brecher, G. Pongs, M. Winterschladen, A. Demmer, S. Lange, T. Bergs, M. Merz, and F. Niehaus, "Development of a compression molding process for three-dimensional tailored free-form glass optics," *Applied Optics,* vol. 45, pp. 6511-18, 2006.

[18] A. Y. Yi and L. Li, "Design and fabrication of a microlens array by use of a slow tool servo," *Optics Letters,* vol. 30, pp. 1707-9, 2005.

[19] J. Kohlscheen, H. R. Stock, and P. Mayr, "Tailoring of diamond machinable coating materials," *Precision Engineering,* vol. 26, pp. 175-182, 2002.

[20] T. P. Leung, W. B. Lee, and X. M. Lu, "Diamond turning of silicon substrates in ductile-regime," *Journal of Materials Processing Technology,* vol. 73, pp. 42-8, 1998.

[21] D. Lee, M. Wells, C. J. Dickson, P. Shore, and P. Morantz, "Development of diamond machined mirror arrays for integral field spectroscopy," USA, 2006, pp. 62731-1.

[22] K. S. Chon, Y. Namba, and K.-H. Yoon, "Precision machining of electroless nickel mandrel and fabrication of replicated mirrors for a soft X-ray microscope," *JSME International Journal, Series C: Mechanical Systems, Machine Elements and Manufacturing,* vol. 49, pp. 56-62, 2006.

[23] C. C. A. Chen, C. Chien-Ming, and C. Jr-Rung, "Toolpath generation for diamond shaping of aspheric lens array," *Journal of Materials Processing Tech.,* vol. 192-193, pp. 194-9, 2007.

[24] T. Kawai, K. Sawada, and Y. Takeuchi, "Ultra-precision micro structuring by means of mechanical machining," Piscataway, NJ, USA, 2001, pp. 22-5.

[25] L. Lei, A. Y. Yi, H. Chunning, D. A. Grewell, A. Benatar, and C. Yang, "Fabrication of diffractive optics by use of slow tool servo diamond turning process," *Optical Engineering,* vol. 45, pp. 113401-1, 2006.

[26] K. M. Rezaur Rahman, M. Rahman, K. S. Neo, M. Sawa, and M. Maeda, "Microgrooving on electroless nickel plated materials using a single crystal diamond tool," *International Journal of Advanced Manufacturing Technology,* vol. 27, pp. 911-17, 2006.

[27] A. Q. Biddut, M. Rahman, K. S. Neo, K. M. Rezaur Rahman, M. Sawa, and Y. Maeda, "Performance of single crystal diamond tools with different rake angles during micro-grooving on electroless nickel plated die materials," *International Journal of Advanced Manufacturing Technology,* vol. 33, pp. 891-9, 2007.

[28] A. Malecki and A. Micek-Ilnicka, "Electroless nickel plating from acid bath," *Surface and Coatings Technology,* vol. 123, pp. 72-7, 2000.

[29] T. Yamaguchi, M. Higuchi, S. Shimada, and T. Kaneeda, "Tool life monitoring during the diamond turning of electroless Ni-P," *Precision Engineering,* vol. 31, pp. 196-201, 2007.

[30] W. Yun, B. Lai, A. A. Krasnoperova, E. Di Fabrizio, Z. Cai, F. Cerrina, Z. Chen, M. Gentili, and E. Gluskin, "Development of zone plates with a blazed profile for hard X-ray applications," *Review of Scientific Instruments,* vol. 70, pp. 3537-41, 1999.

[31] Y. Hirai, Y. Inamoto, K. Sugano, T. Tsuchiya, and O. Tabata, "Moving mask UV lithography for three-dimensional structuring," *Journal of Micromechanics and Microengineering,* vol. 17, pp. 199-206, 2007.

[32] M. R. Wang and S. Heng, "Laser direct-write gray-level mask and one-step etching for diffractive microlens fabrication," *Applied Optics,* vol. 37, pp. 7568-76, 1998.

[33] C. M. Waits, B. Morgan, M. Kastantin, and R. Ghodssi, "Microfabrication of 3D silicon MEMS structures using gray-scale lithography and deep reactive ion etching," *Sensors and Actuators A (Physical),* vol. 119, pp. 245-53, 2005.

[34] T. Shiono and K. Setsune, "Blazed reflection micro-Fresnel lenses fabricated by electron-beam writing and dry development," *Optics Letters,* vol. 15, pp. 84-6, 1990.

[35] W. H. Wong and E. Y. B. Pun, "Exposure characteristics and three-dimensional profiling of SU8C resist using electron beam lithography," *Journal of Vacuum Science & Technology B (Microelectronics and Nanometer Structures),* vol. 19, pp. 732-5, 2001.

[36] C. Marxer, C. Thio, M. A. Gretillat, N. F. de Rooij, R. Battig, O. Anthamatten, B. Valk, and P. Vogel, "Vertical mirrors fabricated by deep reactive ion etching for fiber-optic switching applications," *Journal of Microelectromechanical Systems,* vol. 6, pp. 277-85, 1997.

[37] Y. Xia and G. M. Whitesides, "Soft lithography." vol. 28 Palo Alto, CA, United States: Annual Reviews Inc, 1998, pp. 153-184.

[38] T.-K. Shih, C.-F. Chen, J.-R. Ho, and F.-T. Chuang, "Fabrication of PDMS (polydimethylsiloxane) microlens and diffuser using replica molding," *Microelectronic Engineering,* vol. 83, pp. 2499-2503, 2006.

[39] C. Thibault, C. Severac, E. Trevisiol, and C. Vieu, "Microtransfer molding of hydrophobic dendrimer," *Microelectronic Engineering,* vol. 83, pp. 1513-1516, 2006.

[40] C. Kuo-Shen, I. K. Lin, and K. Fu-Hsang, "Fabrication of 3D polymer microstructures using electron beam lithography and nanoimprinting technologies," *Journal of Micromechanics and Microengineering,* vol. 15, pp. 1894-903, 2005.

[41] D. K. Cai, A. Neyer, R. Kuckuk, and H. M. Heise, "Optical absorption in transparent PDMS materials applied for multimode waveguides fabrication," *Optical Materials,* vol. 30, pp. 1157-61, 2008.

[42] M. A. Unger, C. Hou-Pu, T. Thorsen, A. Scherer, and S. R. Queke, "Monolithic microfabricated valves and pumps by multilayer soft lithography," *Science,* vol. 288, pp. 113-16, 2000.

[43] Y. Hongbin, Z. Guangya, C. F. Siong, W. Shouhua, and L. Feiwen, "Novel polydimethylsiloxane (PDMS) based microchannel fabrication method for lab-on-a-chip application," *Sensors and Actuators, B: Chemical,* vol. 137, pp. 754-761, 2009.

[44] C. Kwon Su, Y. Namba, K. Kyong-Woo, K. Sunghoon, and Y. Kwon-Ha, "Fabrication of a soft X-ray microscope mirror using an epoxy replication method," *Optical Engineering,* vol. 47, pp. 1-6, 2008.

[45] V. K. Parashar, A. Sayah, M. Pfeffer, F. Schoch, J. Gobrecht, and M. A. M. Gijs, "Nano-replication of diffractive optical elements in sol-gel derived glasses," Lugano, Switzerland, 2003, pp. 710-719.

[46] A. C. Liou and R. H. Chen, "Injection molding of polymer micro- and sub-micron structures with high-aspect ratios," *International Journal of Advanced Manufacturing Technology,* vol. 28, pp. 1097-1103, 2006.

[47] F. Erlsmann, "Design of a plastic aspheric Fresnel lens with a spherical shape," *Optical Engineering,* vol. 36, pp. 988-91, 1997.

[48] A. Pramanik, K. S. Neo, M. Rahman, X. P. Li, M. Sawa, and Y. Maeda, "Cutting performance of diamond tools during ultra-precision turning of electroless-nickel plated die materials," Switzerland, 2003, pp. 308-13.

[49] Y. Tamagawa and Y. Ichioka, "Efficiency of blazed diffractive optics produced by diamond turning," *Optical Review,* vol. 5, pp. 291-4, 1998.

[50] L. Seok Woo and S. S. Lee, "Shrinkage ratio of PDMS and its alignment method for the wafer level process," *Microsystem Technologies,* vol. 14, pp. 205-8, 2008.

[51] J. R. Anderson, D. T. Chiu, R. J. Jackman, O. Chemiavskaya, J. C. McDonald, H. Wu, S. H. Whitesides, and G. M. Whitesides, "Fabrication of topologically complex three-dimensional microfluidic systems in PDMS by rapid prototyping," *Analytical Chemistry,* vol. 72, pp. 3158-3164, 2000.

[52] J.-S. Kim and D. R. Knapp, "Miniaturized multichannel electrospray ionization emitters on poly(dimethylsiloxane) microfluidic devices," *Electrophoresis,* vol. 22, pp. 3993-3999, 2001.

[53] Z. Guangya, V. J. Logeeswaran, F. E. H. Tay, and C. Fook Siong, "Diffraction grating scanner using a micromachined resonator," Piscataway, NJ, USA, 2004, pp. 45-8.

[54] M. A. Forastiere, S. Pelli, G. C. Righini, A. Verciani, C. Gomez-Reino, L. R. Staronski, and Z. Jaroszewicz, "Diffractive structures in integrated optics," New York, NY, USA, 1995, pp. 795-9.

[55] L. R. Lindvold, "Commercial aspects of diffractive optics," *DOPS-NYT,* vol. 16, pp. 62-6, 2001.

[56] B. Lai, W. B. Yun, D. Legnini, Y. Xiao, J. Chrzas, P. J. Viccaro, V. White, S. Bajikar, D. Denton, F. Cerrina, E. Di Fabrizio, M. Gentili, L. Grella, and M. Baciocchi, "Hard X-ray phase zone plate fabricated by lithographic techniques," *Applied Physics Letters,* vol. 61, pp. 1877-9, 1992.

[57] E. Hecht, *Optics*, 4th ed. Reading, Mass.: Addison-Wesley, 2002.

[58] M. Daimon and A. Masumura, "Measurement of the refractive index of distilled water from the near-infrared region to the ultraviolet region," *Applied Optics,* vol. 46, pp. 3811-20, 2007.

[59] *Optical shop testing*, 3rd ed. Hoboken, N.J.: John Wiley, 2007.

[60] D. A. Buralli, G. M. Morris, and J. R. Rogers, "Optical performance of holographic kinoforms," *Applied Optics,* vol. 28, pp. 976-83, 1989.

[61] J. Dyson, "Common-Path Interferometer for Testing Purposes," *J. Opt. Soc. Am.,* vol. 47, pp. 386-387, 1957.

[62] K. Goto, M. Sasaki, S. Okuma, and K. Hane, "A double-focus lens interferometer for scanning force microscopy," *Review of Scientific Instruments,* vol. 66, pp. 3182-3185, 1995.

[63] L. Pei-Yih, H. P. D. Shieh, J. Jau-Jiu, T. Shin-Ter, Y. Tsung-Ming, C. Tsung-Kai, and L. Jiin-Song, "A novel dual focus objective lens for DVD/CD pick-up head," USA, 1998, pp. 462-4.

[64] H. Kinoshita, K. Hoshino, K. Matsumoto, and I. Shimoyama, "A thin camera with a zoom function using reflective optics," *Sensors and Actuators, A: Physical,* vol. 128, pp. 191-196, 2006.

[65] H. B. Yu, G. Y. Zhou, F. S. Chau, F. W. Lee, S. H. Wang, and H. M. Leung, "A liquid-filled tunable double-focus microlens," *Optics Express,* vol. 17, pp. 4782-4790, 2009.

[66] R. Barakat and A. Houston, "Transfer Function of an Annular Aperture in the Presence of Spherical Aberration," *J. Opt. Soc. Am.,* vol. 55, pp. 538-539, 1965.

[67] J. Ojeda-Castaneda, P. Andres, and A. Diaz, "Annular apodizers for low sensitivity to defocus and to spherical aberration," *Optics Letters,* vol. 11, pp. 487-9, 1986.

[68] B. Dubik, S. Koth, J. Nowak, and M. Zajac, "Hybrid lens with corrected sphere-chromatic aberration," *Optics and Laser Technology,* vol. 27, pp. 315-19, 1995.

[69] L. Yat Hei and R. Leonhardt, "Aspherical lenses for terahertz spectroscopy," USA, 2007, pp. 68011-1.

[70] Z. Zhong and V. C. Venkatesh, "Semi-Ductile Grinding and Polishing of Ophthalmic Aspherics and Spherics*," *CIRP Annals - Manufacturing Technology,* vol. 44, pp. 339-342, 1995.

[71] J. Durnin, J. J. Miceli, Jr., and J. H. Eberly, "Diffraction-free beams," *Physical Review Letters,* vol. 58, pp. 1499-501, 1987.

[72] A. Vasara, J. Turunen, and A. T. Friberg, "Realization of general nondiffracting beams with computer-generated holograms," *Journal of the Optical Society of America A (Optics and Image Science),* vol. 6, pp. 1748-54, 1989.

[73] W. T. Welford, "Use of Annular Apertures to Increase Focal Depth," *J. Opt. Soc. Am.,* vol. 50, pp. 749-752, 1960.

[74] H. Wang and F. Gan, "Phase-Shifting Apodizers for Increasing Focal Depth," *Appl. Opt.,* vol. 41, pp. 5263-5266, 2002.

[75] J. Ojeda-Castaneda, and A. Diaz, "High focal depth by quasibifocus," *Appl. Opt.,* vol. 27, pp. 4163-4165, 1988.